GALACTIC PLANE SURVEYS

C. Motch

Observatoire de Strasbourg, 11 rue de l'Université, 67000 Strasbourg, France

ABSTRACT

We review the main results obtained from recent Galactic Plane X-ray surveys carried out by XMM-Newton and Chandra, limiting our discussion to the faint discrete sources. The wide X-ray band-pass, high sensitivity and good spectral resolution of these new instrumentations offer for the first time the opportunity to explore the X-ray source populations of our own Galaxy in the medium to low X-ray luminosity regime ($L_X < 10^{35}$erg s^{-1}). At very low latitudes ($b \sim 0°$) the vast majority of the soft (0.5-2.0 keV) sources are identified with active stars whereas at galactic latitudes above a few degrees the background of AGN dominates log N(>S)-log S curves down to a few 10^{-15}erg cm^{-2} s^{-1} at all energies. The large number of stellar identifications allows to study with unprecedented depth the distribution of young stars up to about 1 kpc. XMM-Newton and Chandra measurements are not strongly biased by interstellar extinction, as were earlier studies based on ROSAT observations restricted to the softer 0.1-2.4 keV band. Current surveys are thus particularly well suited for the study of the hard X-ray emitting low luminosity population which has mostly escaped ROSAT scrutiny. Chandra and XMM-Newton observations indeed reveal the presence of a population of low X-ray luminosity hard galactic sources exhibiting a marked concentration in the central parts of the Galaxy. Several source types such as cataclysmic variables, Be/X-ray binaries, RS CVn's or low luminosity stages of classical X-ray binaries predicted by theories of evolution could contribute to this population. Follow-up optical observations provide constraints on the nature of these sources and even positive identifications in a number of cases. The numerous sources detected close to the center could be associated with the nuclear bulge and the nuclear cluster. Their nature remains so far uncertain.

Key words: X-ray; Surveys; Accreting sources.

1. INTRODUCTION

In the early 70's the Uhuru satellite (Forman et al. 1978) discovered a concentration of bright X-ray sources along the galactic plane, the most prominent of them being Sco X-1. A number of other satellites completed the bright source mapping, such as Ariel V (Warwick et al. 1981) and HEAO-1 (Wood et al. 1984). These experiments have lead to the discovery of the first accreting neutron stars and black holes and opened a rich and exciting new field of astrophysics. However, the collimator design of these instruments limited their detection efficiency and only the brightest X-ray sources with X-ray luminosities above $\sim 10^{36}$erg s^{-1} at the distance of the galactic center could be detected. At present, XTE and INTEGRAL are continuously detecting new luminous transient galactic sources and very significantly extend our understanding of the various kinds of accreting neutron star and black hole binaries.

From 1978 till 1981, the *Einstein* satellite was the first to fly a relatively large X-ray imaging telescope equipped with detectors sensitive to the soft X-rays (0.5-4.5 keV). *Einstein* discovered the high energy emission of many galactic sources such as cataclysmic variables (CVs) (Hertz & Grindlay 1984) and revealed the unexpected X-ray emission from many young stars all along the HR diagram. In the first years of the 90's, ROSAT conducted the first all-sky soft (0.1-2.4 keV) X-ray map ever made followed by a large number of pointed observations. Among the many galactic discoveries which can be attributed to ROSAT are the super soft sources, already suspected by *Einstein*, and the thermal emission of radio-quiet isolated neutron stars. Although many faint accreting binaries (CVs, Be/X-ray systems) were found in the galactic plane, the number source count remained dominated by active stars (Motch et al. 1997). With its hard X-ray (0.7-10 keV) sensitive imaging instrument, ASCA provided the first detailed view on the population of faint hard X-ray sources in the Galaxy (Sugizaki et al. 2001).

The new generation of imaging X-ray satellites, Chandra and XMM-Newton offer a much improved spatial resolution and collecting area compared to previous experiments. In the hard X-rays, the sensitivity of XMM-Newton and Chandra are roughly a factor 10 and 100 better than that of ASCA respectively. A similar situation is encountered in the soft band where XMM-Newton and Chandra do better than the deepest ROSAT pointings by similar factors. Apart from the improved sensitivity, Chandra also provides the excellent positions required to identify galactic sources in the crowded fields prevailing at low latitude. As for XMM-Newton it delivers good spectra and light curves for many sources.

The excellent hard X-rays capabilities of Chandra and XMM-Newton offer the unique opportunity to unveil low luminosity sources ($L_X \sim 10^{31}$erg s^{-1}) shinning through large amounts of interstellar material up to the distance of the galactic center and to explore to much larger distances the population of soft sources (CVs, active coronae, etc.) discovered by *Einstein* and ROSAT. Galactic plane X-ray surveys are a vast topic and the present review concentrates on the discussion of the properties of the faint sources, typically F_X(0.5-12 keV) $< 10^{-12}$ erg cm^{-2} s^{-1} which make the vast majority of the new sources discovered in Chandra and XMM-Newton observations at low galactic latitudes. We furthermore restrict our presentation to the "classical" $E < 12$ keV X-ray range and to discrete sources. A review on the various components contributing to the diffuse galactic emission in presented by R. Warwick in this volume.

2. SCIENCE DRIVERS

The study of the nature of the X-ray source population of our own Galaxy in the medium to low luminosity regime ($L_X \sim 10^{29}$ - 10^{35} erg s^{-1}) brings essential information on accretion power, star formation and end points of stellar evolution throughout the Galaxy. Their distribution in the Galaxy and their connection to different galactic structures such as the disc, the bulge and the central regions yield important information on their evolutionary status. In addition, the knowledge of the log N(>S)-log S curves down to faint fluxes is prerequisite to separate truly diffuse from unresolved emission, a very debated issue in the framework of the Galactic Ridge (Warwick 2005).

Because of the steep decay of X-ray luminosity with age, soft X-ray surveys unveil the young (age $\leq$ 2 Gyr) stellar population much more efficiently than at optical wavelength and allows to study the evolution of the scale height with age and the mechanism leading to the "heating" of the disc stars. Number counts and distribution in distances give access to the recent stellar formation rate. Clustering structures, such as the Gould Belt enhancement revealed by ROSAT (Guillout et al. 1998) can also be discovered. Current estimates are that our Galaxy could harbour about 10^6 to 10^7 CVs. However, CV demography is based on local estimates and their scale height and distribution at large distances in the disc and bulge of the Galaxy are essentially unknown. This problem has impact on our knowledge of the actual novae rate and connects with the origin of low-mass X-ray binaries (LMXBs) and SN1a supernovae.

The binary evolution scenarios leading to the low and high mass X-ray luminous accreting binaries predict the existence of a number of low X-ray luminosity stages, which in most cases have no yet been observed. Before entering their high mass transfer states, LMXBs should go through a long lived, close, detached neutron star - red dwarf phase during which accretion of the stellar wind onto the neutron star may produce a detectable X-ray luminosity excess above the coronal stellar activity (Bleach 2002). Willems and Kolb (2003) predict that between 10^4 and 10^5 such pre-LMXBs could exist in the Galaxy among which a large fraction will emit X-ray luminosities of the order of 10^{31}erg s^{-1}. All Be/X-ray binaries known so far display direct evidences (pulsations) or indirect evidences (X-ray spectrum) of an accreting neutron star (Negueruela 1998). In high mass binaries, the large mass transfer which may occur during the evolution of the primary star can lead to the creation of a white dwarf (WD) remnant instead of a neutron star in a large number of cases. Averaging over all spectral types, the number of Be + WD should be 7 to 10 times that of Be + neutron stars (Raguzova 2001). Although a number of candidate systems, the γ-Cas analogs, exist (Lopes de Oliveira et al. 2005), the presence of an accreting white dwarf has not yet been confirmed in any of these candidates. Neutron stars accreting from the wind of a relatively unevolved companion could also account for a large number of low luminosity sources ($L_X < 10^{35}$erg s^{-1}; Pfahl et al. 2002). Their expected number may be of the order of 10^5 and should be dominated by intermediate mass primaries (M = 3-8 $M_\odot$). Although some neutron stars accreting from the wind of massive supergiant stars are known, no neutron star has yet been seen accreting from the wind of a main sequence star. The absence of X-ray detection of any of these low L_X states could be partly due to observational biases. It remains however somewhat puzzling and could cast some doubts on binary evolution theories or may indicate that the efficiency with which X-rays are produced considerably drops at low mass accretion rates. Finally, the detection of thermal emission from isolated compact neutron stars either cooling, similar to those discovered by ROSAT or accreting from the interstellar medium could give valuable information on the past or recent massive star formation and end points. The detection of isolated accreting black holes may also be within the reach of the current instruments provided the efficiency with which accretion from the interstellar medium produces X-rays is large enough.

3. A TYPICAL GALACTIC LANDSCAPE

At the level of sensitivity of the Chandra and XMM-Newton instruments (F_X(0.5-12 keV) $\sim 10^{-15}$ erg cm^{-2} s^{-1}) various populations contribute to the source content of low galactic latitude fields. The total galactic photoelectric absorption is often large enough to absorb completely the soft X-rays emission from background AGNs and many soft sources are relatively nearby active coronae. At higher energies, the galaxy becomes transparent to X-rays and the dense background of AGNs sources becomes progressively dominant. The detectability of a genuine population of hard X-ray galactic sources over the extragalactic contribution depends considerably on the galactic direction, total galactic absorption and flux range.

Chandra and XMM-Newton are currently conducting several surveys of various regions of the galactic plane. In this section we focus on the discrete source content of a typical region of the galaxy, i.e. away from the central regions and void of any known structure such as local absorbing clouds, star clusters or star forming regions.

Probably the most ambitious galactic plane survey carried out by Chandra is the Champlane program (Grindlay et al. 2005) which aims at surveying about 8 deg^2 spread over 154 fields distributed over the entire galactic plane. More than 8000 sources are detected above a sensitivity of $F_X \geq 5\ 10^{-16}$ erg cm^{-2} s^{-1} in the 0.5 to 2.0 keV band and $F_X \geq 3\ 10^{-15}$ erg cm^{-2} s^{-1} in the 2 to 10 keV band. Champlane includes a large wide-field optical and IR imaging program as well as spectroscopy. First analysis of the source content in 14 fields located in the anti-center direction (Grindlay et al. 2005) shows that $\sim$ 40% of them have optical counterparts fainter than R = 24.5. The statistics of identification hint at a CV density of $n \sim 10^{-5}$ pc^{-3}, about one third of that estimated locally (Schwope et al. 2002).

Ebisawa et al. (2005) have conducted a somewhat deeper survey concentrated on a small field (0.07 deg^2) located in a region void of bright sources at l = 28.5°and b = 0.0°. Sources detected in the soft (0.5-2.0 keV) and hard (2-10 keV) bands have little overlap. Follow-up near infrared photometry allows to classify them on the basis of their X-ray and IR properties. Almost all soft sources have counterparts with near-infrared (NIR) colours consistent with those of late type star counterparts and only 22% of the hard sources have NIR counterparts. Soft sources with NIR counterparts have stellar-like X-ray spectra, hard sources with NIR counterparts have CV like X-ray spectra and hard sources without NIR counterparts have AGN compatible X-ray spectra. The authors conclude that there are evidences for a genuine hard X-ray galactic population, but that the vast majority of the hard sources are extragalactic and that consequently, the diffuse X-ray galactic ridge emission detected in this field cannot be due to the unresolved contribution of discrete galactic sources.

Hands et al. (2004) report results from the XGPS survey which consist of $\sim$ 400 sources detected in relatively shallow dedicated pointings covering 3 deg^2 at l = 19°-22° and $b = \pm 0.6°$. The 2-10 keV sensitivity is $\sim 2\ 10^{-14}$ erg cm^{-2} s^{-1}, roughly 10 times brighter than that of Chandra. Again, there is little overlap between sources detected in soft (0.4-2 keV) and hard (2-6 keV) X-rays. Soft sources are best fitted by 0.25 keV + 1.5 keV thin thermal spectra (active coronae like) while hard sources have spectra consistent with a power law (Γ = 1.6) with varying N_H= 0.6 - 4 $10^{22}\mathrm{cm}^{-2}$. Fig 1 shows that the log N(>S)-log S curves observed by ASCA and Chandra nicely merge with that derived from the XGPS. An inflection occurs in the log N(>S)-log S curve at $F_X \sim 10^{-12}$ erg cm^{-2} s^{-1} which reflects the transition between a high and low L_X population dominance. The observed hard X-ray log N(>S)-log S is significantly above the expected extragalactic curve, clearly revealing the presence of a galactic population of hard X-ray sources in the XGPS flux regime ($F_X \sim$ 2 - 100 10^{-14} erg cm^{-2} s^{-1}; 2-10 keV). Extragalactic sources account for the majority of sources below $\sim 10^{-13}$ erg cm^{-2} s^{-1} (2-10 keV) with a predominant galactic component above this threshold.

Table 1. Optical identifications of bright XGPS sources

Class	Nbr	mean HR
INS candidate	1	–0.82
Late type stars	19	–0.68
Early type stars	4	–0.68
CVs	3	+0.19
Unidentified	14	+0.61
Be/X-ray	3	+0.85
WR star	1	+1.00

As part of its galactic plane survey (see below), the Survey Science Center (SSC) of the XMM-Newton satellite undertook the optical identification of the 45 brightest XGPS sources in the broad (0.4-6 keV) band. Table 1 summarizes the statistics of optical identifications as function of the mean hardness ratio. Negative HR values indicate soft spectra. Most soft sources are indeed positively associated with active coronae or shocked wind emission from early type stars. Cataclysmic variables exhibit significantly medium hard spectra and are among the sources detected in both soft and hard bands. Their appearance in the soft band probably reflects the fact that they were optically bright enough and therefore close enough to be identified, although one of them was as faint as V = 23.3. Be/X-ray systems are intrinsically much brighter in the optical and can thus be identified at larger distances than CVs with a comparatively higher interstellar absorption and therefore harder spectrum. It is worth noting, however, that the identification essentially relies on the presence of a Balmer Hα line which can also be heavily absorbed. Near infrared spectroscopy in the region of the Paschen series could allow the identification of several more such massive X-ray binaries. The extremely hard spectrum of the WR star is probably partly intrinsic to the source. Unidentified sources have hardness ratio mostly consistent with those expected from background AGNs but could also be consistent with accreting galactic sources. In the F_X range between 10^{-12} and 10^{-13} erg cm^{-2} s^{-1} (2-10 keV), among 20 XGPS sources investigated, 8 have galactic counterparts and 12 are possibly extragalactic with no optical identification brighter than R$\sim$ 23. These numbers ($\sim$ 40% of galactic sources) are in good agreement with the log N(>S)-log S curves shown in Fig. 1.

Thanks to its wide field of view (30′ dia) and good spatial resolution maintained over the whole field, the XMM-

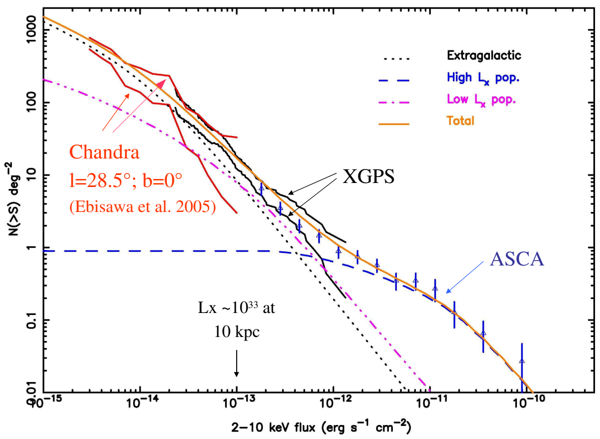

Figure 1. Combined ASCA, XMM-Newton and Chandra hard X-ray log N(>S)-log S curves at l = 19-28.5° and b $\sim$ 0°.

Newton telescope optics provide an excellent opportunity to conduct a large and sensitive X-ray survey. The potential of XMM-Newton surveys was recognised by ESA in setting up a dedicated XMM-Newton Survey Science Center to facilitate the exploitation of the XMM-Newton Serendipitous Sky Survey by providing a public archive of data products and carrying out a carefully coordinated follow-up programme to characterise the overall X-ray source population (Watson et al. 2001). One of the most demanding mission devoted to the SSC is the "statistical" identification of all serendipitous EPIC sources. To achieve this goal, the SSC is conducting optical identification campaigns on samples of $\sim$ 1000 sources at various galactic latitudes and flux limits which will be later used as "calibration" for the statistical identification. Optical identification of the low galactic latitude sample constitutes the core of the XMM/SSC galactic plane survey ($|b|$ $\leq$ 20°; Motch et al. 2003; Motch et al. 2005). The program uses wide field optical and IR imaging and optical spectroscopy at 2 to 8m class telescopes. At present, the SSC has searched for the optical counterparts of more than 400 sources located in 1.8 deg^2 with $F_X > 3\ 10^{-15}$ erg cm^{-2} s^{-1} (0.5-2 keV) and $F_X >$ 3 10^{-14} erg cm^{-2} s^{-1} (2-12 keV), in addition to $\sim$ 80 sources selected on the basis of their X-ray and optical properties. The identification statistics (see Tab. 2) reveal the strong dependency of the source content on galactic latitude. At the limiting R magnitude of 19-22 reached for spectroscopic identification, only few accreting binaries can be positively identified. Clearly, deeper optical and near infrared spectroscopy are needed to identify the faint CVs at large distances and high-mass X-ray binaries in the most absorbed directions. At very low galactic latitudes, background AGNs are in most cases too absorbed to be within the reach of the current optical and near infrared instrumentation.

The nature of the accreting binaries, CVs and Be/X-ray binaries, identified in the XMM/SSC survey is not different from what is already known. In particular, no neutron

Table 2. Statistics of optical identifications in the XMM/SSC galactic plane survey

Fields	Nbr of sources	Stars	EG	Accre-ting	Unid
$b \sim 0^o$	233	40%	$\sim$ 1%	$\sim$ 1%	58%
$b \sim$ 3-12^o	125	27%	14%	$\sim$ 1%	58%

star accreting from the wind of an unevolved companion has been discovered yet. A small number of relatively bright optical objects fall in the 90% confidence error circle of hard sources (typically 3-4$''$ radius). So far optical observations of these candidates have failed to detect any spectral signature such as Balmer or He II λ4686 line emission or radial velocity variations which could reveal the presence of an accreting compact object. A small group of hard and low X-ray luminosity Be stars is however emerging in XMM-Newton surveys and is now also recognized in HEAO-A1 and ROSAT surveys (Lopes de Oliveira et al. 2005). The common characteristics of these Be stars are: a narrow range of B0.5-1 V-IIIe spectral types, Hα EW of $\sim$ -30 Å, relatively stable Balmer line profiles, hard X-ray spectra (thin thermal kT $>$ 8 keV or power law with Γ = 1.5-2.0 + possible presence of a softer component), relatively strong H-like, He-like and low-ionization Fe-K line emission, stable X-ray luminosity over years time scales, soft X-ray luminosities slightly above the mean $L_X \sim 10^{-7}\ L_{bol}$ relation for normal OB stars, hard (0.5-12 keV) X-ray luminosities of a few 10^{32}erg s^{-1}, hour time scale modulations + rapid X-ray variability on short time scales ($\tau <$ 10-100 s), but absence of stable periodicity (Motch et al. 2006). These properties are essentially those of the so far unique and puzzling X-ray emitting Be star γ-Cas. Their X-ray spectra, luminosity and also time behaviour in some cases appear amazingly similar to those of some dwarf novae cataclysmic variables. This has been long considered as the main argument for the Be + WD model and has caught even more attention because of the expected frequency of such systems predicted by evolutionary scenarios. However, a number of correlated X-ray, UV and optical behaviours can hardly be explained in this model and find a better interpretation if one assumes that the flaring X-ray emission arises close to the surface of the Be star in magnetically confined regions and are partially absorbed and reprocessed in colder material located in the circumstellar disc (Smith et al. 1998). This latter model, is however, not free of problems and the origin of the hard X-ray emission of this particular group of Be stars still remains elusive.

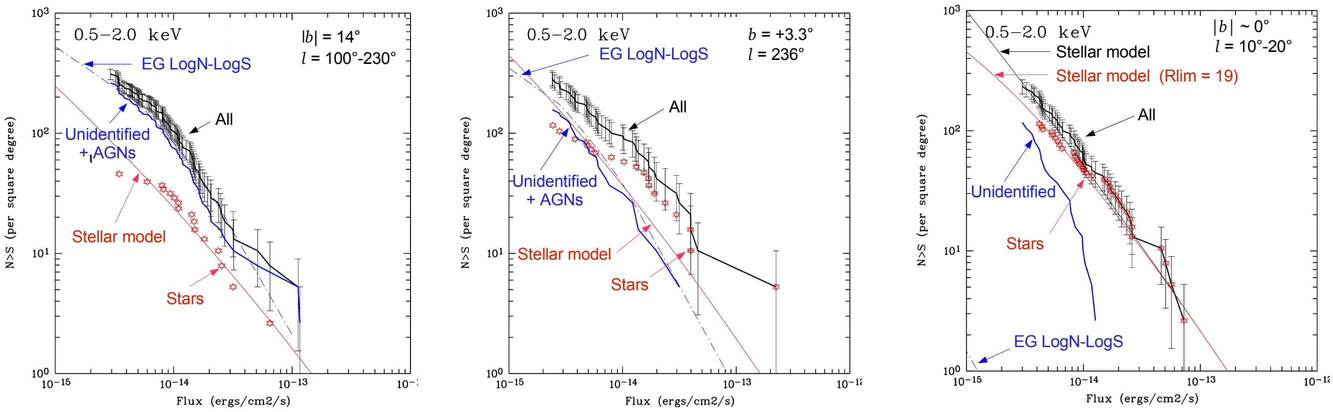

Figure 2. Variation of the stellar and extragalactic + unidentified log N(>S)-log S curves as a function of galactic latitude. Data are extracted from the XMM/SSC galactic plane survey.

4. THE X-RAY STELLAR POPULATION

Active stars constitute the bulk of the identification of soft X-ray sources. At low latitudes, X-ray emitting stars are dominated by the young population (age $\leq$ 750 Myr). XMM-Newton can detect them up to $\sim$ 1 kpc in a typical exposure. As mentioned in section 2, the distribution of the properties of active stars can provide extremely valuable information on some essential galactic parameters such as the variation of the scale height with age for instance. Comparing various observable quantities (log N(>S)-log S curves, distributions in distance, spectral types, colours, etc..) with model predictions is the best suited method to constrain these parameters. The X-ray stellar population model used in the framework of the XMM/SSC survey of the galactic plane is that of Guillout et al. (2005) and Herent et al. (2005) which includes the latest luminosity functions and a description of the dependency of the X-ray energy distribution on age and spectral type. These models also allow to take into account the limiting magnitude of the optical identifications and the presence of enhanced and uneven absorption on the line of sight. Model predictions are in excellent agreement with the observations over six orders of magnitude at high galactic latitude (Herent et al. 2005). At low galactic latitudes, the agreement between model and observations is generally good, except in some regions having pathological distributions of the absorption in distance (Guillout et al. 2005). This overall agreement suggests that the galactic structure parameters of young stars assumed in the model are probably close to their true values.

5. GALACTIC AND EXTRAGALACTIC CONTRIBUTIONS

In a typical low galactic field and at a given flux level, the relative number of galactic and extragalactic sources depends on the energy band considered and on the latitude, longitude and total galactic absorption on the line of sight. The source identification records of the XMM/SSC galactic plane survey can be used to quantify these effects in the range of flux F_X = 3 - 100 10^{-15} erg cm^{-2} s^{-1} (0.5-2 keV) and F_X = 3 - 50 10^{-14} erg cm^{-2} s^{-1} (2-12 keV) covered by this survey. Fig. 2 shows the evolution of the galactic and extragalactic soft X-ray populations as the line of sight plunges toward low galactic latitudes. At $|b|$ = 14° and l = 100°-230°, the number of active stars amounts to roughly a quarter of the total number of soft sources. The log N(>S)-log S curve made from the sum of the identified extragalactic sources and of the unidentified sources (which have too faint counterparts) matches well that expected for the extragalactic component, taking into account the total galactic N_H. At b = 3.3° and l = 236°, the number of stars rises significantly, reaching on average about half of the total number of sources. Again, the expected extragalactic log N(>S)-log S curve fits well the distribution of identified extragalactic sources plus unidentified sources. Finally, at $|b| \sim 0°$ and l = 10°-20°, stars account for the totality of the identifications and the background of AGN is completely shielded. In general, the identified stellar log N(>S)-log S curves are in good agreement within the error bars with the predictions of the stellar population model. This gives confidence in the source identification process at the telescope and indicates that no strong bias for or against a particular population was introduced at this stage. Because of the absorption and of the higher F_X/F_{opt} of the young stars which concentrate in the deep plane (Herent et al. 2005), at $b \sim 0°$, it is necessary to consider the limiting magnitude (R $\sim$ 19) at which it is possible to identify positively an active corona at the telescope. Taking this bias into account allows to fit properly the log N(>S)-log S curve of the identified stellar component while the stellar model without magnitude limit represents well the log N(>S)-log S curve of the total source sample. This is a strong indication that most of the unidentified soft sources are probably optically faint active coronae. Amazingly, in spite of the drastic change in composition of the soft source content, the increase of the number of stellar sources when moving down in

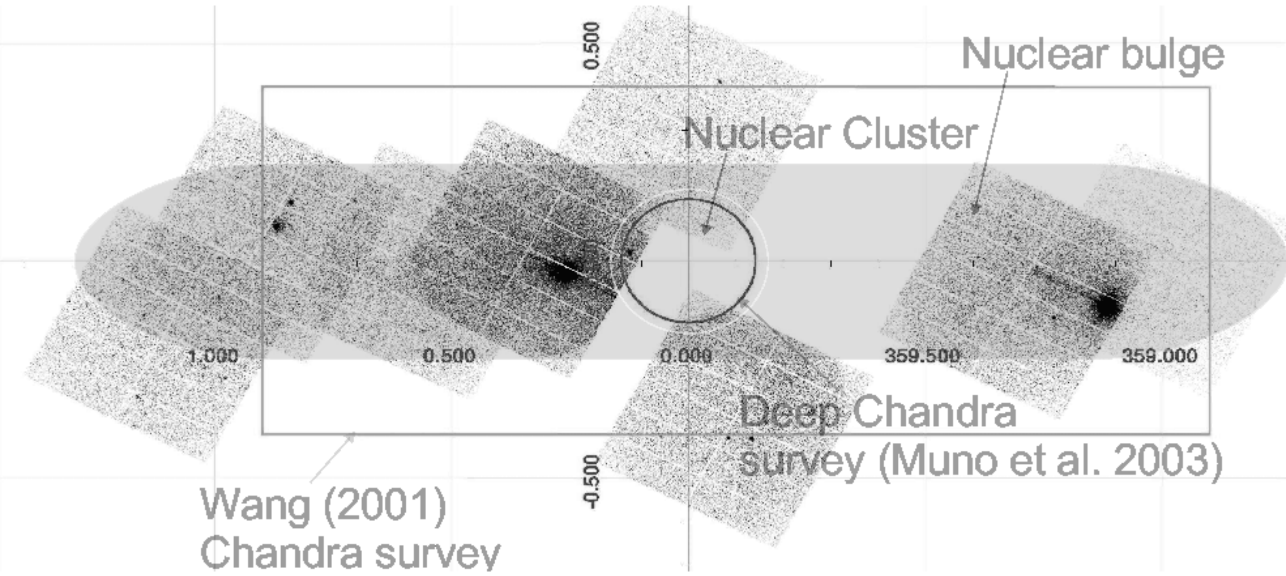

Figure 3. A map showing the location of the main observations carried out by XMM-Newton and Chandra in the region of the galactic center. The size of the nuclear bulge and cluster are not exactly to scale.

the deep plane is almost counterbalanced by the simultaneous decrease of the number of extragalactic sources bright enough to shine through the increasing interstellar absorption.

In the hard X-rays (2-12 keV), AGN completely dominate source counts at $|b|$ = 14° and b = 3.3° in the XMM/SSC galactic plane survey. In the $|b| \sim 0°$ field (l = 10°-20°), there is a clear excess of hard sources above the expected extragalactic background, similar to that found in the XGPS by Hands et al. (2004).

6. THE GALACTIC CENTER REGION

The galactic center region has been the target of all major X-ray telescopes such as, *Einstein*, GRANAT, ROSAT, BeppoSAX and ASCA. XMM-Newton and Chandra are now collecting deep observations of this important region. Fig. 3 shows the XMM-Newton images of the deepest public observations around the galactic center (Wijnands et al. 2005). The XMM-Newton pointings on the center itself are not shown for clarity reasons. The positions of the large scale Chandra survey conducted by Wang et al.(2002) and of the extremely deep pointing of Muno et al. (2003) are also shown. Also sketched on this figure are the positions of the ”nuclear bulge” and of the ”nuclear cluster”. The nuclear bulge, not to be confused with the galactic bulge, is a flat disc-like structure of radius $\sim$ 230 pc, scale height $\sim$ 45 pc with a high stellar density and ongoing stellar formation. Its total mass is $\sim$ 1.4 $10^9 M_\odot$ (Launhardt et al. 2002). The nuclear cluster is a central concentration of stars with a R^{-2} distribution.

Chandra has intensively observed the inner parts of the Galaxy. The first survey published is that of Wang et al. (2002) which covers about 0.8° in latitude, 2° in longitude approximately centered on Sgr A*. About 800 new X-ray sources are detected in this area above a minimum flux of $\sim 10^{-14}$ erg cm^{-2} s^{-1}(2 - 8 keV) corresponding to a detection limit of 8 10^{31}erg s^{-1} at 8 kpc. The He-like Fe Kα line mainly arises from the discrete sources. The number and the hard spectra of the discrete sources indicate the presence of numerous accreting white dwarfs, neutron stars or black holes in that region. Most of the X-ray flux is in the diffuse component which is apparently following known interstellar structures and may be related to regions of recent star formation.

Muno et al. (2003) have obtained a very long 590 ksec Chandra exposure centered on Sgr A*. The 17 by 17 arcminute ACIS-I field corresponds to a 40 pc$\times$ 40 pc area at the distance of the galactic center and therefore essentially covers the nuclear cluster. The survey completeness limit is $L_X \sim 10^{31}$erg s^{-1} at the distance of the galactic center. A total of 2357 sources were detected, mostly above 1.5 keV. Their radial distribution drops as θ^{-1} when moving away from Sgr A* and thus follows the infrared distribution of stars in the nuclear cluster. The density of faint hard sources is extremely high, being more than one order of magnitude above the expected extragalactic background of sources. Their spectra are very hard with power law photon index below 1.0 and exhibit strong lines from low ionization, He-like and H-like iron. Some of these sources display variability on day or month time scales (Muno et al. 2004). Both spectral and timing properties are compatible with magnetically accreting white dwarfs and wind accreting neutron stars. On the other hand, soft sources are uniformly distributed on the sky as expected from a local stellar population.

XMM-Newton has repeatedly observed the galactic center area, focusing on Sgr A* and on the very faint transients located within $\sim$ 1° of the galactic center (Wij-

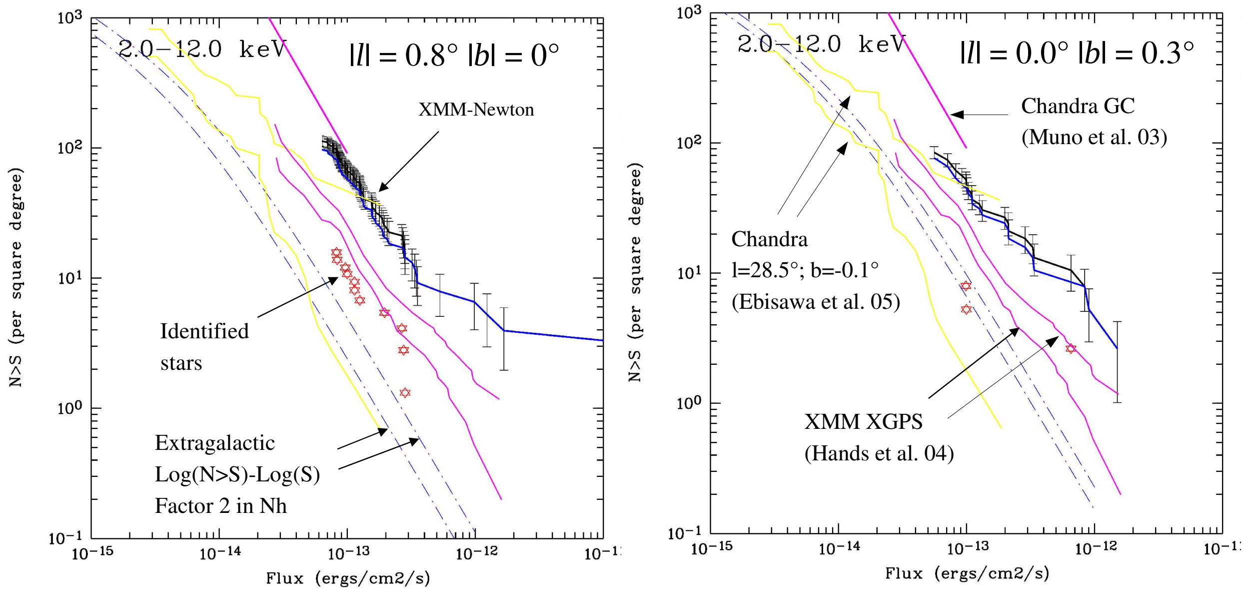

Figure 4. log N(>S)-log S curves observed by XMM-Newton in the central regions of the Galaxy.

nands et al. 2005). We have used the series of 'GC' fields shown in Fig. 3 to study the spatial distribution of the hard sources in the central regions. Fig. 4 (left panel) displays the log N(>S)-log S curves derived from XMM-Newton fields GC2, GC3, GC4 and G8 which are clear of strong diffuse emission. The sources were extracted from the 1XMM catalogue and are therefore in principle free of spurious sources if one imposes a maximum likelihood larger than 8 and a sum flag greater than 0. The log N(>S)-log S curve of the XGPS survey, that derived from the deep Chandra pointing at l =28.5°, $b\sim$0° and the log N(>S)-log S curve computed by Muno et al. (2003) at the center of the deep Sgr A* fields are also shown for comparison. At a 2-12 keV flux of $\sim$ 7 10^{-14} erg cm^{-2} s^{-1}, corresponding to $L_X \geq$ 5 10^{32}erg s^{-1}at 8 kpc, the source density $\sim$ 0.8° away from the galactic center is about 3 times that observed in the XGPS at l = 20° and an order of magnitude above the estimated extragalactic contribution. Since a sizable fraction of the hard XGPS sources are extragalactic, the density increase of galactic sources from $|l|$ = 20° to $|l|$ = 0.8° is even larger. There is however no clear evidence of variation of the source density with longitude in these pointings. The direction of the nuclear bulge is thus very rich in hard X-ray sources and its source density is only surpassed by that measured at the center of the nuclear cluster by Muno et al. (2003). Fig. 4 (right panel) also shows the log N(>S)-log S curve derived from the two XMM-Newton pointings north and south of Sgr A*, GRO J1744 and GC10, which have a mean galactic latitude of $|b|$ = 0.33°(corresponding to 46 pc at 8 kpc). At $|b|$ = 0.33°, the density of galactic sources is about half of that at $|b|$ = 0.0 for F_X= 7 10^{-14} erg cm^{-2} s^{-1}. If confirmed, this steep density drop with galactic latitude may indicate that the majority of the hard sources have an origin in the nuclear bulge which has a scale height of $\sim$ 45 pc.

Optical identifications are severely hampered by the huge interstellar absorption toward the central regions. The GC2 field l=+0.8, b=+0.07 was selected for the XMM/SSC galactic plane survey. Unfortunately, the optical wavelength and the medium size (4-m) of the telescope used for this project did not allow to identify any of the hard sources. A majority of the soft sources were identified with F-K + Me stars. This picture is consistent with the idea that all sources detected in this direction at F_X(0.5-2.0 keV) $\geq$ 5 10^{-15}erg cm^{-2} s^{-1} are nearby active coronae. Interestingly, their source densities are similar to those seen at other galactic longitudes, reinforcing the idea that soft sources represent a local population. Clearly, only an infrared instrumentation on a large telescope can obtain discriminating information on the nature of the hard sources. Bandyopadhyay et al. (2005) find K band counterparts for $\sim$ 75% of a sample of sources in the nuclear bulge region surveyed by Wang et al. (2002) ($F_X \geq$ 4 10^{-14} erg cm^{-2} s^{-1}) suggesting a galactic population. The near-infrared magnitudes and colours of the candidate objects are consistent with highly reddened stars. Laycock et al. (2005) have obtained deep infrared imaging showing that there is no significant excess of bright counterparts in the nuclear stellar cluster (5′ away from Sgr A*). They conclude that high mass X-ray binaries cannot account for more than 18% of the identifications.

The nature of the low X-ray luminosity sources encountered in large number very close to the galactic center remains weakly constrained. Massive X-ray binaries are unlikely to be the dominant population and CVs, in particular the magnetic ones, appear as the best candidate population, although a large population of wind accreting neutron stars could still be present.

7. CONCLUSIONS

Background AGNs and active stars account for a majority of the 0.5-12 keV sources detected in the Galactic Plane at mid galactic latitudes. AGN dominate source counts in both soft and hard bands down to relatively low latitudes ($|b| \sim 3°$, depending on galactic longitude). Stellar population models match so far remarkably well the properties of identified stars. The decrease of the stellar density with increasing galactic latitude should provide a sensitive test of the evolution of scale height with age. At very low galactic latitudes stellar coronae (very young stars) dominate in the soft X-rays and their spatial density which mainly depends on relatively local absorption does not vary much with longitude. A population of hard galactic sources appears above $\mathrm{F_X} \sim 5\ 10^{-14}$erg cm^{-2} s^{-1} (2-10 keV) at $l \leq 30°$and $b \sim 0°$. Optical follow-up observations confirm their galactic nature since a sizable fraction of these hard sources are identified with accreting binaries (Be/X-ray and CVs). Chandra and XMM-Newton have unveiled a dense population of low X-ray luminosity hard galactic sources peaking in the central $\pm 1°$ region of the Galaxy. Two components associated with the nuclear cluster and the nuclear bulge may be present. The nature of these sources, cataclysmic variable or wind accreting neutron stars, remains uncertain.

ACKNOWLEDGMENTS

I acknowledge support from many collaborators from the Survey Science Center of the XMM-Newton satellite.

REFERENCES

Bandyopadhyay, R.M., Miller-Jones, J.C.A., Blundell, K.M., Bauer, F.E., Podsiadlowski, Ph. et al. 2005, MNRAS, in press, astro-ph/0509346

Bleach, J.N., 2002, MNRAS, 332, 689

Ebisawa, K., Tsujimito, M., Paizis, A., Hamaguchi, K., Bamba, A., et al. 2005, ApJ, in press

Forman, W., Jones, C., Cominsky, L., Julien, P., Murray, S., et al. 1978, ApJS, 38, 357

Grindlay, J.E., Hong, J., Zhao, P., Laylock, S., van den Berg, M. et al. 2005, ApJ, in press

Guillout, P., Sterzik, M.F., Schmitt, J.H.M.M., Motch, C., Neuhuser, R. 1998, A&A, 337

Guillout, P., Herent, O., Motch, C. 2005, these proceedings

Hands, A.D.P., Warwick, R.S., Watson, M.G., Helfand, D.J. 2004, MNRAS, 351, 31

Herent, O., Motch, C., Guillout, P. 2005, these proceedings

Hertz, P., Grindlay, J.E. 1984, ApJ, 278, 137

Launhardt, R., Zylka, R., Mezger, P. G. 2002, A&A, 384, 112

Laycock, S., Grindlay, J., van den Berg, M., Zhao, P., Hong, J., et al. 2005, ApJ, in press

Lopes de Oliveira, R., Motch, C., Haberl, F., Negueruela, I., Janot-Pacheco, E., 2005, submitted to A&A

Motch, C., Guillout, P., Haberl, F., Pakull, M.W., Pietsch et al. 1997, A&A, 318, 111

Motch.,C., Herent, O., Guillout, P, et al. 2003, AN, 324, 51

Motch, C., et al., 2005, in preparation

Motch, C., Lopes de Oliveira, R., Negueruela, I., Haberl, F., Janot-Pacheco, E. 2006, in proceedings of the conference on "Active OB stars", Sapporo Sept 2005, Eds. S. Stefl, S. Owocki, A. Okazaki

Muno, M.P., Baganoff, F.K., Bautz, M.W., Brandt, W.N., Broos, P.S., et al. 2003, ApJ, 589, 225

Muno, M.P., Arabadjis, J.S., Baganoff, F.K., Bautz, M.W., Brandt, W.N., et al. 2004, ApJ, 613, 1179

Negueruela, I. 1998, A&A, 338, 505

Pfahl, E., Rappaport, S., Podsiadlowski, P. 2002, ApJ, 571, L37

Raguzova, N.V. 2001, A&A, 367, 848

Schwope, A., Brunner, H., Buckley, D., Greiner, J., Heyden, K. v.d. et al. 2002, A&AS, 396, 895

Smith, M.A., Robinson, R.D., & Corbet, R.H. 1998, ApJ, 503, 877

Sugizaki, M., Mitsuda, K., Kaneda, H., Matsuzaki, K., Yamuchi, S.et al. 2001, ApJS,134, 77

Wang, Q.D., Gotthelf, E.V., Lang, C.C. 2002, Nature, 415, 148

Warwick, R. S., Marshall, N., Fraser, G. W., Watson, M. G., Lawrence, A., et al. 1981, MNRAS 197, 865

Warwick, R., 2005, this Volume

Watson, M. G., Augures, J.-L., Ballet, J., Barcons, X., Barret, D., et al. 2001, A&A, 365, L51

Wijnands, R., in't Zand, J.J.M., Rupen, M., Maccarone, T., Homan, T. et al. 2005, A&A, in press.

Willems, B., Kolb, U. 2003, MNRAS, 343, 949

Wood, K. S., Meekins, J. F., Yentis, D. J., Smathers, H. W., McNutt, et al. 1984, ApJS, 56, 507

INVESTIGATING GALAXY EVOLUTION WITH *CHANDRA*

G. Fabbiano

Harvard-Smithsonian Center for Astrophysics,60 Garden St., Cambridge MA 02138, USA

ABSTRACT

Chandra observations show the importance of the X-ray band for studying the evolution of galaxies. Binary X-ray sources are an easily detectable tracer of the stellar population. *Chandra* studies of these populations are giving us insights into the nature and formation of these binaries, and provide the basis for diagnostics of galaxy evolution. With *Chandra* and *XMM-Newton* we can explore relatively poorly known aspects of the black hole population of the universe: ultra-luminous X-ray sources, that may be connected with the 'missing' intermediate mass black holes predicted by hierarchical galaxy and black hole formation scenarios; and quiescent supermassive nuclear black holes and their surroundings, as a way of understanding the full range of the AGN phenomenon. Finally, the X-ray band provides the only way to explore hot plasmas in galaxies; recent observations are revealing the importance of these plasmas as vehicles of both chemical enrichment and energy.

1. INTRODUCTION

This talk would not have been possible without *Chandra*. Although *XMM-Newton* has contributed significantly to the study of the nearest galaxies, the sub-arcsecond resolution of *Chandra* is essential for detecting populations of X-ray sources in galaxies to the Virgo Cluster and beyond, at the luminosities of the bright Galactic X-ray binaries.

This resolution is also needed to explore the X-ray emission of normal galaxies at high redshift, to obtain sensitive data on the emission and the surroundings of the silent supermassive black holes found at the nuclei of most large galactic bulges, and to study the relatively uncontaminated emission of hot plasmas in galaxies.

2. STELLAR EVOLUTION IN X-RAY BINARIES

It is well known that the Milky Way hosts both old and young X-ray source populations, reflecting its general stellar make up. With *Chandra*'s sub-arcsecond angular resolution, combined with CCD photometric capabilities (Weisskopf *et al.* 2000), we can now study these X-ray populations in galaxies of all morphological types, down to typical limiting luminosities in the 10^{37} ergs s^{-1} range. At these luminosities, the old population X-ray sources are accreting neutron star or black-hole binaries with a low-mass stellar companion, the LMXBs (life-times ~10^{8-9} yrs). The young population X-ray sources, in the same luminosity range, are dominated by neutron star or black hole binaries with a massive stellar companion, the HMXBs (life-times ~ 10^{6-7} yrs; see Verbunt & van den Heuvel 1995 for a review on the formation and evolution of X-ray binaries), although a few young supernova remnants (SNRs) may also be expected. At lower luminosities, reachable with *Chandra* in Local Group galaxies, Galactic sources include accreting white dwarfs and more evolved SNRs. With *Chandra*'s angular and spectral resolution, populations of point-like sources are easily detected above a generally cooler diffuse emission from the hot interstellar medium (fig. 1). Note that luminous X-ray sources are relatively sparse by comparison with the underlying stellar population, and can be detected individually with the *Chandra* sub-arcsecond resolution, with the exception of those in crowded circum-nuclear regions.

To analyze this wealth of data two principal approaches have been taken: (1) a photometric approach, consisting of X-ray color-color diagrams and color-luminosity diagrams, and (2) X-ray luminosity functions (XLFs). Whenever the data allow it, time and spectral variability studies have also been pursued. Optical and radio identifications of X-ray sources and association of their position with different galaxian components are now being increasingly undertaken.

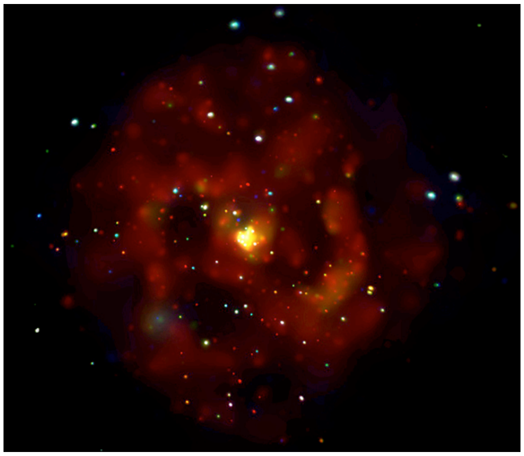

Fig. 1 – *Chandra* image of M83 (red is low energy and blue high energy), from the *Chandra* web page (Soria & Wu 2003)

Given the lack of standard X-ray photometry to date, different definitions of X-ray colors have been used in different works; in the absence of instrument corrections, these colors can only be used for comparing data obtained with the same observational set up. Colors, however, have the advantage of providing a spectral classification tool when a limited number of photons are detected from a given source, which is certainly the case for most X-ray population studies in galaxies. Also, compared with the traditional derivation of spectral parameters via model fitting, color-color diagrams provide a relatively assumption-free comparison tool. *Chandra*-based examples of this approach can be found in Zezas *et al.* 2002a, b and Prestwich *et al.* 2003, among others. The X-ray color-color diagram of Prestwich *et al.* 2003 (fig. 2) illustrates how colors offer a way to discriminate among different types of X-ray sources.

XLFs are increasingly used to characterize the X-ray source populations of different galaxies. Compared to the Milky Way, external galaxies provide clean source samples, all at the same distance. Moreover, the detection of X-ray source populations in a wide range of different galaxies allows us to explore global population differences that may be connected with the age and or metallicity of the parent stellar populations (see review of Fabbiano & White 2005 and references therein; Kong *et al.* 2003; Belczynski *et al.* 2004). In general, X-ray sources associated with young stellar populations follow a significantly flatter XLF than that of the X-ray sources in old stellar systems. A good example is provided by M81, where the XLF of the spiral arm stellar population is flatter than that of the inter-arm and bulge regions, consistent with the prevalence of short-lived luminous HMXBs in younger stellar populations (Tennant *et al.* 2001, fig. 3; Swartz *et al.* 2002).

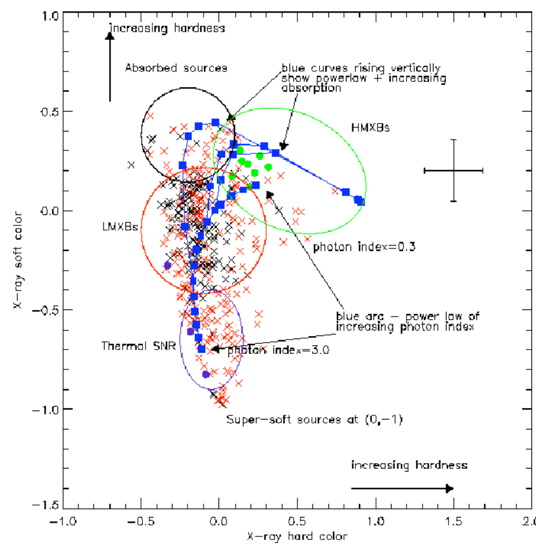

Fig. 2 – *Chandra* color-color diagram from Prestwich *et al.* 2003

The same trend is found comparing the X-ray populations of actively star-forming galaxies with those of E and S0s. While the total number of X-ray sources in star-forming galaxies (the normalization of the XLF) is driven by the star formation rate, in E and S0 galaxies total stellar mass appears to be the driving factor, with the specific frequency of globular clusters as a second order effect (e.g., Zezas & Fabbiano 2002; Kilgard *et al.* 2002; Grimm, Gilfanov & Sunyaev 2003; Gilfanov 2004; Kim & Fabbiano 2004).

The tools that are being developed for characterizing and understanding the X-ray source populations of nearby galaxies lay the foundation of future work in X-ray population synthesis (see Belczynski *et al.* 2004). We know from the co-added statistical detections of high redshift galaxies in deep *Chandra* surveys that there is X-ray evolution with redshift (Lehmer *et al.* 2005) in galaxies. The next step will be to use what we are learning from the nearby universe, together with the observational constraints derived from observations of the high *z* universe, to put firm observational and theoretical constraints on the evolution of X-ray binary populations (e.g. Ghosh & White 2001).

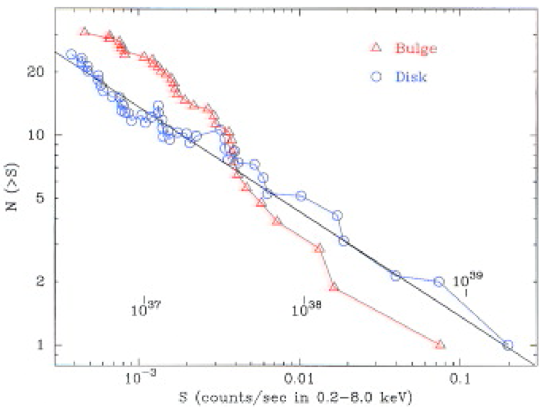

Fig. 3 – Bulge and disk XLFs of M81 (Tennant *et al.* 2001).

3. BLACK HOLES AND THEIR ENVIRONMENT

One of the current hot topics in astrophysics and cosmology is the formation and evolution of black holes and their relation to the formation of galaxies. X-ray observations can help constrain some of these scenarios. I will discuss here two topics related to understanding the entire spectrum of black holes: ultra-luminous X-ray sources (ULXs), and silent nuclear supermassive black holes.

3.1 ULXs

The most widely used observational definition of ULXs is that of sources detected in the X-ray observing band-pass with luminosities of at least 10^{39} erg s^{-1}, implying bolometric luminosities clearly in excess of this limit. This ULX luminosity is significantly in excess of the Eddington limit of a neutron star ($\sim 2 \times 10^{38}$ erg s^{-1}), suggesting accreting objects with masses of 100 $M_{\odot}$ or larger. Since these masses exceed those of stellar black holes in binaries (up to ~30 $M_{\odot}$, Belczynski, Sadowski & Rasio 2003), ULXs could then be a new class of astrophysical objects, possibly unconnected with the evolution of the normal stellar population of a galaxy. ULXs could represent the missing link in the black hole mass distribution, bridging the gap between stellar black holes and the super-massive black holes found in the nuclei of early type galaxies. These 'missing' black holes have been called intermediate mass black holes (IMBH), and could be the remnants of hierarchical merging in the early universe (Madau & Rees 2001), or could be forming in the core collapse of young dense stellar clusters (e.g. Miller & Hamilton 2002).

While ULXs have been known for the last ~20 years, the detection of large samples of these sources has required the observations of many galaxies, and in particular active star-forming systems, where they are copious. *Chandra* and *XMM-Newton* observations have shown that ULXs tend to be associated with very young stellar populations (such as that of the Antennae galaxies, where 14 such sources are found; Fabbiano *et al.* 2004a). These results have suggested the alternative view that ULXs could just represent a particular high-accretion stage of X-ray binaries, possibly with a stellar black hole accretor (King *et al.* 2001; see also Grimm, Gilfanov & Sunyaev 2003; Rappaport, Podsiadlowski & Pfahl 2005), or even be powered by relativistic jets in microquasars (Koerding, Falke & Markoff 2002). *Chandra* and *XMM-Newton* work has confirmed that ULXs are compact accreting sources (as suggested by *ASCA* results, Makishima *et al.* 2000; Kubota *et al.* 2001). Flux-color transitions have been observed in a number of ULXs, suggesting the presence of an accretion disk. Some of these spectra and colors are consistent with or reminiscent of those of black hole binaries (e.g., in the Antennae, Fabbiano *et al.* 2003a, b, 2004a). However, these results do not constrain unequivocally the mass of the compact accretor

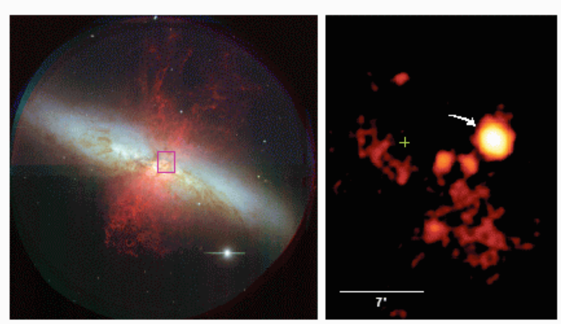

Fig. 4 - M82, left, and the *Chandra* image of the area in the marked rectangle (right), with the ULX marked by the arrow; from Fabbiano (2005b)

My present view (based on the observational results to date) is that ULXs may be a mixed bag of sources, perhaps a few are the elusive IMBHs, but most may be more normal black hole binaries (see Fabbiano 2005b).

3.2 Silent supermassive black holes

It is now established that supermassive nuclear black holes are ubiquitous in large E and S0 galaxies and in spiral bulges (e.g. Tremaine *et al.* 2002). Only a small fraction of these black holes are luminous AGN, while low-level activity is more widespread. Some of these nuclei are 'silent' (Ho, Filippenko & Sargent 2003). With *Chandra* we can now explore the emission properties of these low-activity and silent supermassive black holes down to luminosities typical of X-ray binary emission; we can also set constraints on the hot fuel available for accretion and examine the surrounding hot interstellar medium for evidence of past outbursts of activity (Fabbiano *et al.* 2003, 2004b, Jones *et al.* 2002). Fig. 5 shows four of these silent nuclei (Soria *et al.* 2005). All these early-type galaxies by selection have measured nuclear masses, and stringent upper limits on optical line and radio emission.

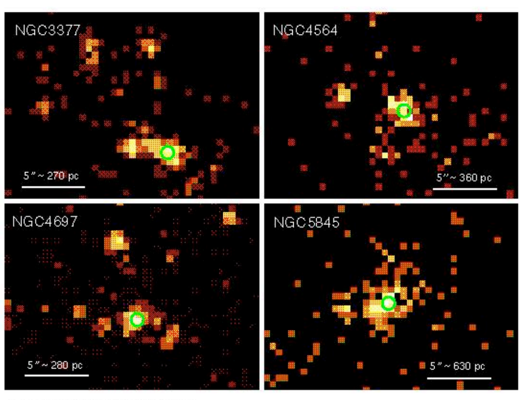

Fig. 5 – Four examples of *Chandra* images of silent supermassive black holes (Soria *et al.* 2005)

The sources we detect with *Chandra* have luminosities in the range 10^{38}-10^{39} erg s^{-1} and tend to be associated with extended emission, from which an estimate of the Bondi accretion parameters can be derived. In these nuclei (see also Fabbiano *et al.* 2004b; Pellegrini 2005), accretion must be inefficient, but ADAF accretion, fueled by both the hot ISM and by stellar out-gassing, can explain the emission. Cyclic activity and outflow cycles (e.g., Binney & Tabor 1995; Ciotti & Ostriker 2001) may avoid accumulating large amounts of material in the immediate surroundings of the black holes.

Why does a black hole awaken? It is not clear. Galaxy interaction and merging have been suggested in the past as triggers of activity, but there isn't yet a strong statistical evidence of this effect. Recent X-ray observations have provided evidence of nuclear activity in strongly interacting galaxies, suggesting that at least in some cases interaction does indeed facilitate nuclear accretion. NGC6240 is a particularly impressive example (Komossa *et al.* 2003). In this late merger galaxy two X-ray hard nuclei have been found with *Chandra* ACIS, and their spectra show clear Fe K emission lines.

If AGN activity is intermittent, perhaps resulting from a feedback cycle (e.g., Ciotti & Ostriker 2001), some evidence of past outbursts may be present in the hot ISM. The spiral-like feature in NGC4636 could be such a remnant (Jones *et al.* 2002), and so perhaps could be a faint elongated structure in NGC821 (Fabbiano *et al.* 2004b). In NGC5128 (Cen A), a huge gaseous ring perpendicular to the jet was discovered with *Chandra*. Its properties are consistent with it being shock heated gas from a past nuclear outburst, possibly connected with the recent merger event in Can A (Karovska *et al.* 2002; fig. 6).

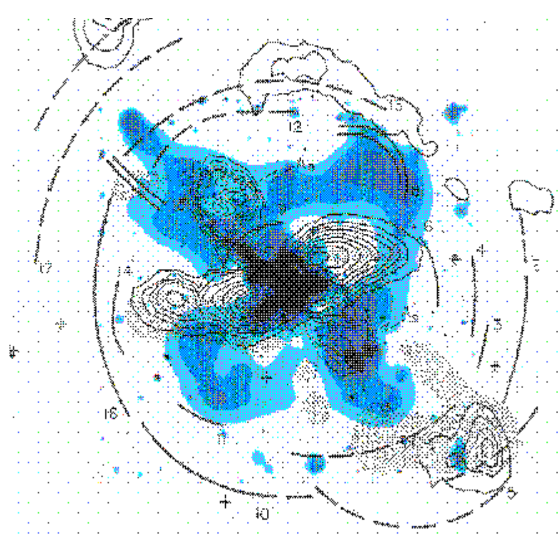

Fig. 6 – In blue is the X-ray emission of NGC5128 detected with *Chandra*. Note the jet and the 'hot ring' surrounding the nucleus (from Karovska *et al.* 2002).

4. HOT WINDS AND THE ECOLOGY OF THE UNIVERSE

Starting with the first Einstein observations (see Fabbiano 1989) it was clear that hot gas and galactic winds are present in actively star-forming galaxies, such as M82 and NC253 in the nearby universe. Through these winds the star-forming galaxies will influence their environment, increasing its entropy, and also depositing newly formed elements into the intergalactic medium. Understanding these winds is therefore important if we want to fully understand the ecology of the universe.

With *Chandra* and *XMM-Newton* we can now get a significantly deeper understanding of these hot gaseous components. I will concentrate here on a recent example, resulting from the deep *Chandra* observations of the Antennae galaxies (NGC4038/39), the prototypical galaxy merger. This system was observed with *Chandra* ACIS for 411 ks. resulting in a spectacular data set (fig. 7, Fabbiano *et al.* 2004a). The hot ISM of the Antennae is discussed in detail by Baldi *et al.* (2005a, b; see also this conference), so I will not talk about it here. I will instead discuss the still mysterious large-scale features seen in this hot ISM, extending well beyond the optical bodies of the merging galaxies. These giant loops extend for ~10kpc to the south of the Antennae, and are embedded in lower surface brightness diffuse emission, that can be traced out to 20 kpc. The loop temperature, from the *Chandra* data, is ~0.3 +/- 0.02 keV,

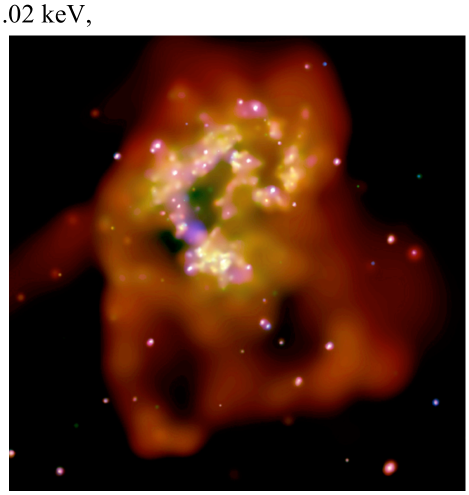

Fig. 7 – Deep *Chandra* image of the Antennae (NGC4038/39), Fabbiano *et al.* (2004a)

significantly larger that the that of the more diffuse halo (0.23 +/- 0.02 keV), possibly suggesting adiabatic cooling and an expanding halo or wind. We do not know what causes these loops, nor what their future evolution will be. Two possibilities are starburst-blown bubbles or merger-induced shocks. From an energy budget point of view, there is plenty of supernova energy deposited in the starburst to cause superbubbles. Given the parameters of the merger, the loops could be propagating with a velocity of 100-1000 km s^{-1}, to be compared with a sound speed of ~200 km s^{-1}. So it is possible that the loops are due to shock-heated gas, but good spectral data are missing. The *Chandra* ACIS data do not have the necessary signal to noise ratio to discriminate among different options. In particular, if the loops are superbubbles, one would expect a cooler interior (Castor, McCray & Weaver 1975). If they are outwardly propagating shocks, the outer rim should be cooler. A deep *XMM-Newton* observation would answer these questions.

The loops could be the result of merger interactions. With accurate temperature and density maps one could attempt a comparison with model simulations (e.g., Barnes 2004). The *Chandra* data do not provide enough statistics for a detailed spectral mapping of these features, but a deep *XMM-Newton* observation could.

Deep *XMM-Newton* data could also address the physical status of the diffuse halo (in equilibrium or expanding), and its metal content. Since we have learned from the deep *Chandra* observation that the hot ISM of the Antennae is metal enriched by SNII events (see Baldi *et al.* 2005a, b), it would be important to measure the metal content of the halo, and compare it with the metal production in the starburst, because this would provide prima facie evidence of how the transport of metals in the intergalactic medium may occur. Obtaining a spectral map of the halo, which would be possible with *XMM-Newton*, would also address crucial questions for the physical status and evolution of the halo. In particular, is the central entropy raised as in galaxy groups (Lloyd-Davies, Ponman & Cannon 2000)? Is the profile at large radii steep and cooler, suggesting winds? We expect that the Antennae will eventually evolve into an elliptical galaxy. Since the mass in the halo is comparable to the amount of diffuse hot gas detected in X-ray faint E and S0 galaxies, and the cooling time is long (Fabbiano 2004a), this type of deep data would provide unique constraints on models of halo development in elliptical galaxies.

Concluding, X-ray observations have discovered a hot gaseous component in galaxies and are now beginning to reveal the physical status and chemical composition of this component. This hot component needs to be included in any simulation of galaxy and merging evolution.

5. PROSPECTS FOR INVESTIGATING GALAXY AND BLACK HOLE FORMATION

We are now witnessing a revolution in the study of galaxies in X-rays. We have progressed from the discovery and characterization phase to using the X-ray window as an important part of our understanding of the evolution of galaxies. Given the connection between HMXB populations and star formation in galaxies, illustrated by X-ray population studies of galaxies with *Chandra*, deep X-ray observations give us a means to measure directly the star-formation rate in the deep universe (e.g., Ranalli, Comastri & Setti 2003; Grimm, Gilfanov & Sunyaev 2003). With *Chandra*'s high-resolution telescope we can directly study the interaction and feedback between nuclear black holes and the host galaxies, an important ingredient in present day cosmological simulations (e.g., Granato *et al.* 2004; Okamoto *et al.* 2005). Moreover, X-ray observations of the hot gaseous component of galaxies have demonstrated that gravity is not the only important force in galaxy formation and evolution. Mergers shock-heat the ISM/IGM and increase its entropy. SN, active nuclei, and perhaps dark jets in X-ray sources all alter the energy budget by heating the ISM, and producing galactic winds. Stellar evolution enriches these winds with chemical elements, and therefore alters the chemistry of the universe at large. X-ray observations provide a direct observational window into these phenomena.

Although *XMM-Newton* has and will contribute substantially to this progress, the sub-arcsecond resolution of *Chandra* has been the true catalyst of this revolution. It is *Chandra*'s resolution, and the resulting sensitivity, that has allowed the detections of samples of X-ray sources d'wn to Galactic XRB luminosities in galaxies more distant than the Virgo Cluster; these samples of X-ray sources have permitted X-ray population studies, providing a probe of the evolution of X-ray binaries in a variety of different environments, and have led to the detection of extreme sources, such as ULXs, in copious numbers. It is *Chandra*'s resolution, and the associated spectral capabilities, that have allowed the separation of point like sources and hot diffuse emission in galaxies, leading to the discovery of metal enrichment in these gases. Finally, it is this resolution that has made possible the study of the faintest reaches of nuclear activity.

While *Chandra* is beautiful, it is a small telescope, and this means that forbiddingly long exposure times are needed to exploit some of these results to the full. For example, a dedicated week of exposure time was needed to obtain the beautiful data on the Antennae that I have shown in this talk. Evolution is only inferred by stacking data on the positions of Hubble deep image galaxies, because individual high redshift galaxies cannot be detected with *Chandra* (Lehmer *et al.* 2005). There is, however, recognition of the potential of X-ray astronomy for studies of cosmology and galaxy and black hole evolution. This recognition has resulted in the *Generation-X* proposal, approved for study by NASA, for a very large future X-ray telescope (~100 square meters mirror), with 0.1 arcsecond resolution. This telescope will not be deployed before 2025.

But this is far away in the future. As a community, we should make sure that this resolution is not lost once *Chandra* stops operating, and that future larger telescopes match or even surpass it. Unfortunately, there are no planned missions (either by NASA or by ESA) that will carry the legacy of *Chandra* forward in the near or foreseeable future. I see this as a serious problem not only for X-ray astronomy, but also for astronomy as a whole.

This work was partially supported under NASA contract NAS8-39073 (CXC).
Some material was also covered in a review talk delivered at the COSPAR Colloquium "Spectra and Timing of Compact X-ray Binaries", held in Mumbai (India), January 17-20, 2005, and in a review talk delivered at the IAU Symposium 230 "Populations of High Energy Sources in Galaxies" held in Dublin (Ireland), August 15-19, 2005.

REFERENCES

Barnes, J. 2004, MNRAS, 350, 798

Belczynski, K., Kalogera, V., Zezas, A. & Fabbiano, G. 2004, ApJ, 601, L147

Belczynski, K., Sadowski, A., Rasio, F. A. 2004, ApJ, 611, 1068

Binney, J., & Tabor, G. 1995, MNRAS, 276, 663

Castor, J.., McCray, R., & Weaver, R. 1975, ApJ 200, L107

Ciotti, L., & Ostriker, J. P. 2001, ApJ, 551, 131

Fabbiano, G. 1989, ARA&A, 27, 87

Fabbiano, G. 2005a, ARA&A, submitted

Fabbiano, G. 2005b, Science, 307, 533

Fabbiano, G., *et al.*. 2003, ApJ, 588, 175

Fabbiano, G., Baldi, A., King, A. R., Ponman, T. J., Raymond, J., Read, A., Rots, A. Schweizer, F. & Zezas, A. 2004a, ApJ, 605, L21

Fabbiano, G., Baldi, A., Pellegrini, S., Siemiginowska, A., Elvis, M., Zezas, A. & McDowell, J. 2004b, ApJ, 616, 730

Fabbiano, G., Zezas, A., King, A. R., Ponman, T. J., Rots, A. & Schweizer, F. 2003a, ApJ, 584, L5

Fabbiano, G., King, A. R., Zezas, A., Ponman, T. J., Rots, A. & Schweizer, F. 2003b, ApJ, 591, 843

Fabbiano, G. & White, N. E. 2005, in Compact Stellar X-ray Sources in Normal Galaxies, eds. W. H. G. Lewin & M. van der Klis, Cambridge: Cambridge University Press, in press

Ghosh, P. & White, N. E. 2001, ApJ, 559, L97

Gilfanov, M. 2004, MNRAS, 349, 146

Grimm, H.-J., Gilfanov, & M., Sunyaev, R. 2003, MNRAS, 339, 793

Granato, G. L., De Zotti, G., Silva, L., Bressan, A., & Danese, L. 2004, ApJ, 600, 580

Jones, C., Forman, W., Vikhlinin, A., Markevitch, M., David, L., Warmflash, A., Murray, S., & Nulsen, P. E. J. 2002, ApJ, 567, L115

Ho, L. C., Filippenko, A. V., & Sargent, W. L. W. 2003, ApJ, 583, 159

Karovska, M., Fabbiano, G., Nicastro, F., Elvis, M., Kraft, R. P., & Murray, S. S. 2002, ApJ, 577, 114

Komossa, S., Burwitz, V., Hasinger, G., Predehl, P., Kaastra, J. S., & Ikebe, Y. 2003, ApJ, 582, L15

Kong, A. K. H., Di Stefano, R., Garcia, M. R. & Greiner, J. 2003, ApJ, 585, 298

Kilgard, R. E., Kaaret, P., Krauss, M. I., Prestwich, A. H., Raley, M. T. & Zezas, A. 2002, ApJ, 573, 138

Kim, D.-W. & Fabbiano, G. 2004, ApJ, 611, 846

King, A. R., Davies, M. B., Ward, M. J., Fabbiano, G. & Elvis, M. 2001, ApJ, 552, L109

Koerding, E., Falke, H. & Markoff, S. 2002, A&A, 382, L13

Kubota, A., Mizuno, T., Makishima, K., Fukazawa, Y., Kotoku, J., Ohnishi, T. & Tashiro, M. 2001, ApJ, 547, L119

Lehmer, B. D., Brandt, W. N., Alexander, D. M., Bauer, F. E., Conselice, C. J., Dickinson, M. E., Giavalisco, M., Grogin, N. A., Koekemoer, A. M., Lee, K.-S., Moustakas, L. A., & Schneider, D. P. 2005, AJ, 129,1

Lloyd-Davies, E. J., Ponman, T. J. & Cannon 2000, D. B. MNRAS, 315, 689

Madau, P. & Rees, M. J. 2001, ApJ, 551, L27

Makishima, K., *et al.* 2000, ApJ, 535, 632

Miller, M. C. & Hamilton, D. P. 2002, MNRAS, 330, 232

Okamoto, T., Eke, V. R., Frenk, C. S., & Jenkins, A. 2005, MNRAS, 363, 1299

Pellegrini, S. ApJ, 624, 155

Prestwich, A. H., Irwin, J. A., Kilgard, R. E., Krauss, M. I., Zezas, A., Primini, F., Kaaret, P. & Boroson, B. 2003, ApJ, 595, 719 Sarazin, C. L., Irwin, J. A. & Bregman, J. N. 2000, ApJ, 544, L101

Ranalli, P., Comastri, A., & Setti, G. 2003, A&A, 399, 39

Rappaport, S. A., Podsiadlowski, Ph. & Pfahl, E. 2005, MNRAS, 356, 401

Soria, R., Fabbiano, G., Graham, A., Baldi, A.., Elvis, M., Jerjen, H., Pellegrini, S., & Siemiginowska, A. 2005, ApJ, in press

Soria, R. & Wu, K. 2003, A&A, 410, 53

Swartz, D. A., Ghosh, K. K., Suleimanov, V., Tennant, A. F. & Wu, K. 2002, ApJ, 574, 382

Tennant, A. F., Wu, K., Ghosh, K. K., Kolodziejczak, J. J., & Swartz, D. A. 2001, ApJ, 549, L43

Tremaine, S. *et al.* 2002, ApJ, 574, 740

Verbunt, F. & van den Heuvel, E. P. J. 1995 in X-Ray Binaries, eds. W. H. G. Lewin, J. van Paradijs & E. P. J. van den Heuvel, Cambridge: Cambridge University Press, p.457

Weisskopf, M., Tananbaum, H., Van Speybroeck, L. & O'Dell, S. 2000, Proc. SPIE, 4012, 2

Zezas, A. & Fabbiano, G. 2002, ApJ, 577, 726

Zezas, A., Fabbiano, G., Rots, A. H., & Murray, S. S. 2002a, ApJS, 142, 239

Zezas, A., Fabbiano, G., Rots, A. H., & Murray, S. S. 2002b, ApJ, 577, 710

AN X-RAY SOURCE POPULATION STUDY OF THE ANDROMEDA GALAXY M 31

W. Pietsch

Max-Planck-Institut für extraterrestrische Physik, Giessenbachstraße, 85741 Garching, Germany

ABSTRACT

Archival *XMM-Newton* EPIC observations reveal the population of X-ray sources of the bright Local Group spiral galaxy M 31, a low-star-formation-rate galaxy like the Milky Way, down to a 0.2-4.5 keV luminosity of 4.4×10^{34} erg s^{-1}. With the help of X-ray hardness ratios and optical and radio information different source classes can be distinguished. The survey detected 856 sources in an area of 1.24 square degrees. Sources within M 31 are 44 supernova remnants (SNR) and candidates, 18 super-soft sources (SSS), 16 X-ray binaries (XRBs) and candidates, as well as 37 globular cluster sources (GlC) and candidates, i.e. most likely low mass XRBs within the GlC. 567 hard sources may either be XRBs or Crab-like SNRs in M 31 or background AGN. 22 sources are new SNR candidates in M 31 based on X-ray selection criteria. Time variability information can be used to improve the source classification. Two GlC sources show type I X-ray bursts as known from Galactic neutron star low mass XRBs. Many of the M 31 SSS detected with *XMM-Newton*, *Chandra* and *ROSAT*, could be identified with optical novae. Soft X-ray light curves can be determined in M 31 center observations for several novae at a time opening a new area of nova research.

Key words: galaxies: individual (M 31), novae, cataclysmic variables, supernova remnants, X-rays: galaxies, X-rays: binaries, X-rays: bursts.

1. INTRODUCTION

In the *XMM-Newton* survey of the Local Group Sc galaxy M 33 (Pietsch et al., 2004a, hereafter PMH2004), 408 sources were detected in a 0.8 square degree field combining the counts of all EPIC instruments, which could be identified and classified using X-ray colors and time variability as well as optical and radio information. This proved to be an efficient way to separate super-soft X-ray sources (SSSs) and thermal supernova remnants (SNRs) in M 33 from Galactic stars in the foreground and "hard" sources. These hard sources may be either X-ray binaries (XRBs) or Crab-like SNRs in M 33 or active galactic nuclei (AGN) in the background of the galaxy. The success of this survey inspired us for a similar analysis of all archival *XMM-Newton* observations of M 31.

The Andromeda galaxy M 31 is located at a distance similar to the one of M 33 (780 kpc, Holland, 1998; Stanek & Garnavich, 1998, i.e. $1''$ corresponds to 3.8 pc and the flux to luminosity conversion factor is 7.3×10^{49} cm^2) and – compared to the near face-on view of M 33 – is seen under a higher inclination (78°). The optical extent of the massive SA(s)b galaxy can be approximated by an inclination-corrected D_{25} ellipse with a large diameter of 153.3' and axis ratio of 3.09 (de Vaucouleurs et al., 1991; Tully, 1988). With its moderate Galactic foreground absorption ($N_{\rm H}$= 7×10^{20} cm^{-2}, Stark et al., 1992), M 31 is well suited to study the X-ray source population and diffuse emission in a nearby spiral similar to the Milky Way. M 31 was a target for many previous imaging X-ray missions. The *Einstein* Observatory detected 108 individual X-ray sources brighter than 5×10^{36} erg s^{-1} (see e.g. Trinchieri & Fabbiano, 1991). The sources were identified with young stellar associations, globular clusters (GCs) and SNRs. The *ROSAT* HRI (Primini et al., 1993) detected 86 sources brighter than $\sim10^{36}$ erg s^{-1} in the central area of M 31. The *ROSAT* PSPC covered the entire galaxy twice in surveys conducted one year apart and detected altogether 560 X-ray sources down to a limit of $\sim5\times10^{35}$ erg s^{-1} and SSS were established as a new class of M 31 X-ray sources (Supper et al., 1997, 2001). The flux of many of the sources varied significantly between the *Einstein* and *ROSAT* observations. Deep *Chandra* ACIS I and HRC observations of the central region (covered areas of 0.08 and 0.27 square degree) resolved 204 and 142 X-ray sources, respectively (Garcia et al., 2000; Kong et al., 2002b; Kaaret, 2002). A synoptic study of M 31 with the *Chandra* HRC covered "most" of the disk (0.9 square degree) in 17 epochs using short observations, and resulted in mean fluxes and long-term light curves for the 166 objects detected (Williams et al., 2004). In these observations, several M 31 SNRs were spatially resolved (Kong et al., 2002a, 2003) and bright XRBs in globular clusters and SSSs and quasi-soft sources (QSSs) could be characterized (Di Stefano et al., 2002, 2004; Greiner et al., 2004).

One of *XMM-Newton*'s most important contributions to galaxy science was a deep survey of the central region around the long axis of M 31 as part of the guaranteed time program. This survey is unique in that it has the greatest depth ($\sim10^{35}$ erg s^{-1}) and best spatial resolution of any existing large area M 31 survey. It has covered almost 3° (>40 kpc) along the major axis of the galaxy and 30' ($\sim$7 kpc) along the central portion of the minor axis. These deep *XMM-Newton* observations have allowed us for the first time to study the short-term time variability ($\sim$100 s and shorter, see below) and spectra of bright X-ray sources in a galaxy outside the Milky Way and the Magellanic Clouds (e.g. Osborne et al., 2001; Barnard et al., 2003, 2005; Mangano et al., 2004). The observations revealed diffuse emission from the hot ISM in the centre and the northern disk (Shirey et al., 2001; Trudolyubov et al., 2001, 2004), and were used to derive source luminosity distributions (Trudolyubov et al., 2002).

Here, I summarize results of our group mainly based on the archival M 31 *XMM-Newton* observations, including X-ray images and a source catalogue for the archival observations of M 31 (Pietsch et al., 2005b, hereafter PFH2005), the detection of type I X-ray bursts in M 31 (Pietsch & Haberl, 2005, hereafter PH2005) and on the detection of optical novae in M 31 as SSSs (Pietsch et al., 2005a, hereafter PFF2005).

2. XMM-NEWTON SURVEY OF M 31

PFH2005 have created merged medium and thin filter images for the three EPIC instruments, in five energy bands (0.2–0.5 keV, 0.5–1.0 keV, 1.0–2.0 keV, 2.0–4.5 keV, and 4.5–12 keV), using only times of low background from the archival *XMM-Newton* M 31 observations which at the time contained four observations of the centre area of M 31 separated by half a year, two pointings in the southern, three in the northern disk, and one short observation in the halo, which all at least partly cover the optical D_{25} ellipse. In total, the observations in the analysis cover an area of 1.24 square degrees (see Fig. 1) with a limiting sensitivity of 4.4×10^{34} erg s^{-1} in the 0.2–4.5 keV band which is a significant improvement compared to the *Chandra* surveys. However, up to now only about 2/3 of the optical M 31 extent (D_{25} ellipse) are covered with a rather inhomogeneous exposure. There were still significant offsets between the observations that had to be corrected for before merging. For the centre observations these offsets were determined from source lists of the individual observations using the USNO-B1, 2MASS, and *Chandra* catalogues to define an absolute reference frame. This finally resulted in a residual systematic position error of less than 0.5". The source detection procedures revealed 856 sources using simultaneously 5×3 images (5 energy bands and PN, MOS1 and MOS2 camera). For the pointings into the disk and halo of M 31 this procedure was applied to the individual observations. The centre pointings strongly overlap and therefore the images were merged to reach higher detection sensitivity.

Figure 1. Combined XMM-Newton EPIC image in the 0.2–4.5 keV band smoothed with a 20" FWHM Gaussian. Orientation and optical D_{25} ellipse are indicated.

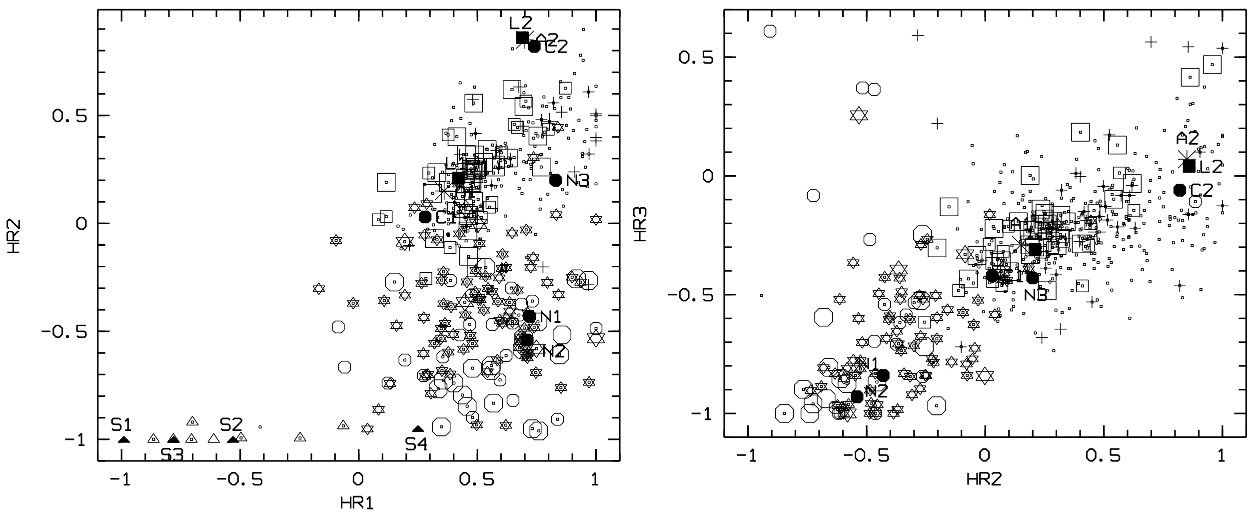

Figure 2. Hardness ratios (HR) detected by XMM-Newton EPIC. Shown as dots are only sources with HR errors smaller than 0.2 on both HRi and $HRi + 1$. Foreground stars and candidate are marked as big and small stars, AGN and candidates as big and small crosses, SSS candidates as triangles, SNR and candidates as big and small hexagons, GlCs and XRBs and candidates as big and small squares. In addition, we mark positions derived from measured XMM-Newton EPIC spectra and models for SSSs (S1 to S4) as filled triangles, low mass XRBs (L1 and L2) as filled squares, SNRs (N132D as N1, 1E 0102.2–7219 as N2, N157B as N3, Crab spectra as C1 and C2) as filled hexagons, AGN (A1 and A2) as asterisk (extracted from Fig. 5 of PFH2005).

Table 1. Summary of identifications and classifications of XMM-Newton X-ray sources in the M 31 and M 33 fields (see PFH2005 and PMH2004).

	M 31		M 33	
Source type	ident.	class.	ident.	class.
fg Star	6	90	5	30
AGN	1	36		12
Gal	1		1	1
GalCl	1	1		
SSS		18		5
SNR	21	23	21+2	23-2
GlC	27	10		
XRB	7	9	2	
hard		567		267

Hardness ratios were calculated only for sources for which at least one of the two band count rates had a significance greater than 2σ (Fig. 2). In search for identifications, the X-ray source positions were correlated with sources in the SIMBAD and NED archives and within several catalogues. The cataloged X-ray sources are "identified" or "classified" based on properties in X-rays (hardness ratios (HR), variability, extent) and of correlated objects in other wavelength regimes. A source is counted as identified, if at least two criteria secure the identification. Otherwise, it is only counted as classified.

Table 1 summarizes identifications and classifications according to the *XMM-Newton* catalogues of M 31 and M 33. For the SNRs in M 33 two new optical counterparts for soft X-ray SNR candidates from the *XMM-Newton* list are indicated (see Ghavamian et al., 2005). Detection of strong time variability in follow-up analysis will certainly move many objects from the "hard" to "XRB" classification. Comparison to earlier X-ray surveys revealed transients not detected with *XMM-Newton*, which add to the number of M 31 XRBs. Up to to now, only low mass X-ray binaries have been identified in M 31, mostly by correlations with globular cluster sources. In M 33, however, besides the ultra-luminous X-ray source close to the nucleus (X–8, most likely a black hole XRB) the only other XRB identified is the eclipsing high mass XRB X–7 with an orbital period of 3.45 d that has been confirmed by the ellipsoidal heating light curve of its optical companion (Pietsch et al., 2004b).

Many foreground stars, SSSs and SNRs can be classified or identified. The number of 44 SNRs and candidates more than doubles the X-ray-detected SNRs. 22 sources are new SNR candidates in M 31 based on X-ray selection criteria. Another SNR candidate may be the first plerion detected outside the Galaxy and the Magellanic Clouds. Additional SNR candidates can be identified by comparing cataloged X-ray sources with optical narrow filter images of the Local Group survey of Massey et al. (2001). Figure 3 gives two examples for two new optical SNR candidates proposed by X-ray source position and a [S II]/Hα ratio of the optical emission characteristic for optical SNRs.

However, besides a few clearly identified XRBs and AGN, and SNR candidates from positions in other wavelengths, we have no clear hardness ratio criteria to se-

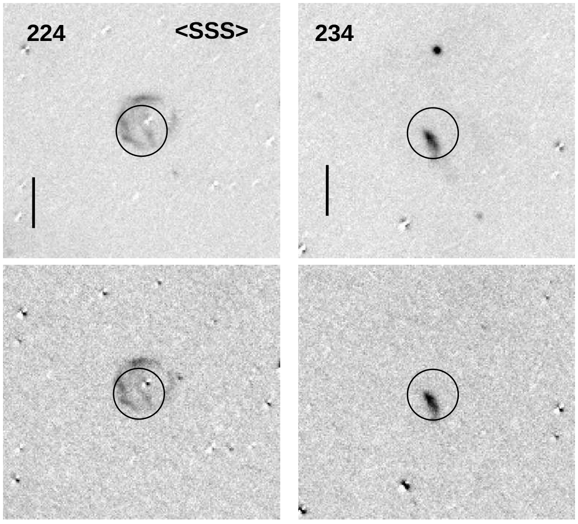

Figure 3. SNR candidates from overlay of Local Group survey images (Hα above, [SII] below): [PFH2005] 224 was classified as SSS candidate, [PFH2005] 234 was unclassified.

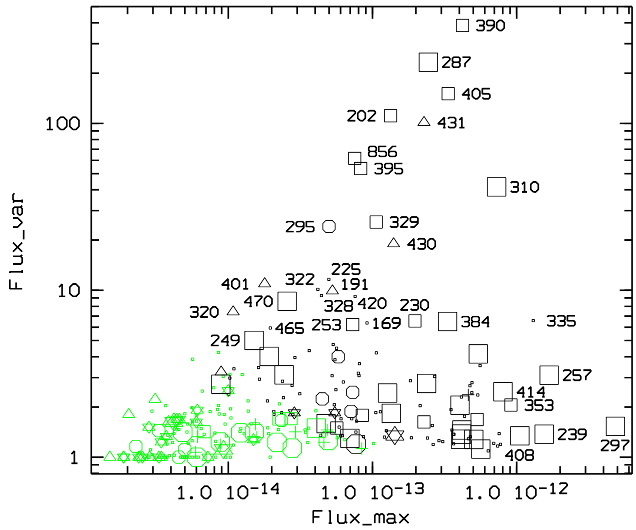

Figure 4. Variability of X-ray sources within four overlapping XMM-Newton observations to the M 31 centre performed from June 2000 to January 2002.

lect XRBs, Crab-like SNR or AGN. They are all "hard" sources (567 sources classified as hard in total). Only additional criteria like short or long term X-ray variability or detailed spectral modeling will reveal their nature. Such methods can be used in the M 31 center area with four overlapping observations in the *XMM-Newton* archive (separated by half a year) and additional observations of the area taken 2.5 yr later (see Fig. 4 and 5).

3. DETECTION OF TYPE I X-RAY BURST SOURCES IN M 31

Within the Milky Way, bright globular cluster X-ray sources were identified as low mass XRBs. Many of them show type I X-ray bursts identifying them as neutron star systems. PH2005 searched for X-ray bursts in *XMM-Newton* archival data of M 31 sources which were identified or classified as globular cluster sources in the PFH2005 catalogue (Fig. 5). Two bursts were detected simultaneously in EPIC pn and MOS detectors and some more candidates in EPIC pn. The energy distribution of the burst photons and the intrinsic luminosity during the peak of the bursts indicate that at least the strongest events were type I radius expansion burst radiating during maximum at the Eddington limit of a 1.4 $M_\odot$ neutron star for hydrogen-poor matter (Fig. 6). Standard type I bursts would show harder spectra and would not be bright enough to be detected by *XMM-Newton*EPIC. The bursts identify the sources as neutron star low mass XRBs in M 31. These type I X-ray bursts are the first detected outside the Milky Way and show that, with the large collecting area of *XMM-Newton*, X-ray bursts can be used to classify neutron star low mass XRBs in Local Group galaxies.

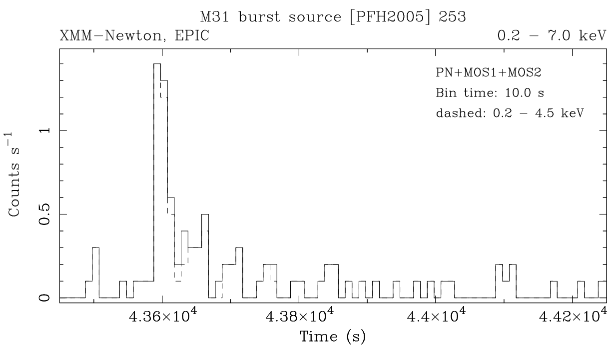

Figure 6. Combined XMM-Newton EPIC light curve of a type I X-ray burst of source [PFH2005] 253 in M31 (Fig. 3 from Pietsch & Haberl, 2005).

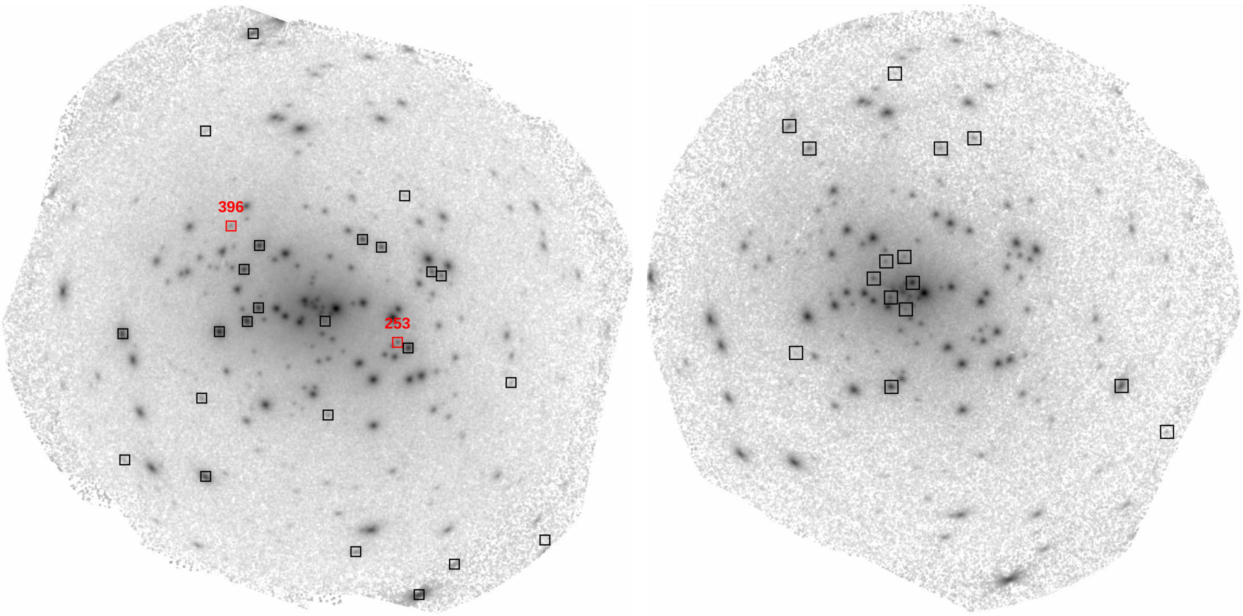

Figure 5. Variability of X-ray sources between combined XMM-Newton M 31 center observations of June 2000 to January 2002 (left, globular cluster sources and candidates marked, burst sources numbered) and observations 2.5 yr later (right). New transients are marked. However, many bright sources from left image are missing.

4. OPTICAL NOVAE AS MAJOR CLASS OF SSS IN M 31

PFF2005 searched for X-ray counterparts to optical novae detected in M 31 and M 33. They combined an M 31 optical nova catalogue from the WeCAPP survey with optical novae reported in the literature and correlated them with the most recent X-ray catalogues from *ROSAT*, *XMM-Newton* and *Chandra*, and – in addition – searched for nova correlations in archival data. They report 21 X-ray counterparts for novae in M 31 (mostly SSS). Their sample more than triples the number of known optical novae with super-soft phase. Most of the counterparts are covered in several observations which allows to constrain X-ray light curves of optical novae (see Fig. 7). Selected brighter sources were classified by their *XMM-Newton* EPIC spectra. Six counterparts are only detected in *Chandra* HRC I (3) or ROSAT HRI (3) observations, i.e. X-ray detectors with no energy resolution, and therefore can not be classified as super-soft. From the well-determined start time of the SSS state in two novae one can estimate the hydrogen mass ejected in the outburst to $\sim 10^{-5} M_{\odot}$ and $\sim 10^{-6} M_{\odot}$, respectively. The super-soft X-ray phase of at least 15% of the novae starts within a year. At least one of the novae shows a SSS state lasting 6.1 years after the optical outburst. Six of the SSSs turned on between 3 and 9 years after the optical discovery of the outburst and may be interpreted as recurrent novae. If confirmed, the detection of a delayed SSS phase turn-on may be used as a new method to classify novae as recurrent. At the moment, the new method yields a ratio of recurrent novae to classical novae of 0.3. Ongoing optical and X-ray monitoring of the central region of M 31, where most of the novae are detected, should allow

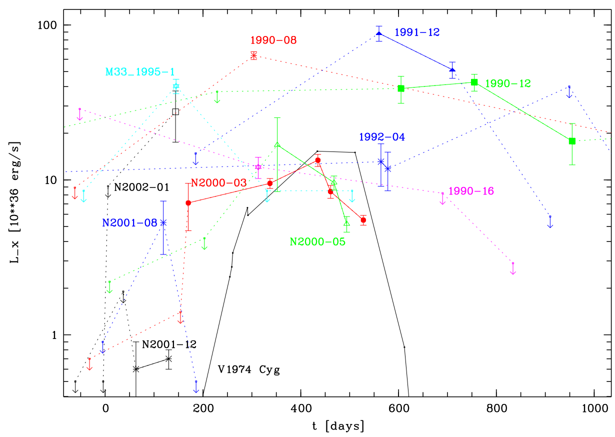

Figure 7. Light curves for M 31 and M 33 novae that were detected within 1000 d after outburst. Detections of individual novae are connected by solid lines, and connections to upper limits are marked by dashed lines (Fig. 3 from Pietsch et al., 2005a).

us to determine the length of the plateau phase of several novae and, together with the nova temperature development, give a handle on the masses of the white dwarfs involved.

5. CONCLUSIONS

The sensitivity of *XMM-Newton* and *Chandra* observations of M 31 combined with the wealth of multi-wavelength data for the galaxy allows a detailed study of the point source population. Many more interesting results can be expected from further monitoring of M 31 with *XMM-Newton* and *Chandra* specifically also in the energy band below 0.5 keV. The first light curves of the SSS state of optical novae proved that these kind of studies can be more efficiently achieved by observing many candidates at the same time in one field in M 31 than by monitoring individual novae in the Milky Way or the Magellanic Clouds. The results of the *Chandra* and *XMM-Newton* observations of M 31 demonstrate the importance of arcsec spatial resolution, broad energy coverage, good energy resolution, and high collecting power – used together with deep images and catalogues at other wavelengths – also for future X-ray source population studies in nearby galaxies.

ACKNOWLEDGMENTS

Based on observations obtained with XMM-Newton, an ESA science mission with instruments and contributions directly funded by ESA Member States and NASA. The *XMM-Newton* project is supported by the Bundesministerium für Bildung und Forschung / Deutsches Zentrum für Luft- und Raumfahrt (BMBF/DLR), the Max-Planck Society and the Heidenhain-Stiftung.

REFERENCES

Barnard, R., Kolb, U., & Osborne, J. P. 2003, A&A, 411, 553

Barnard, R., Kolb, U., & Osborne, J. P. 2005, A&A, submitted (astro-ph/0508284)

de Vaucouleurs, G., de Vaucouleurs, A., Corwin, H. G., et al. 1991, Third Reference Catalogue of Bright Galaxies (Volume 1-3, XII, 2069 pp. 7 figs.. Springer-Verlag Berlin Heidelberg New York)

Di Stefano, R., Kong, A. K. H., Garcia, M. R., et al. 2002, ApJ, 570, 618

Di Stefano, R., Kong, A. K. H., Greiner, J., et al. 2004, ApJ, 610, 247

Garcia, M. R., Murray, S. S., Primini, F. A., et al. 2000, ApJ, 537, L23

Ghavamian, P., Blair, W. P., Long, K. S., et al. 2005, AJ, 130, 539

Greiner, J., Di Stefano, R., Kong, A., & Primini, F. 2004, ApJ, 610, 261

Holland, S. 1998, AJ, 115, 1916

Kaaret, P. 2002, ApJ, 578, 114

Kong, A. K. H., Garcia, M. R., Primini, F. A., & Murray, S. S. 2002a, ApJ, 580, L125

Kong, A. K. H., Garcia, M. R., Primini, F. A., et al. 2002b, ApJ, 577, 738

Kong, A. K. H., Sjouwerman, L. O., Williams, B. F., Garcia, M. R., & Dickel, J. R. 2003, ApJ, 590, L21

Mangano, V., Israel, G. L., & Stella, L. 2004, A&A, 419, 1045

Massey, P., Hodge, P. W., Holmes, S., et al. 2001, Bulletin of the American Astronomical Society, 33, 1496

Osborne, J. P., Borozdin, K. N., Trudolyubov, S. P., et al. 2001, A&A, 378, 800

Pietsch, W., Fliri, J., Freyberg, M. J., et al. 2005a, A&A, 442, 879

Pietsch, W., Freyberg, M., & Haberl, F. 2005b, A&A, 434, 483

Pietsch, W. & Haberl, F. 2005, A&A, 430, L45

Pietsch, W., Misanovic, Z., Haberl, F., et al. 2004a, A&A, 426, 11

Pietsch, W., Mochejska, B. J., Misanovic, Z., et al. 2004b, A&A, 413, 879

Primini, F. A., Forman, W., & Jones, C. 1993, ApJ, 410, 615

Shirey, R., Soria, R., Borozdin, K., et al. 2001, A&A, 365, L195

Stanek, K. Z. & Garnavich, P. M. 1998, ApJ, 503, L131

Stark, A. A., Gammie, C. F., Wilson, R. W., et al. 1992, ApJS, 79, 77

Supper, R., Hasinger, G., Lewin, W. H. G., et al. 2001, A&A, 373, 63

Supper, R., Hasinger, G., Pietsch, W., et al. 1997, A&A, 317, 328

Trinchieri, G. & Fabbiano, G. 1991, ApJ, 382, 82

Trudolyubov, S., Kotov, O., Priedhorsky, W., Cordova, F., & Mason, K. 2004, ApJ, submitted (astro-ph/0401227)

Trudolyubov, S. P., Borozdin, K. N., & Priedhorsky, W. C. 2001, ApJ, 563, L119

Trudolyubov, S. P., Borozdin, K. N., Priedhorsky, W. C., Mason, K. O., & Cordova, F. A. 2002, ApJ, 571, L17

Tully, R. B. 1988, Nearby galaxies catalog (Cambridge and New York, Cambridge University Press)

Williams, B. F., Garcia, M. R., Kong, A. K. H., et al. 2004, ApJ, 609, 735

THE HOTTEST WHITE DWARFS IN THE LOCAL GROUP

M. Orio

INAF- Turin Observatory, Strada Osservatorio 20, I-10025 Pino Torinese (TO) , Italy
and Dept. of Astronomy, University of Wisconsin, 475 N. Charter Str., Madison, WI 53706, USA

ABSTRACT

The nature of the progenitor stars of supernovae of type Ia, the "standard candles" on which much of what we know on the dynamics and geometry of the Universe is based, is still a matter of debate. Close binary supersoft X-ray sources (CBSS) are among likely progenitors: they are often observed, yet are still elusive for many observational and technical difficulties involved. Our own galactic backyard, the Local Group, is ideal to study these stars, because of to the low column density of neutral hydrogen (N(H)). I compare XMM-Newton observations of the sample of these sources in known in the Local Group galaxies. Because of the peculiar spectrum of these sources, it turns out that the first, basic parameter that determines what type of population we detect, is the intrinsic absorption inside the galaxy or a given region of it. This poses a large bias in comparing these populations. For instance supersoft X-ray sources found in the SMC, observed with very low N(H), have a surprisingly constant or almost constant X-ray flux. However, apparent variability in regions of much higher N(H), like some peripheral areas of M31, may be due to poor statistics or to only very small fluctuations in X-ray flux. Nevertheless, there are "hints" of some intrinsic differences in the populations. Some of the LMC sources seem to be be intrinsically very variable, more than sources observed in M31 and the SMC. I discuss the possibility that the symbiotics among CBSS, and SSS that seem to exceed Eddington luminosity and be regulated by a wind, may be important as type Ia supernova progenitors.

Key words: binaries: close–novae, cataclysmic variables–galaxies: stellar content– galaxies: individual, LMC, SMC,M31– X-rays: galaxies.

1. INTRODUCTION

Supersoft X-ray sources (SSS) are defined phenomenologically as X-ray sources that have virtually no counts above 1 keV. Their spectra can be approximately fitted with a blackbody at temperature in the range 20-100 eV, and they are intrinsically extremely luminous (10^{36-38} erg s^{-1} but very absorbed. These sources are detected at large distances, but only if the equivalent column density of neutral hydrogen, N(H), is low. The Local Group is ideal to discover and study SSS, which as a matter of fact were first discovered in the Magellanic Clouds.

SSS are a non-homogeneous class, but they are mostly thought to include very hot white dwarfs, of which many are undergoing thermonuclear burning of hydrogen in an accreted shell in a close binary. Close binary supersoft sources (CBSS) are extremely interesting as type Ia supernovae progenitors. More than a quarter of the CBSS are classical novae. However, no recurrent novae (RN) so far were observed as SSS for a significant amount of time. This is interesting because RN may be very relevant as SNe Ia progenitors, but only if they are observed as bright, hydrogen burning sources after the outburst, because this means they retain accreted material and the WD can grow towards the Chandrasekhar mass. CBSS can be wind/nebular sources (e,g. Cal 87, Greiner et al. 2004 and Orio et al. 2004, usually in low end of luminosity distribution), but often we may be seeing a hot WD atmosphere (e.g. Cal 83, on the high end of luminosity distribution). Although we now know a statistically significant number of SSS, it turns out that caution is necessary in order to derive statistics. Single white dwarfs like PG 1059 stars and planetary nebulae nuclei may appear as SSS, and in addition also supernova remnants (SNR), neutron stars in the foreground and not, background AGN may be all be picked up in the phenomenological classification. We would gain very important astrophysical information if we could sort them out in a statistically significant way.

Recently, Di Stefano and Kong (2003, 2004) and Di Stefano et al. (2004) have studied SSS in external galaxies, even outside the Local Group, using Chandra's ACIS-S detector. ACIS-S offers has the necessary spatial resolution to resolve sources even in the 2 innermost arcminutes[2] in the inner core off M31, inaccessible to EPIC because of source confusion), and it sensitive to softest X-ray range. However, the above authors had to propose an "ACIS-S-suitable" definition of SSS. Di Stefano & Kong (2003) studied therefore an algorithm based

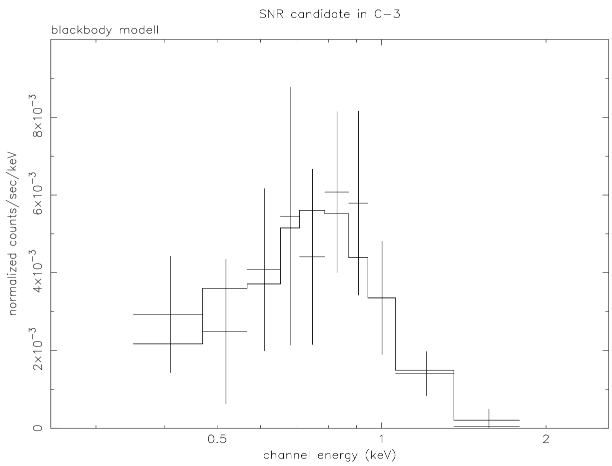

Figure 1. The spectrum of a SNR in M31, RX J004344.1+411219.

on broad bands, especially with a very broad "soft" S band 0.2-1 keV. The reason for this choice is that ACIS-S is not very sensitive in the S band, unlike Chandra HRC (which however cannot be used because it does not offer spectral resolution) or the XMM-Newton EPIC detectors (which lack sufficiently good spatial resolution). Searching faint sources, in external galaxies, the band has to be broad enough to collect photons and not miss sources. Previous definitions adopted in ROSAT investigations (e.g. Supper et al. 1997, 2002) included more CBSS. The new definition has the disadvantage of selecting more different types of sources, like foreground neutron stars and especially SNR, and less CBSS, making SSS an even less homogeneous class. The spectrum shown in Fig.1 is not the softest SNR in M31, yet most of the flux is below 1 keV. It is obvious that soft SNR of this type may be classified as SSS, although probably only the youngest SNR of M31, the remnant associated with S And, would remain a CBSS in the Supper et al. 91997) definition. Another problem of the Chandra-suitable algorithm is the difficulty to adapt it to XMM-Newton EPIC pn and MOS, which do not have a sensitive M band (1.1-2 keV). For the EPIC instruments the ratio of number of photons collected in the S and M band is disproportionately high. However, this may have been the price to pay to compare SSS in the Local Group and in galaxies outside it.

2. A COMPARISON BETWEEN THE LOCAL GROUP GALAXIES

The only way to attempt a statistical study and obtain at least a preliminary census is to examine the spectrum in detail, when possible, and to limit the study to the Local Group, especially using XMM-Newton EPIC, which is extremely sensitive in the band 0.2-0.5 keV. Up to now, extrapolating from the ROSAT surveys and from partial coverage of M31 with XMM-Newton and ACIS-S, we know that about 40 SSS are observed in M31 at a given time, of which 25-30% are novae within 10 years from outburst (Orio 2005). 7 SSS were observed in the LMC (see Greiner 2000). The LMC sources are a nova, a wind source (Cal 87, which incidentally seems to be the only only non variable one, except for X-ray flux modulation with the orbital period: see Orio et al. 2004), a recurrent source, two transient ones, and another variable one.

The catalog of Kahabka et al. (1999) of the SMC includes 9 SSS, of which at least 7 are confirmed as SMC sources. The SMC however has only 1/5th the luminous mass of the LMC and one 80th the one of M31. A thorough search in the archives reveals that 6 SMC sources are persistent SSS, including two planetary nebulae, two symbiotics, and a not yet identified object known to be a constant and strong U source. Finally, 5 SSS were observed in M33 (one of them was also nova , see Pietsch et al. 2005); and one source was observed in the dwarf spheroidal Draco galaxy (a symbiotic, see Mürset et al. 1997).

The comparison shows that there are probably more transient/ highly variable sources in the LMC. We find many low temperature, softer sources in the SMC. This however may be just an effect of low N(H) and smaller population. The value of N(H) plays a very important role in SSS discovery and detection. Are these softer sources systematically missed in other galaxies? If this is the case, rather than being an effect of the low metallicity, statistical comparisons may be heavily biased. A possible solution would be to compare a number of regions of low and comparable N(H) in both the LMC, SMC and M31.

3. MASS ACCRETION REGULATED BY A WIND

Two variable SSS in M31 are extremely interesting. They are called r2-12 and r3-8 in the Chandra catalogs, and reach a luminosity of a few times 10^{39} erg s^{-1}. Such high luminosity seems to be also a characteristic of SSS detected outside the Local Group. One can only speculate that there may be a mechanism at work which is the same as in Ultraluminous X-ray Sources (ULX). The spectrum of the less variable of these two sources, r2-12, is shown in Fig.2. The core of M31 was observed four times with XMM-Newton: it seems that when these two sources reach high luminosity, the spectrum becomes harder, and even has a power-law component for r2-12. Although there is no identification of these sources at optical wavelength, this phenomenon can be understood in the framework of a CBSS: probably a wind that starts when the luminosity is above Eddington (e.g.) and implies that $\dot{m}$ is very high, of order 10^{-7} $M_\odot$ year^{-1}. With such a high transfer rate, it would be crucial to study the optical spectrum of such sources and find out whether they are loosing a significant amount of mass in a wind. If this is not the case, they may reach the Chandrasekhar mass and become type Ia SNe.

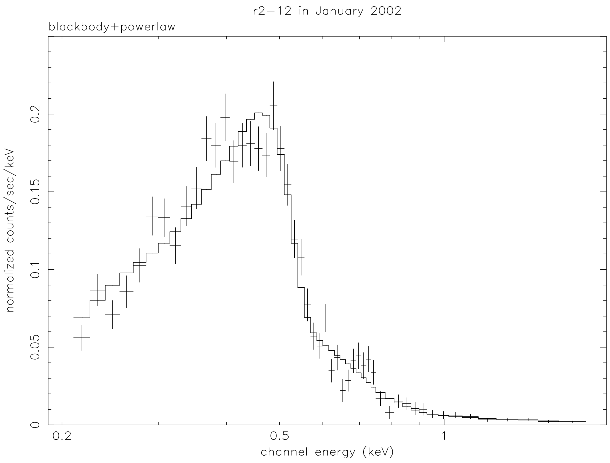

Figure 2. The spectrum of the super-luminous SSS r2-12 in M31: it is fitted with a blackbody at temperature ≈60 eV and a power law component.

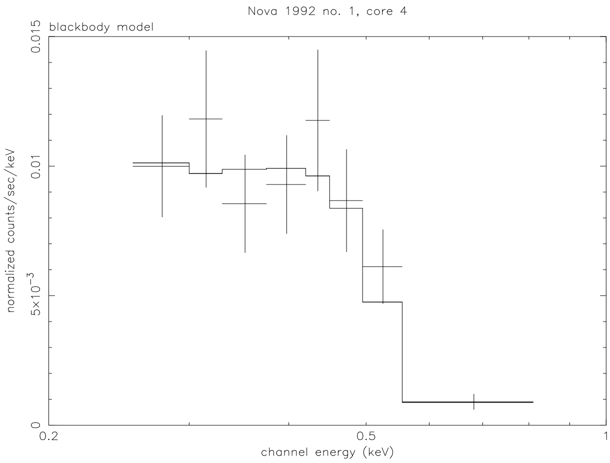

Figure 3. The very soft spectrum of nova 1992-1 in M31. This spectrum, approximately fit with a blackbody at 55 eV, is typical for a SSS nova a few years after the outburst.

4. THE ROLE OF NOVAE AND SYMBIOTIC STARS

Interestingly, three SSS in the Local Group were identified with symbiotics, but only in two very metal poor galaxies: the SMC and Draco (Mürset et al. 1997). The three symbiotics do not have any recorded nova outbursts. They have all been luminous in supersoft X-rays for several years, the two in the SMC for more than 10 years (Orio et al. 2005b). There is a possibility that they may be just accreting "quietly" at too high a rate to undergo nova eruptions with mass loss. Could they eventually reach the Chandrasekhar mass and become SNe Ia? The hope is that in the future we will be able to determine the WD mass in these systems, using large telescopes.

Only about 10-30% of post-outburst novae remain SSS for more than a couple of months and for up to 10 years (Orio et al. 2002, Orio 2005), even if novae make up a significant fraction of SSS in M31 (Orio 2005, Pietsch et al. 2005). Only one nova was observed among 10 novae observed within 10 years from the outburst with ROSAT in the LMC (Orio & Greiner 1998, Orio et al. 2002). The fraction among SSS in M31 seems to be higher, although probably only close to 30%. This is unlikely to be a metallicity effect, since the SSS phase should be shorter with higher metallicity (Sala & Hernanz 2005).

As Fig. 3 shows, the spectrum of classical novae is really extremely soft, and although the ejecta also emit X-ray flux, the supersoft spectrum is due to the hot WD.

5. SUPERSOFT X-RAY SOURCES IN THE XMM-NEWTON OBSERVATIONS OF M31

Fig. 4 shows the innermost 6x6 arcmin of the M31 core, observed with EPIC-pn and with Chandra ACIS-S. It appears immediately that the sources at the center cannot be resolved. If we look closely, we realize however that source confusion is a problem only in the innermost 2x2 arcmin (see close up in Fig. 5). Using the criteria of Di Stefano et al. (2004), 21 sources are selected as SSS in the XMM-Newton observations, which cover about a 4th of the area of the galaxy, by far the most crowded part (Orio 2005): the core and most of the regions along the axis. 5 of them are SNR, of which 4, however, would not be selected as SSS with ROSAT-like criteria, the very young remnant associated with S And being probably the exception. 5 of the M31 SSS observed with XMM-Newton are classical novae that exploded in 1992, 1995 (2), 1996 and 2000. As mentioned above, only ≈10% of novae of the last 25 years are SSS, and none after 10 years. We do not have information on symbiotic stars of M31. Of the other sources, only two were real transient, and the above mentioned r3-8 is seen to vary in flux by more than one order of magnitude on time scales of months. Most other sources disappear from the X-ray window only of they are faint and in areas of high N(H), so large variations are not necessary to explain that they are not repeatedly observed. As a matter of fact, most of the ROSAT SSS that are no longer visible in the new M31 observations done with Chandra and XMM-Newton, are quite faint and/or in regions of high N(H).

6. CONCLUSIONS

Although XMM-Newton and Chandra observations so far have not significantly increased the population of SSS and identify new CBSS in the Magellanic Clouds, significant new statistics of SSS have been obtained for M31. A large enough number of sources are known by now, that statistical comparisons are beginning to be possible. We can definitely say that softer, persistent sources have been detected in the SMC, as opposed to harder, more variable sources in other galaxies and especially in the LMC. Classical novae are a significant fraction of the

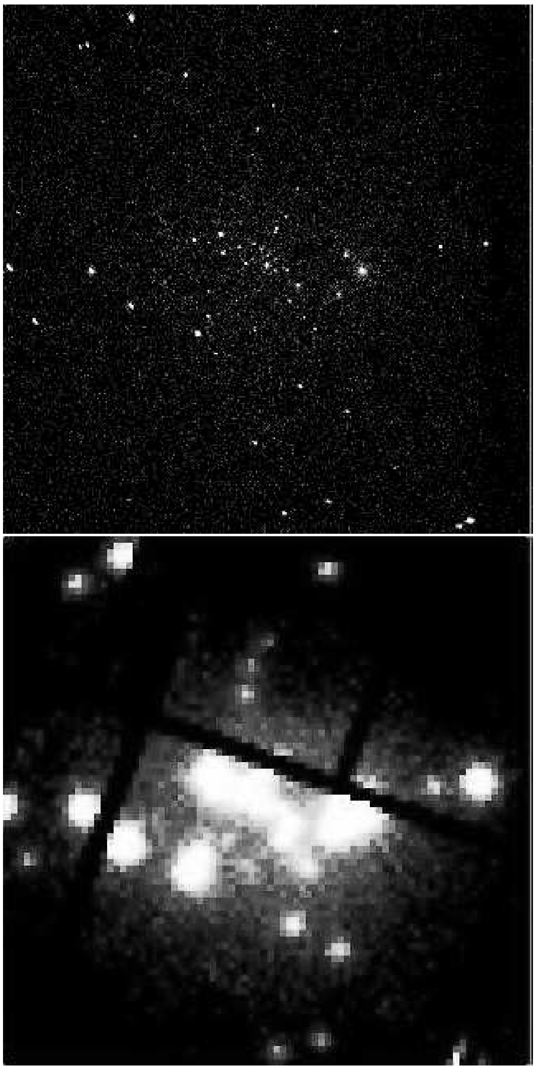

Figure 4. The central 6 arcmin of the core of M31 imagined with XMM-Newton EPIC-pn and with Chandra ACIS-S. The junctions between CCDs and the rows of picsels flagged as "bad" are black and the images are not smoothed or elaborated in any way.

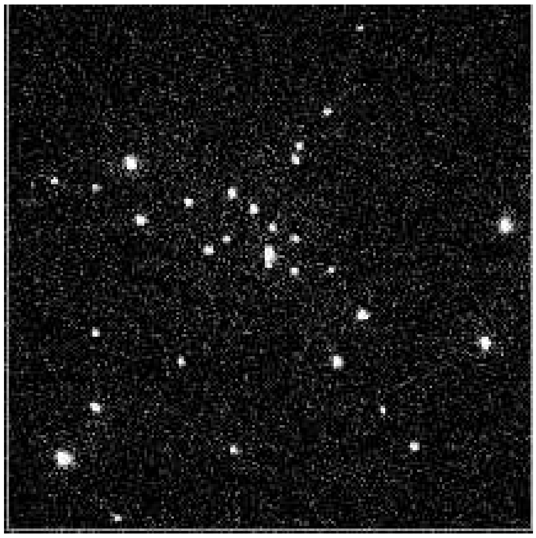

Figure 5. A close up of the innermost 2x2 arcmin with Chandra ACIS-S.

CBSS population, but they are not necessarily interesting as type Ia SN progenitors. On the other hand, a few symbiotics and very luminous "wind-regulated sources" are observed the Local Group galaxies. These two last classes may indeed be relevant as type Ia supernova progenitors, if it can be proved that no significant mass loss occurs.

REFERENCES

Di Stefano, R. & Kong, A. 2003, ApJ, 592, 884

Di Stefano, R. & Kong, A. 2004, ApJ, 609, 710

Di Stefano, R., et al. 2004, ApJ, 610, 247

Greiner, J. 2000, NewA, 5, 37

Greiner, J., & Di Stefano, R. 2002, A&A, 578, L59

Greiner, J., & Di Stefano, R., Kong, A., Primini, F. 2004, ApJ, 610, 261

Greiner, J., et al. 2004b, in Compact Binaries in the Galaxy and Beyond, IAU Coll. 194, E. Sion & G. Tovmassian editors, RevMexAA(SC), 20, 182

Kahabka, P., Pietsch, W., Filipovic, M. D., & Haberl, F. 1999, A&AS, 136,81

Kong, A.K.H., Garcia, M.R., Primini, F.A. & Murray, S.S., 2002, ApJ, 580, L125

Mürset, U., Schild, H., Vogel, M. 1997, A&A, 307, 516

Orio, M., & Greiner, J. 1999, A&A, 344, L13

Orio, M., Hartman, W., Still, M., & Greiner, J. 2003, ApJ, 594, 435

Orio, M., Ebisawa, K., Heise, J., & Hartmann, W. 2004, in Compact Binaries in the Galaxy and Beyond, IAU Coll. 194, E. Sion & G. Tovmassian editors, RevMexAA(SC), 20, 210

Orio, M. et al. 2005, preprint

Pietsch, W., Freyberg, M., & Haberl, F. 2005, A&A, 434, 483

Pietsch, W. et al. 2005, astro-ph/0504321

Sala, G. & Hernanz, M. 2005, 439, 1061

Supper, R. et al. 1997, A&A, 317, 328

Supper, R. et al. 2001, A&A, 373, 63

LOW MASS X-RAY BINARIES AND GLOBULAR CLUSTERS IN EARLY-TYPE GALAXIES

Craig L. Sarazin[1], Greg R. Sivakoff[1], Adrienne M. Juett[1], Andrés Jordán[2], and Patrick Côté[3]

[1]Department of Astronomy, University of Virginia, Charlottesville, VA 22903-0818, USA
[2]European Southern Observatory, Karl-Schwarzschild-Str. 2, 85748 Garching bei München, Germany
[2]Astrophysics, Denys Wilkinson Building, University of Oxford, 1 Keble Road, Oxford, OX1 3RH, UK
[3]Herzberg Institute of Astrophysics, 5071 W. Saanich Road, Victoria, BC V9E 2E7, Canada

ABSTRACT

Chandra observations have allowed the detection of a large number of low mass X-ray binaries (LMXBs) in early-type galaxies. Comparisons to catalogs of globular clusters (GCs) from Hubble Space Telescope observations have shown that a high fraction of the LMXBs in early-type galaxies are associated with GCs. The fraction of LMXBs associated with globular clusters increases along the Hubble sequence from spiral bulges to S0s to Es to cDs. On the other hand, the fraction of globular clusters which contain X-ray sources appears to be roughly constant (∼4% for $L_X \gtrsim 10^{38}$ ergs/s, ∼10% for $L_X \gtrsim 10^{37}$ ergs/s). There is a strong tendency for the X-ray sources to be associated with the optically more luminous GCs. There is a trend for the X-ray sources to be found preferentially in redder, more metal-rich GCs, which is independent of optical luminosity correlation. The relative role of formation of LMXBs in GCs and in situ formation in the field is uncertain. One of the best ways to study this is to compare the spatial distribution of GC-LMXBs, field LMXBs, GCs, and optical light in the galaxies. Theoretical models and results of fits to the observed distributions are presented. Our multiple observations of NGC 4365 and NGC 4697 over several years allow us to study the variability of LMXBs. We have detected very luminous X-ray flares from three sources in NGC 4697 with durations of ∼70 to ∼3000 seconds, which have no clear analogue in our Galaxy. One suggestion is that these are due to micro-blazars; X-ray binaries with accreting black holes with jets which are pointed in our direction.

Key words: early-type galaxies; globular clusters; X-ray binaries .

1. INTRODUCTION

Chandra observations have resolved most of the X-ray emission in X-ray-faint early-type galaxies into individual point-like sources (e.g., Sarazin, Irwin, & Bregman, 2000). Given their properties and the stellar populations in these galaxies, these X-ray sources are assumed to be Low Mass X-ray Binaries (LMXBs). A significant fraction (∼20-70%) of the LMXBs are associated with globular clusters in the host galaxies (Sarazin et al., 2001; Angelini et al., 2001). The fraction of LMXBs located in GCs is much higher than the fraction of optical light, which indicates that stars in GCs are much more likely (by a factor of ∼500) to be donor stars in X-ray binaries than field stars. As has been known for a number of years, a similar result applies to our own Galaxy and to the bulge of M31 (e.g., Hertz & Grindlay, 1983). This is generally believed to result from stellar dynamical interactions in globular clusters, which can produce compact binary systems.

X-ray observations with *ASCA* indicated that the total luminosity of LMXBs in early-type galaxies correlated better with the number of GCs than with the optical luminosity of the galaxy (White et al., 2002). This is somewhat surprising, as a nontrivial fraction (∼ 50%) of the LMXBs in most of the early-type galaxies observed so far with *Chandra* are not identified with GCs. This suggests that most (perhaps all?) of the LMXBs in early-type galaxies were made in GCs (Grindlay, 1984; Sarazin et al., 2001; White et al., 2002). The field LMXBs might have been ejected from globular clusters individually by stellar dynamical processes (or possibly by supernova kicks), or emerged when globular clusters were destroyed by tidal effects. Alternatively, the field LMXBs may have been made in situ from primordial binaries.

2. STATISTICS OF LMXBS AND GC POPULATIONS

The fraction of LMXBs in a galaxy which are associated with GCs increases along a Hubble sequence from spiral bulges (∼10%) to S0s (∼20%) to giant ellipticals (∼50%) to cD galaxies (∼70%) (Sarazin et al., 2003). There is a well-established trend for the specific fre-

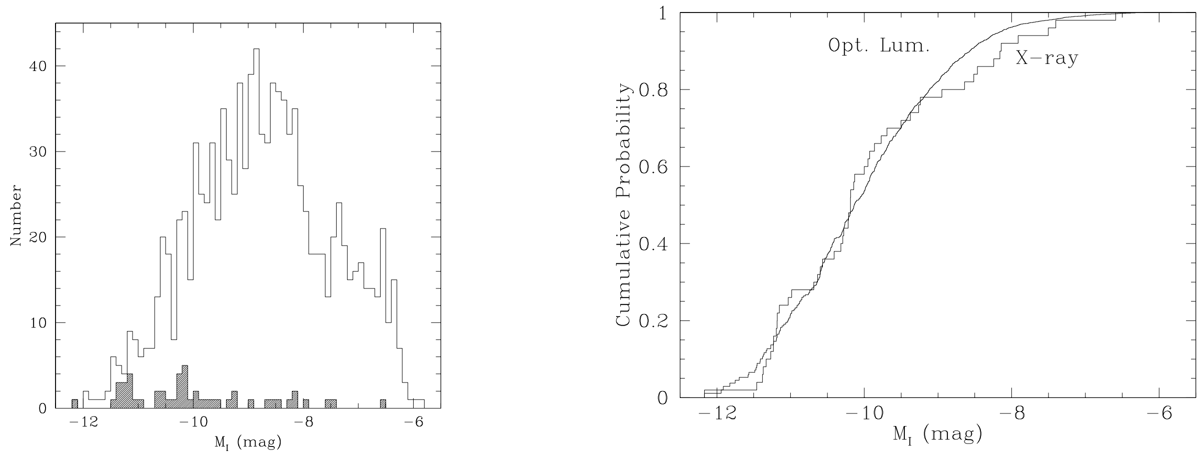

Figure 1. (a) Histograms of the number of globular clusters versus their absolute magnitude M_I in a sample of galaxies with Chandra data (Sarazin et al., 2003). The upper histogram is for all of the GCs in the galaxies. The lower shaded histogram shows the GCs which contain identified LMXBs. (b) Cumulative distribution functions for the probability that a GC contains an X-ray source ("X-ray") and for the optical luminosity of GCs ("Opt. Lum.").

quency of GCs in galaxies (S_N, the number of GCs per optical luminosity) to increase along the same Hubble sequence (e.g., Harris, 1991). The detailed correlation of the fraction of LMXBs in GCs with S_N is more consistent with most of the field LMXBs being made in situ in the field (Juett 2005; see also Maccarone et al. 2003; Sarazin et al. 2003). On the other hand, Irwin (2005) argued recently that a significant portion of the field LMXBs in S0 galaxies may have come from disrupted GCs.

The fraction of globular clusters which contain X-ray sources appears to be roughly constant from galaxy to galaxy. For samples of LMXBs with a high limiting X-ray luminosity, $L_X \gtrsim 10^{38}$ ergs/s, the fraction is $\sim$4% (Kundu et al., 2002; Sarazin et al., 2003). For NGC 4697, a nearby elliptical with deep X-ray and GC observations, the fraction reaches $\sim$10% for $L_X \gtrsim 10^{37}$ ergs/s (Sivakoff et al., 2006).

3. PROPERTIES OF GCS CONTAINING LMXBS

Figure 1(a) shows histograms of the absolute I magnitude, M_I, of the total GC sample (upper histogram) and of the GCs containing LMXBs (shaded histogram). The LMXBs seem to be associated preferentially with the more optically luminous GCs (Angelini et al., 2001; Kundu et al., 2002; Sarazin et al., 2003). For example, the median value of M_I for non-X-ray GCs is -8.7, while the corresponding value for the X-ray GCs is -10.2. Using the Wilcoxon or equivalent Mann-Whitney rank-sum tests, the distribution of X-ray and non-X-ray GC luminosities are found to disagree at more than the 6σ level.

Of course, a correlation between optical luminosity and the probability of having an X-ray source is not unexpected. LMXBs contain normal stars, and globular clusters which have higher luminosities have more stars as potential donors in LMXBs. Thus, it is interesting to test the hypothesis that the probability that a GC contains a LMXB is proportional to its optical luminosity. Figure 1(b) compares the cumulative probability distribution of LMXBs versus the cumulative distribution of the optical luminosity in GCs. The two cumulative distribution functions track one another fairly well. For example, half of the optical luminosity comes from GCs brighter than $M_I = -10.1$, while the medium absolute magnitude of GCs with LMXBs is -10.2. The KS two-sample test was used to compare the two distributions; they are not significantly different. Thus, the current data indicate that optically bright GCs are much more likely to contain LMXBs than faint GCs, but the distribution is consistent with a constant probability per unit optical luminosity (Kundu et al., 2002; Sarazin et al., 2003). Recently, Jordán et al. (2004) found a correlation between the density of stars in M87 GCs and the occurrence of LMXBs. This would be consistent with the formation of LMXBs by dynamical collision processes in GCs, although the detailed form of the correlation found by Jordán et al. (2004) was also nearly equivalent to a simple dependence on the number of stars.

Figure 2 shows histograms of the $V - I$ colors for the total GC sample (upper histogram) and for the GCs containing LMXBs (shaded histogram). Because the sample contains a number of different galaxies, the overall color distribution may be less obviously bimodal than that seen in some individual galaxies. The LMXBs appear to be associated preferentially with the redder GCs (larger values of $V - I$) (Angelini et al., 2001; Kundu et al., 2002; Sarazin et al., 2003). The median color of the non-X-ray GCs is $V - I = 1.07$, while the corresponding median for the X-ray GCs is 1.14. Using the Wilcoxon or Mann-Whitney rank-sum tests or the KS test, the probabilities that the two color distributions where drawn from the same distribution are $<0.2\%$. Roughly, red GCs are three times as likely to harbor a LMXB as blue GCs.

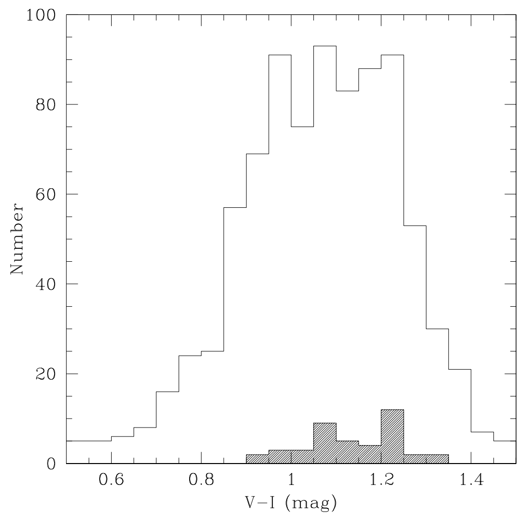

Figure 2. Histograms of the number of GCs versus their optical color, $V - I$ (Sarazin et al., 2003). The upper histogram is for all of the GCs, while the lower shaded histogram shows the GCs which contain LMXBs.

4. SPATIAL DISTRIBUTIONS OF STARS, GCS, AND LMXBS

The radial distribution of GCs in elliptical galaxies is more extended than that of the field stars; in particular, the optical light profiles of ellipticals typically show a central cusp, whereas the spatial distribution of GCs has a constant surface density core. This may indicate that GCs never formed in the central regions, or that the GCs which were initially formed there were disrupted by tidal effects. One way to test this would be to search the central regions of ellipticals for a stellar population which is characteristic of GCs. This is difficult for optical stars; however, as noted above, LMXBs are preferentially produced in GCs. At the same time, we would like to know what fraction of the field LMXBs were made in GCs. Some of the GC LMXBs might have escaped individually due to stellar dynamical interactions, or they may have been released when their host GC was disrupted by tidal effects. In either case, these field LMXBs would have a spatial distribution which reflected the initial spatial distribution of the GCs. Thus, by studying the spatial distributions of the optical light, GCs, and field and GC LMXBs in galaxies, we can constrain models for the formation and destruction of GCs and the origin of LMXBs.

Figure 3 shows models for the spatial distribution of field and GC LMXBs in an elliptical galaxy (Sarazin, 2006). The stellar and GC distribution were based on observations of NGC 4365, and the X-ray sources are from our earlier Chandra observation of this galaxy (Sivakoff et al., 2003). Here, I show only three extreme models. In Model 1, all field LMXBs were made in situ. This model probably provides an adequate fit to the existing data. Note the general result that the observed LMXB distribution is broader than that of the stars, reflecting the contribution of GC LMXBs. In Model 2, all LMXBs are made in GCs, and the field LMXBs were individually ejected from GCs. In this model, the predicted distribution of the LMXBs is broader than that observed. Finally, in Model 3, all LMXBs are also made in GCs, but the only mechanism for the release of the field LMXBs is the tidal disruption of GCs. In this model, the predicted distribution of field LMXBs is more strongly peaked than that observed due to the high rates of GC destruction at the center of the galaxy. Although better data are needed, the comparison of the models with the present data indicate that at least half of the field LMXBs were made in situ.

5. VARIABILITY OF LMXBS: DISCOVERY OF LUMINOUS X-RAY FLARES

In order to detect fainter LMXBs and to study the variability of these sources, we have performed multi-epoch observations of two nearby, optically luminous, X-ray faint elliptical galaxies, NGC 4697 and NGC 4365. Each galaxy was observed a total of five times over about five years for a total exposure of about 200 ksec. (The fifth and final observation of NGC 4365 is scheduled for 2005 November; in this paper, we discuss only the observations from NGC 4697.) Hubble observations of the centers of these galaxies (Côté et al. , 2004; Jordán et al., 2004), reveal the globular clusters (GCs). Flanking fields of both galaxies will be observed in HST Cycle 14, providing essentially complete coverage of their GCs.

Variability studies of LMXBs in the Milky Way and in E/S0s are very complementary. Galactic LMXBs can be studied in great detail during both active ($L_X \gtrsim 10^{36}$ ergs s^{-1}) and quiescent ($L_X \lesssim 10^{34}$ ergs s^{-1}) states across all wavelengths. From this, binary properties (e.g., donor type, compact object mass, orbital period, jet presence) can be determined, allowing for a better understanding of LMXB formation and evolution. However, there are several limitations in studying Galactic LMXBs: source distances are known for only a small subset, it is difficult to observe the whole Galaxy at once, absorption columns vary from source to source, and the size of the observed sample is limited. The latter limitation means that we are less likely to encounter rare phenomena, particularly those associated with the more luminous sources. The large number of luminous LMXBs in each elliptical galaxy provides a significant chance to detect very unusual objects.

We developed a new technique for detecting and characterizing short flares from faint X-rays sources, which is based on searching the arrival times of individual photons for cases where a larger number of photons arrive within a short period.

In NGC 4697, we have discovered three sources which undergo very luminous X-ray flares (Sivakoff, Sarazin, & Jordán , 2005). Two sources (CXOU J124837.8−054652 and CXOU J124831.0−054828) show ~ 1000 s flares with $L_{\rm bol} > 4 \times 10^{38}$ ergs s^{-1}. Both of these LMXBs appear to be located in GCs. Although the timescale of the

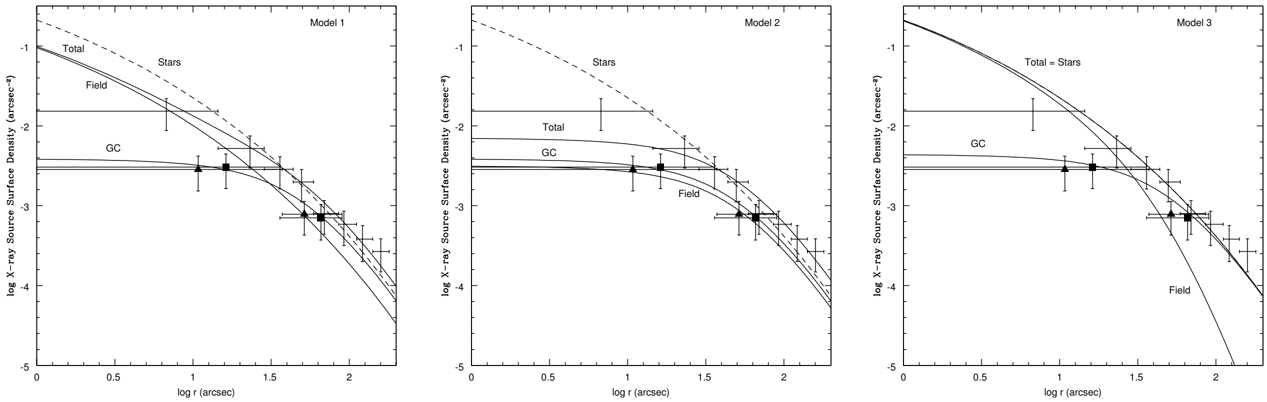

Figure 3. Predicted surface densities distributions of X-ray sources in elliptical galaxies (Sarazin, 2006). The solid curves labeled GC, Field, and Total show the surface densities of LMXBs in GCs, in the field, and in total, respectively. The dashed curve shows the total X-ray distribution if the X-ray sources followed the distribution of field stars. The data points are from NGC 4365. The error bars with triangles are the field LMXBs, those with squares are the GC sources, and the plain error bars are the total source distribution. Model 1 assumes that no GC LMXBs are lost from GCs either due to individual ejection or GC destruction. In Model 2, all LMXBs are made in GCs, no GCs are destroyed, but all of the field LMXBs were individually ejected from GCs. In Model 3, all LMXBs are made in GCs, and all field LMXBs result from the tidal disruption of GCs.

flares is similar to superbursts, the luminosity is higher than expected for a neutron star (NS). Furthermore, the recurrence timescale of flares is probably on the order of $\sim$10 hours, much shorter than the approximately year-long timescale of Galactic superbursts. Recently, Maccarone (2003) proposed that these sources are slightly eccentric binaries in GCs which flare at periastron.

An even more perplexing source (CXOU J124839.0$-$054750) with recurrent $\sim 70\,\mathrm{s}$ flares was also found, with a flaring luminosity of $L_X \gtrsim 5 \times 10^{39}$ erg s^{-1} (Fig. 4). This source is not coincident with a GC. The flare behavior of CXOU J124839.0$-$054750 does not have a clear analog in our own Galaxy. Its peak luminosity is clearly super-Eddington for an NS; the flare is at least 8 times the Eddington luminosity of a helium burning NS. This shows it is not a Type-I X-ray burst. Since NGC 4697 is an elliptical galaxy, it is unlikely that this source is an HMXB like LMC X$-$4 or V4641 Sgr. The flare timescale is similar to rapid transients seen in the BH-XRBs, GRS1915+105 and V4641 Sgr.

One possibility is that CXOU J124839.0$-$054750 (and possibly the other two flaring sources as well) are related to Galactic microquasar sources. Microquasars are XRBs with accreting BHs which produce relativistic jets (e.g., Mirabel & Rodríguez, 1999). In most of the known Galactic examples, we are observing the sources at a large angle from the jet axis (see, however, Orosz et al., 2001). The very high luminosity of CXOU J124839.0$-$054750 might be explained if we are seeing this source along the jet axis. In analogy to their AGN counterparts, microquasars observed along the jet axis are referred to as microblazars (Mirabel & Rodríguez, 1999). Blazars are known to undergo relatively short timescale outbursts; the same phenomena, scaled to microblazars, might account for the X-ray flares in CXOU J124839.0$-$054750.

ACKNOWLEDGMENTS

This work was supported by the National Aeronautics and Space Administration through Chandra Award Numbers GO3-4099X, AR4-5008X, GO4-5093X, GO5-6081X, and GO5-6086X, and Hubble Space Telescope Award Number HST-GO-10003.01-A.

REFERENCES

Angelini, L., Loewenstein, M., & Mushotzky, R. F. 2001, ApJ, 557, L35

Côté, P., et al. 2004, ApJS, 153, 223

Grindlay, J. E. 1984, AdSpR, 3, 19

Harris, W. E. 1991, ARA&A, 29, 543

Hertz, P., & Grindlay, J. E. 1983, ApJ, 275, 105

Irwin, J. A. 2005, ApJ, 631, in press

Jordán, A., Côté, P., Ferrarese, L., Blakeslee, J. P., Mei, S., Merritt, D., Milosavljević, M., Peng, E. W., Tonry, J. L., & West, M. J. 2004, ApJ, 613, 279

Juett, A. M. 2005, ApJ, 621, L25

Kundu, A., Maccarone, T. J., & Zepf, S. E. 2002, ApJ, 574, L5

Maccarone, T. J. 2005, MNRAS, in press

Maccarone, T. J., Kundu, A., & Zepf, S. E. 2003, ApJ, 586, 814

Mirabel, I. F., & Rodríguez, L. F. 1999, ARAA, 37, 409

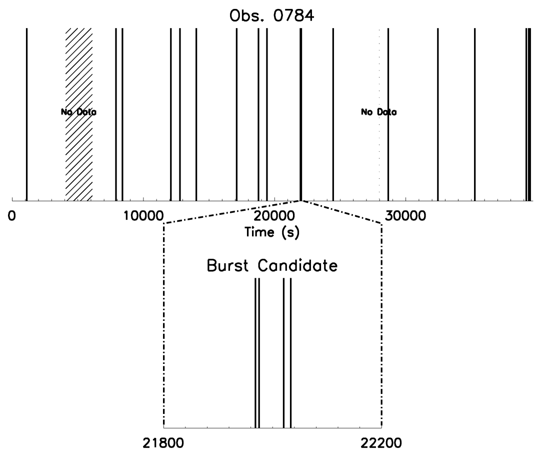

Figure 4. Impulse diagram indicating the time of arrival of photons from the flaring source CXOU J124839.0-054750 in NGC 4697. This source has a ∼70 sec flare.

Orosz, J. A., et al. 2001, ApJ, 555, 489

Sarazin, C. L. 2006, ApJ, submitted

Sarazin, C. L., Irwin, J. A., & Bregman, J. N. 2000, ApJ, 544, L101

—. 2001, ApJ, 556, 533

Sarazin, C. L., Kundu, A., Irwin, J. A., Sivakoff, G. R., Blanton, E. L., & Randall, S. W. 2003, ApJ, 595, 743

Sivakoff, G. R., Sarazin, C. L., & Irwin, J. A. 2003, ApJ, 599, 218

Sivakoff, G. R., Sarazin, C. L., & Jordán, A. 2005, ApJ, 624, L17

Sivakoff, G. R., et al. 2006, ApJ, submitted

White, R. E., Sarazin, C. L., & Kulkarni, S. R. 2002, ApJ, 571, L23

THE MULTI-PHASE GASEOUS HALOS OF LATE-TYPE SPIRALS

R. Tüllmann[1], W. Pietsch[2], J. Rossa[3], D. Breitschwerdt[4], and R.-J. Dettmar[1]

[1]Astronomisches Institut, Ruhr-Universität Bochum, 44780 Bochum, Germany
[2]Max-Planck Institut für extraterrestrische Physik, 85748 Garching, Germany
[3]Space Telescope Science Institute, Baltimore, MD 21218, U.S.A.
[4]Institut für Astronomie, Universität Wien, 1180 Wien, Austria

ABSTRACT

First results from an X-ray mini-survey carried out with XMM-Newton are presented in order to investigate the diffuse Hot Ionized Medium in the halos of nine star-forming edge-on galaxies. Diffuse X-ray halos were detected in eight of our targets, covering a wide range of star formation rates from quiescent to starburst cases. EPIC X-ray contour maps overlaid onto Hα imaging data revealed that the presence of X-ray halos is correlated with Diffuse Ionized Gas. Moreover, these halos are associated with non-thermal cosmic ray halos, as evidenced by radio continuum observations. UV-data obtained with the OM-telescope reveal that Diffuse Ionized Gas is well associated with UV emission originating in the disk. We found very strong indications that spatially correlated multi-phase gaseous halos are associated with star forming processes in the disk. By including multi-wavelength data of other star forming spirals, we obtained a sample of 23 galaxies which allow us to test key parameters which trigger the formation of multi-phase halos. We found that diffuse soft (0.3-2.0 keV) X-ray luminosities correlate well with Hα, B-band, FIR, UV, and radio continuum luminosities, with SFRs and with the energy input rate by SNe. X-ray luminosities are found to not correlate with HI mass and baryonic mass. All this implies that gaseous halos are indeed created by star forming processes. Moreover, there seems to exist a critical SFR threshold above which these halos form.

Key words: Galaxy halos; extended X-ray emission; ISM; starburst and quiescent galaxies.

1. INTRODUCTION

What causes the formation of multi-phase gaseous halos in star forming late-type spiral galaxies? It is commonly believed that supernova (SN) explosions, galactic winds or stellar winds from young and hot stars are the main triggering mechanisms. Theoretical models predict an intense transport of gas and momentum between the disk plane and the halo (so called disk-halo interaction, DHI). The combined power of SNe explosions in star forming regions produce overpressured flows of hot gas which is driven off the disk into the halo. This process gives rise to phenomena known as galactic fountains (de Avillez, 2000) or chimneys (Norman & Ikeuchi, 1989).

The results of the violent energy input are visible in different wavelength regions, such as in the radio, in the optical or in X-rays. Superbubbles and filaments as well as extended worm structures have been observed in the Milky Way (e.g., Heiles, 1984; Koo et al., 1992; Reynolds et al., 2001) as well as in several other galaxies (e.g., Devine & Bally, 1999; Tüllmann et al., 2000, 2003).

Independent evidence of an interstellar DHI comes from the presence of a thick extraplanar layer (1.5 – 10 kpc) of ionized hydrogen, called "Diffuse Ionized Gas" (DIG) which is most likely also blown out into the halo by correlated SNe (see Dettmar (2004) for a recent review). During the last five years significant progress was achieved in this field, e.g., by carrying out a comprehensive Hα survey of 74 edge-on spirals, by estimating the ejected DIG mass, and deriving an empirical set of parameters which indicates the presence of prominent DIG halos (Rossa & Dettmar, 2000, 2003a,b). It turned out that the star formation rate (SFR) per unit area determines whether or not starburst and normal star forming galaxies possess DIG halos. As the SFR is related to the energy input rate by SNe, this directly supports star formation induced galaxy halos.

Moreover, it was shown that filamentary DIG structures (traced by Hα), radio continuum emission, and magnetic field vectors are well aligned in the halos of some star forming spirals (e.g., Dahlem et al., 1997; Tüllmann et al., 2000). This was verified also for at least 13 of the survey galaxies for which radio data are available (Rossa & Dettmar, 2003a,b). Beside this purely morphological correlation, additional studies also found correlations between FIR, B, and X-ray luminosities (e.g., Condon,

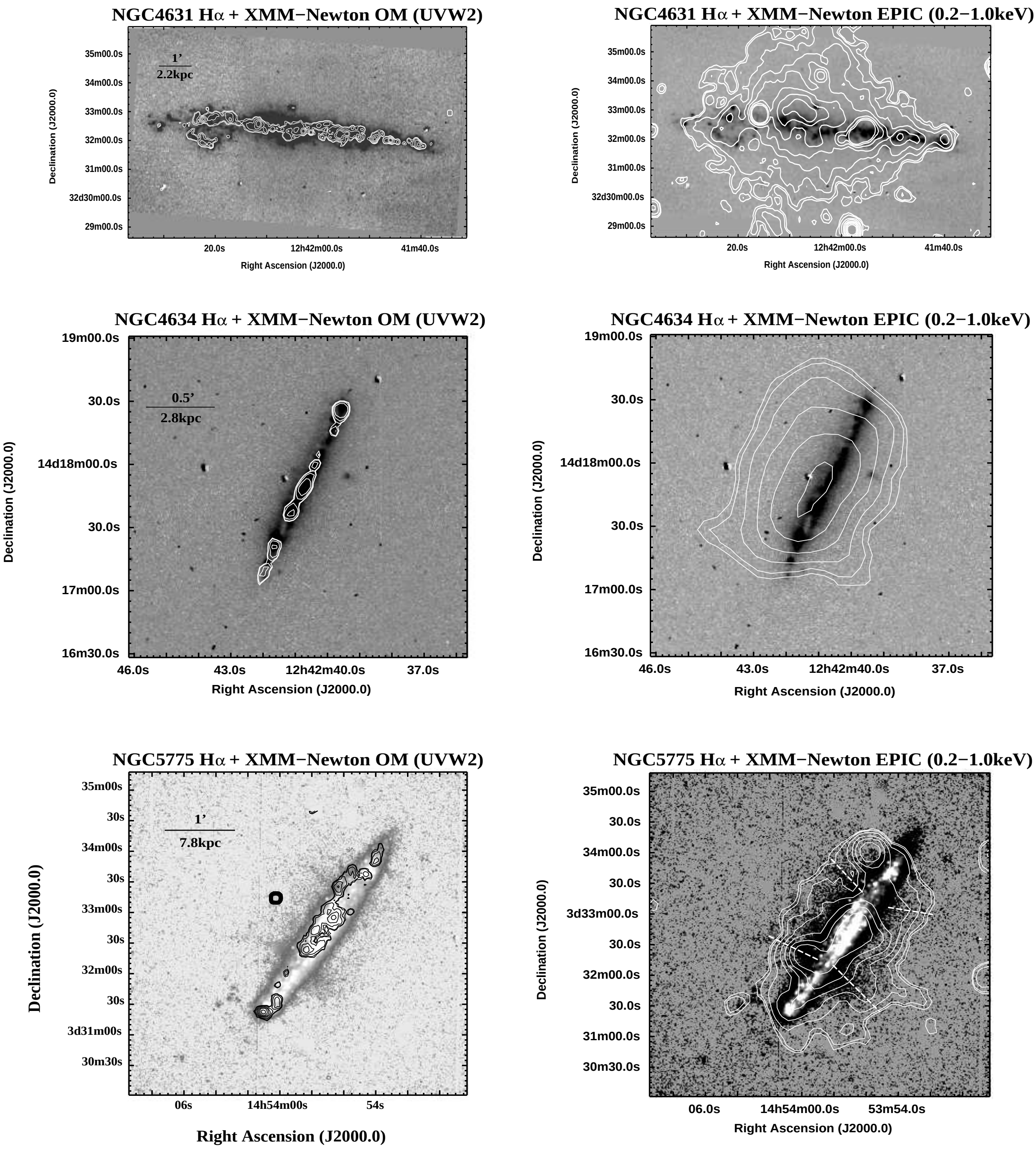

Figure 1. The UV contours maps of NGC 4631, NGC 4634, and NGC 5775 (left panels) obtained with the Optical Monitor (UVW2 filter) and overlaid onto corresponding Hα images nicely confirm the tight relation between DIG and UV continuum emission. The appropriate EPIC X-ray images (right panels) were created from merged pn and MOS eventlists in the soft energy-band (0.2 - 1.0 keV) and give evidence to the presence of soft extended X-ray halos.

1992; Read & Ponman, 2001). For starburst galaxies, a multi-phase correlation could be established making extensive use of the Chandra satellite (Strickland et al., 2002, 2004a,b) and XMM-Newton (Stevens et al., 2003; Ehle, 2005). For normal star forming spirals, however, it was dubious, until we started to investigate the above relation with XMM-Newton for lower energy input rates.

What causes the coexistence of multi-phase gaseous halos? This can be understood by considering the origin of the radiation observed in certain wave bands. The FIR emission is most likely produced by young dust enshrouded stars whose UV flux is absorbed by dust grains and re-emitted at infrared wavelengths. Synchrotron emission originates in the radio continuum and traces

Table 1. Derived plasma parameters

Galaxy	D	$\|z\|$	$kT_{\rm soft}$	$kT_{\rm hard}$	$L_{\rm X,soft}$	$n_{\rm e,soft}$	$n_{\rm e,hard}$	$<M_{\rm gas}>$
	[Mpc]	[kpc]	[keV]		$[10^{40}$ erg s$^{-1}]$	$\times 10^{-3}/\sqrt{f}$ [cm^{-3}]		$\times 10^{8} f$ [M$_\odot$]
	(1)	(2)	(3)	(4)	(5)	(6)	(7)	(8)
NGC 4631	7.5	10.6	0.062 ± 0.037	0.196 ± 0.074	0.02	0.5 ± 0.2	0.6 ± 0.3	$0.01\pm\leq0.01$
		9.00	0.069 ± 0.032	0.245 ± 0.041	0.03	0.7 ± 0.2	0.8 ± 0.3	$0.01\pm\leq0.01$
		7.40	0.096 ± 0.038	0.211 ± 0.075	0.07	0.9 ± 0.1	1.1 ± 0.2	0.07 ± 0.02
		5.80	0.103 ± 0.019	0.274 ± 0.035	0.12	1.3 ± 0.2	1.5 ± 0.3	0.10 ± 0.03
		4.20	0.173 ± 0.031	0.284 ± 0.057	0.15	1.5 ± 0.2	1.8 ± 0.3	0.11 ± 0.04
		0.0	0.234 ± 0.012	0.867 ± 0.019	0.25	0.7 ± 0.1	0.9 ± 0.2	0.44 ± 0.10
		2.90	0.173 ± 0.029	0.372 ± 0.093	0.08	1.0 ± 0.1	1.2 ± 0.2	0.09 ± 0.03
		4.50	0.151 ± 0.037	0.266 ± 0.124	0.04	0.8 ± 0.1	0.9 ± 0.2	0.06 ± 0.02
		6.10	0.122 ± 0.028	0.271 ± 0.181	0.02	0.6 ± 0.1	0.7 ± 0.1	0.03 ± 0.01
NGC 4634	19.1	3.30	0.093 ± 0.012	0.191 ± 0.089	0.03	1.3 ± 0.2	1.5 ± 0.4	$0.02\pm\leq0.01$
		1.90	0.108 ± 0.032	0.267 ± 0.113	0.05	1.8 ± 0.3	2.0 ± 0.6	0.03 ± 0.01
		0.0	0.227 ± 0.035	0.848 ± 0.207	0.03	1.3 ± 0.2	1.8 ± 0.3	$0.03\pm\leq0.01$
		2.00	0.113 ± 0.027	0.305 ± 0.130	0.04	1.4 ± 0.2	1.6 ± 0.5	0.03 ± 0.02
NGC 5775	26.7	6.90	0.067 ± 0.031	0.251 ± 0.101	0.16	0.6 ± 0.2	0.7 ± 0.3	0.28 ± 0.19
		4.20	0.085 ± 0.022	0.280 ± 0.053	0.36	0.9 ± 0.2	1.0 ± 0.3	0.41 ± 0.22
		0.0	0.263 ± 0.049	0.940 ± 0.191	0.37	2.6 ± 0.1	3.6 ± 0.2	1.65 ± 0.22
		4.40	0.125 ± 0.033	0.358 ± 0.136	0.42	1.0 ± 0.2	1.1 ± 0.3	0.45 ± 0.18
		7.05	0.099 ± 0.029	0.350 ± 0.168	0.24	0.7 ± 0.2	0.8 ± 0.3	0.34 ± 0.20

Notes: Col (1): Distance to the target in Mpc. Col. (2): Height above/below the disk plane where the spectrum was extracted. Cols. (3) and (4): Temperatures for the soft and hard component as derived from spectral fitting (see Tüllmann et al. 2005 for details). Col. (5): Diffuse soft X-ray luminosities (0.3 – 2.0 keV), based on distances listed in Col. (1). Cols. (6) to (7): Electron densities for the soft and hard component. Col. (8): Averaged gas masses within the extracted volume, based on averaged electron densities calculated from Cols. (6) and (7).

high energy cosmic ray (CR) electrons produced by SNe or Supernova remnants (SNRs). B-band and UV luminosities are indicators of the continuum radiation of hot and young stars, whereas Hα is a good tracer of gas photoionized by OB-stars and of the above mentioned DHI. X-ray emission, finally, is typical for X-ray binaries, SNRs, superwinds, and diffuse hot plasmas generated by these objects.

2. THE SAMPLE

Our initial XMM-Newton sample consists of nine star forming late-type spiral galaxies which cover the starburst as well as the quiescent case. All targets are nearby to gain good spatial resolution and seen nearly edge-on to allow a clear discrimination between the soft emission originating in the disk and the halo. The sample was chosen from the aforementioned Hα survey of edge-on galaxies (Rossa & Dettmar, 2003a) by selecting galaxies with the highest $L_{\rm FIR}/D_{25}^2$ values and exceeding a IRAS S_{60}/S_{100} ratio of 0.3. These parameters are considered to be a good discriminator for starburst and normal star forming spiral galaxies (e.g., Lehnert & Heckman, 1996; Rossa & Dettmar, 2003a; Strickland et al., 2004a). It should be stressed that our sample is neither complete nor free from selection effects.

3. RESULTS

In the following we concentrate on presenting representative results for two starburst galaxies (NGC 4631 and NGC 5775) and one actively star forming spiral galaxy (NGC 4634). We used merged EPIC pn and MOS contour maps (0.2 –1.0 keV) overlaid onto Hα images and of Optical Monitor (OM) UV imagery carried out with the UVW2 filter in order to systematically investigate the spatial correlation of multi-phase gaseous galaxy halos. A detailed description of our multi wavelength approach and relevant results from our XMM-Newton observations are given in the first of a series of papers (Tüllmann et al., 2005).

3.1. XMM-Newton EPIC and OM imaging

Fig. 1 nicely confirms that the extraplanar DIG emission is well associated with sites where the UV-flux in the disk is enhanced. In case of NGC 5775, one likely can interpret the extraplanar DIG as the limb brightened walls of giant outflow cones and thus make the connection with the central UV sources which seem to be the main drivers of the outflow. Hence, in all three cases a clear correlation between DIG and UV continuum originating in the disk plane exists. As DIG also correlates with diffuse soft X-ray emitting gas in the halo (see right-hand panels), it is self-evident to also consider a correlation between the hot ionized gas and stellar feedback processes (traced by UV radiation).

Beside a DIG and a soft X-ray halo, all three targets also show an extended radio continuum halo at 1.4 GHz, indicating the presence of CRs at extraplanar distances. Hence, we conclude that multi-phase gaseous halos are indeed created by star forming activity rather than by accretion from the IGM/halo as suggested by Benson et al. (2000) or Toft et al. (2002).

What, however, is the critical energy threshold above which multi-phase halos start to form? We address this question in subsection 3.3.

3.2. XMM-Newton EPIC pn spectroscopy

Essential parameters of the halo gas, such as electron densities, gas temperatures, and gas masses, were determined by means of EPIC pn spectroscopy carried out at several offset positions above the disk (see Table 1). In order to determine these quantities we fitted all spectra with a simple 3-component model, consisting of a photoelectric absorber to account for the foreground absorption and two thermal Raymond-Smith (RS) plasma models. Both RS components (a hard and a soft one) are fixed to cosmic metal abundances. The individual $N_{\rm H}$ values have been taken from Dickey & Lockman (1990) and are not allowed to vary during the χ^2-minimization process.

Spectra are fitted only for energy channels with a significant number of counts per time and energy interval. For the halo this is the range between 0.3 – 2 keV, which nicely demonstrates that diffuse X-ray halos are indeed very soft. From Fig. 2 it is directly evident that there is a temperature and density gradient in the halo. Gas temperatures and electron densities decrease with increasing height above the disk. As a consequence of declining densities, the hot ionized gas mass in every extracted region decreases, too. The trends shown in Fig. 2 are consistent with starburst-driven Galactic wind models (Breitschwerdt, 2003).

3.3. Multi-frequency correlations

Provided our hypothesis of star formation induced multi-phase galaxy halos is correct, there also should exist (in addition to phenomenological analogies) strong correlations between different star formation tracers. Such tracers could be star formation rates (SFRs), SN energy input rates ($\dot{E}_{\rm A}^{\rm tot}$) and $L_{\rm FIR}/D_{25}^2$ ratios, but also multi-frequency luminosities of the integrated radio continuum, FIR, Hα, B-band, UV, and X-ray emission.

In order to carry out a statistical correlation analysis of these quantities, we increased our initial sample by

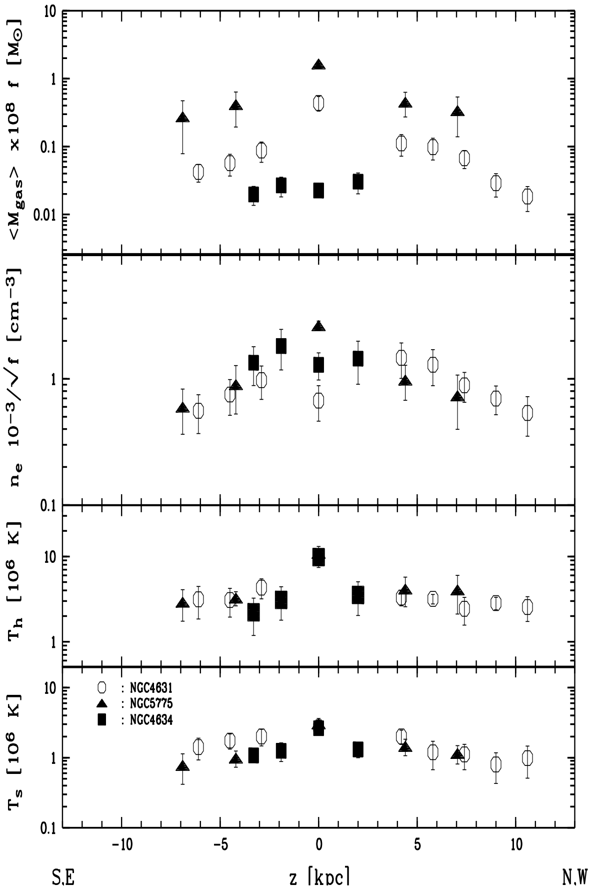

Figure 2. Derived gas parameters plotted as a function of z. Soft and hard temperatures have been derived by fitting the emission spectra with a photoelectric absorber and two RS plasma models of different temperatures. Electron densities and gas masses within the ionized volume are averages of the soft and the hard component and are calculated from soft X-ray luminosities.

searching the literature for appropriate targets. The following sample selection criteria were applied: all galaxies had to be late-type spirals (Sc-Sd), relatively nearby (< 50 Mpc), and seen nearly edge-on ($i > 70°$). Moreover, they had to be previously investigated in the wave bands listed above. No constraints were imposed on the $S60/S100$ and $L_{\rm FIR}/D_{25}^2$ ratios to reach the largest possible coverage of the parameter space. Our extended sample consists now of 23 galaxies which allow us to perform least-squares fitting (assuming $Y = mX + b$) and Spearman rank-order correlation analysis, to test the significance of the correlation between the investigated pairs of parameters. Results are shown in Fig. 3.

We find very strong linear correlations between star formation indicators and multi-frequency luminosities. In addition to the well established $L_{\rm FIR}/L_{1.4{\rm GHz}}$ relation, highly significant linear dependencies between soft X-ray luminosities (0.3 – 2.0 keV) and integrated FIR, radio continuum (1.4 GHz), Hα, B-band, and UV luminosities can be established. Moreover, soft X-ray lumi-

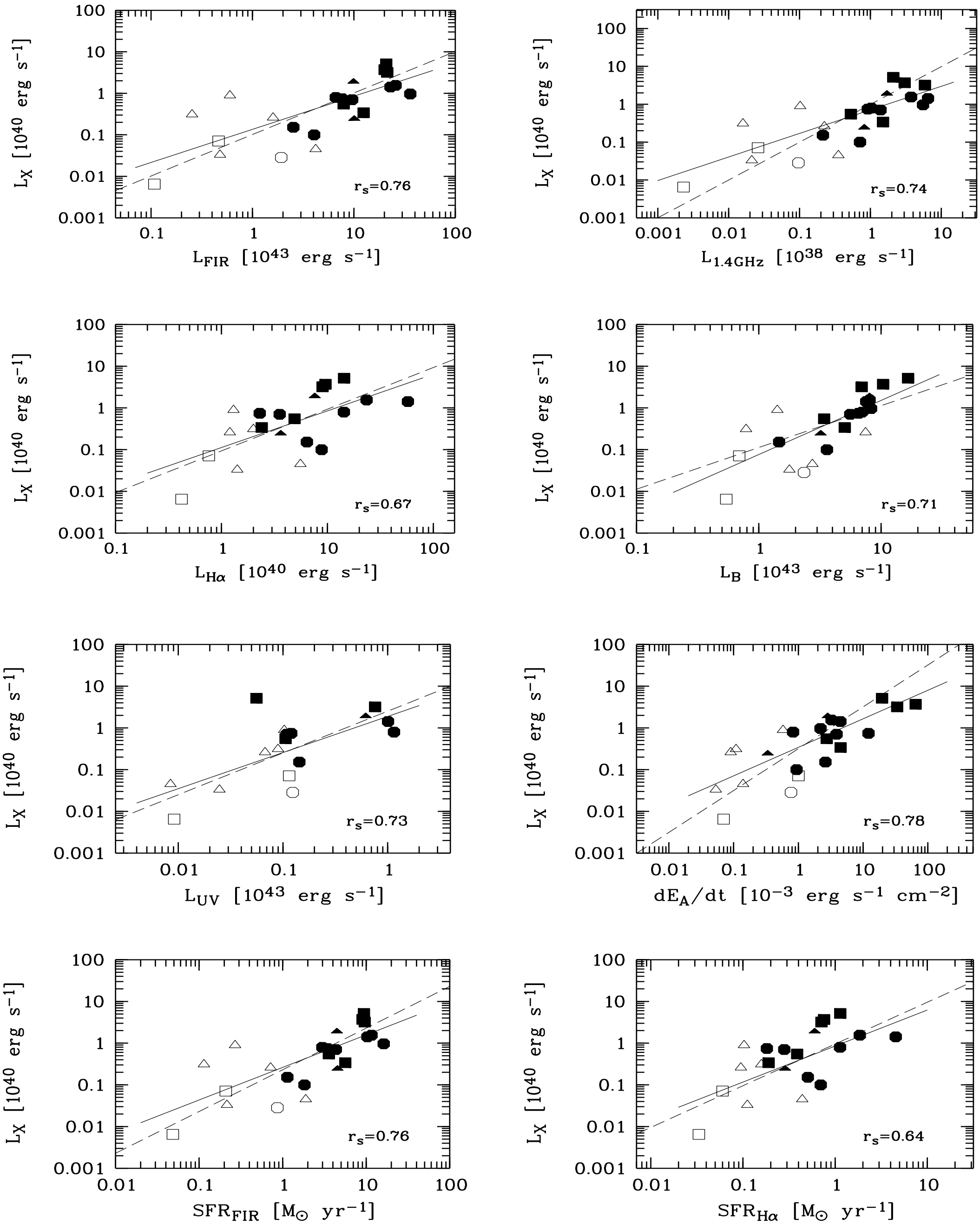

Figure 3. The strong linear correlations between X-ray luminosities, FIR, 1.4 GHz, Hα, broadband B, and UV luminosities, SFRs, and energy input rates $\dot{E}_{\rm A}$, indicate that star forming processes in the disk are the likely driver of multi-phase gaseous halos. Filled (open) symbols represent galaxies with(out) multi-phase halo detections. Solid lines represent the best linear fits to the data whereas the dashed line indicates a relation with unity slope (see Tüllmann et al. (2005b) for details and the full set of correlations). r_s denotes the Spearman rank-order correlation coefficient.

nosities correlate well with star formation rates and the energy input rate by SNe into the ISM. Only weak correlations are found between the dust mass of a galaxy and the corresponding soft X-ray luminosity. X-ray luminosities are found to not correlate with baryonic and H I gas masses. These statistical results also support that multi-phase gaseous galaxy halos in late-type spiral galaxies are created by outflowing gas produced in star forming related events in the disk plane.

However, in order to achieve a more comprehensive picture on the evolution of galaxy halos in different wave bands, we need to answer the question of the threshold SFR (or equivalently the SN energy input rate $\dot{E}_A$) required to create multi-phase gaseous halos. From Fig. 3 we cannot tell precisely, as the lower energy end of our correlations is statistically not well covered. It appears, however, that for multi-phase halos to evolve a critical threshold needs to be exceeded (e.g., a $SFR_{\rm FIR} \geq 1.0\,{\rm M}_{\odot}$/yr). Interestingly, DIG seems to coexist with other gas components if a Hα star formation rate per unit area of $(3.2 \pm 0.5) \times 10^{40}$ erg s^{-1} kpc^{-2} is exceeded (Rossa & Dettmar, 2003b).

In this context it is important to point out that the quantification of the threshold and the progress of understanding the physics of gaseous galaxy halos now depends on galaxies with no or only little halo emission than on "well understood" targets.

4. SUMMARY AND CONCLUSIONS

With a sample of 23 normal star forming galaxies and by adding additional wave bands (Hα and UV), we found remarkably strong linear correlations between 1.4GHz radio continuum, FIR, Hα, B-band, UV, and X-ray luminosities. Strong correlations also exist if X-ray luminosities are plotted against SFRs, $L_{\rm FIR}/D_{25}^2$, or the energy input rate by SNe per unit area, expressed by $\dot{E}_{\rm A}$ (cf. Fig. 3). X-ray luminosities neither correlate with the H I nor with the baryonic mass of a galaxy. Our results clearly imply that multi-phase halos are the consequence of stellar feedback processes in the disk plane. They conflict with the concept of halos being due to infalling gas from the IGM.

REFERENCES

Benson, A. J., Bower, R. G., Frenk, C. S., & White, S. D. M. 2000, MNRAS, 314, 557

Breitschwerdt, D. 2003, RevMexAA, 15, 311

Condon, J. J. 1992, ARA&A, 30, 575

Dahlem, M., Petr, M., Lehnert, M. D., Heckman, T. M., & Ehle, M. 1997, A&A, 320, 731

de Avillez, M. A., 2000, MNRAS, 315, 479

Dettmar, R.–J. 2004, Ap&SS, 289, 349

Devine, D., & Bally, J. 1999, ApJ, 510 197

Dickey, J. M., & Lockman, F. J. 1990, ARA&A, 28, 215

Ehle, M. 2005, in: "Extra-planar Gas", ed. R. Braun, ASP Conf. Series, 331, 337

Heiles, C. 1984, ApJS, 55, 585

Koo, B.-C., Heiles, C., & Reach, W. T. 1992, ApJ, 390, 108

Lehnert, M. D., & Heckman, T. M. 1996, ApJ, 472, 546

Norman, C. A., & Ikeuchi, S. 1989, ApJ, 345, 372

Read, A. M., & Ponman, T. J. 2001, MNRAS 328, 127

Reynolds, R. J., Sterling, N. C., & Haffner, L. M. 2001, ApJ, 558, L101

Rossa, J., & Dettmar, R.–J. 2000, A&A, 359, 433

Rossa, J., & Dettmar, R.–J. 2003a, A&A, 406, 493

Rossa, J., & Dettmar, R.–J. 2003b, A&A, 406, 505

Stevens, I. R., Read, A. M., & Bravo-Guerrero, J. 2003, MNRAS, 343, L47

Strickland, D. K., Heckman, T. M., Weaver, K. A., Hoopes, C. G., & Dahlem, M. 2002, ApJ, 568, 689

Strickland, D. K., Heckman, T. M., Colbert, E. J. M., Hoopes, C. G., & Weaver, K. A. 2004a, ApJS, 151, 193

Strickland, D. K., Heckman, T. M., Colbert, E. J. M., Hoopes, C. G., & Weaver, K. A. 2004b, ApJ, 606, 829

Toft, S., Rasmussen, J., Sommer-Larsen, J., & Pedersen, K. 2002, MNRAS, 335, 799

Tüllmann, R., Dettmar, R.–J., Soida, M., Urbanik, M., & Rossa, J. 2000, A&A, 364, L36

Tüllmann, R., Rosa, M. R., Elwert, T., Bomans, D. J., Ferguson, A. M. N., & Dettmar, R.–J. 2003, A&A, 412, 69

Tüllmann, R., Pietsch, W., Rossa, J., Breitschwerdt, D., & Dettmar, R.-J. 2005a, accepted for publication in A&A, astro-ph/0510079

Tüllmann, R., Pietsch, W., Rossa, J., Breitschwerdt, D., & Dettmar, R.-J. 2005b, in prep.

THE HOT ISM OF THE ANTENNAE OBSERVED WITH CHANDRA: DISCOVERY OF CHEMICAL ENRICHMENT

A. Baldi[1], J. Raymond[1], G. Fabbiano[1], A. Zezas[1], A. Rots[1], F. Schweizer[2], A. King[3], and T. Ponman[4]

[1]Harvard-Smithsonian Center for Astrophysics, 60 Garden Street, Cambridge, MA 02138, USA
[2]Carnegie Observatories, 813 Santa Barbara Street, Pasadena, CA 91101, USA
[3]Theoretical Astrophysics Group, University of Leicester, Leicester LE1 7RH, UK
[4]School of Physics & Astronomy, University of Birmingham, Birmingham B15 2TT, UK

ABSTRACT

An analysis of the properties of the hot ISM in the merging pair of galaxies known as The Antennae (NGC 4038/39), performed using the deep 411 ks Chandra ACIS-S data set is presented. These deep observations and Chandra's high angular resolution allow us to investigate the properties of the hot ISM with unprecedented spatial and spectral resolution. Through a spatially resolved spectral analysis, we find a variety of temperatures (0.3–0.7 keV), densities (3×10^{-2}–1.5×10^{-1} cm^{-3}), and N_H (up to 2×10^{21} cm^{-2}). Metal abundances for Ne, Mg, Si, and Fe vary dramatically throughout the ISM from sub-solar values ($\sim$0.2) up to $\sim$20 times the solar abundance. Comparison of the abundances with the average stellar yields predicted by theoretical models of SN explosions points to Type II SNe as the main contributors of metals to the hot ISM. No evidence of correlation between radiooptical star formation indicators and the metal abundances is found. Although uncertainties in the average density cannot exclude that mixing may have played some important role, the time required to produce the observed metal masses ($\sim$3 Myr) suggests that the correlations are unlikely to be destroyed by the presence of efficient mixing. More likely a significant fraction of Type II SNe ejecta may be in a cool phase, in grains, or escaping in the wind.

Key words: galaxies: peculiar; galaxies: individual(NGC4038/39); galaxies: interactions; X-rays: galaxies; X-rays: ISM.

1. INTRODUCTION

Massive stars deeply influence the baryonic component of the Universe. Their ionizing radiation and the supernovae (SNe) return kinetic energy and metal-enriched gas to the interstellar medium (ISM) from which the stars formed (a process called "feedback"). Feedback exercises an influence not only on the gas-phase conditions in the immediate environment of the clusters hosting massive stars (e.g. Pudritz & Fiege 2000), but also on the phase structure and energetics of the ISM on galactic scales (e.g. McKee & Ostriker 1977) and on the thermodynamics and enrichment of the inter-galactic medium (IGM) on scales of several Mpc (e.g. Heckman 1999).

The vast range of spatial scales involved is only one of the difficulties encountered in attempting to study feedback. Even restricting the discussion to purely mechanical feedback from SNe and stellar winds (SN feedback), another difficulty is the broad range of complicated gas-phase physics, which includes (magneto)hydrodynamic effects such as shocks and turbulence, thermal conduction, and non-ionization equilibrium (NEI) emission processes.

Several attempts at putting quantitative constraints on the metal enrichment caused by SN feedback in starburst galaxies have been made in the recent past. From a small sample of edge-on starburst galaxies observed by ROSAT and ASCA, Weaver, Heckman, & Dahlem (2000) obtained abundances completely consistent with solar values and no evidence of super-solar ratios of the α elements with respect to Fe, as required by type-II SN feedback (e.g., Gibson, Lowenstein, & Mushotzky 1997). Moreover, they concluded that the technique of measuring abundances through X-ray spectral fitting is highly uncertain because of ambiguities in the fits (e.g., a degeneracy between the temperature and metallicity), and strongly dependent on the model choice (see also Dahlem et al. 2000; Strickland et al. 2002, 2004). The advent of Chandra, with its sub-arcsecond angular resolution, allowed a better subtraction of the point sources from the galactic diffuse emission, simplifying the spectral fitting. However, the low resolution spectra of the Chandra ACIS CCDs (Weisskopf et al. 1996) did not allow a dramatic improvement in the accuracy of abundance measures. Notwithstanding the limits of ACIS spectral resolution, Martin, Kobulnicky, & Heckman (2002), observing the dwarf starburst galaxy NGC 1569, claimed to obtain ratios of α elements to Fe 2 – 4 times higher than the solar value.

While X-ray observations of the halos of nearby edge-on disk galaxies may provide the best single probe of the action of mechanical feedback on galactic scales, observations of the disks of *face-on* nearby spiral galaxies may provide useful insights into the physics and enrichment of the hot gas. Such observations allow a spatially resolved analysis of the hot ISM in the disk that is much less affected by internal absorption than in the case of edge-on galaxies.

The Antennae are the nearest pair of colliding, relatively face-on spiral galaxies involved in a major merger (D = 19 Mpc for $H_0 = 75$ km s^{-1} Mpc^{-1}). Hence, this system not only allows a study of the properties of the ISM relatively unaffected by internal absorption, but it also provides a unique opportunity to get the most detailed insight possible into the consequences of a galaxy merger, such as induced star formation and its effect on the ISM.

The presence of an abundant hot ISM in The Antennae was originally suggested by the first *Einstein* observations of this system (Fabbiano & Trinchieri 1983), and has since been confirmed by observations with several major X-ray telescopes (*ROSAT*: Read, Ponman, & Wolstencroft 1995, Fabbiano, Schweizer, & Mackie 1997; and *ASCA*: Sansom et al. 1996). The first *Chandra* ACIS observation of The Antennae in 1999 gave us for the first time a detailed look at this hot ISM, revealing a complex, diffuse, and soft emission component responsible for about half of the detected X-ray photons from the two merging galaxies (Fabbiano, Zezas & Murray 2001; Fabbiano et al. 2003, hereafter F03). The spatial resolution of *Chandra* is at least 10 times superior to that of any previous X-ray observatory, which allows us to resolve the emission on physical scales of $\sim$75 pc (for D=19 Mpc) and to detect and subtract individual point-like sources (most likely X-ray binaries; see Zezas et al. 2002).

While the first *Chandra* data set demonstrated the richness of the ISM in The Antennae, the number of detected photons was insufficient to study its detailed small-scale morphology and spectral properties. A deep monitoring observing campaign of The Antennae with *Chandra* ACIS has produced a detailed and rich data set. This data-set revealed a complex diffuse emission, with signatures of strong line emission coming from some of the hot ISM regions, pointing to high α element abundances (Fabbiano et al. 2004, Baldi et al. 2005a,b). Here we resume the physical properties of the hot gas and we investigate its enrichment by SN explosions.

2. IMAGING AND SPECTRAL ANALYSIS

NGC 4038/39 was observed with *Chandra* ACIS-S seven times during the period between December 1999 and November 2002, for a total of $\sim$411 ks. The data products were analyzed with the CXC CIAO v3.0.1 software and XSPEC package. Full details about the data processing and reduction are given in Baldi et al. (2005a, hereafter Paper I).

Paper I presents a mapped-color image of the diffuse emission in The Antennae, representing contributions from three different energy bands: 0.3–0.65 keV, 0.65–1.5 keV and 1.5–6 keV. Before combining the images from the three bands, all point sources were subtracted and an adaptive gaussian kernel was applied to each of the three images. A similar procedure was applied to generate a line-strength map for the emission lines from O+Fe+Ne (0.6–1.16 keV), Mg (1.27–1.38 keV), and Si (1.75–1.95 keV) in different regions of the hot ISM.

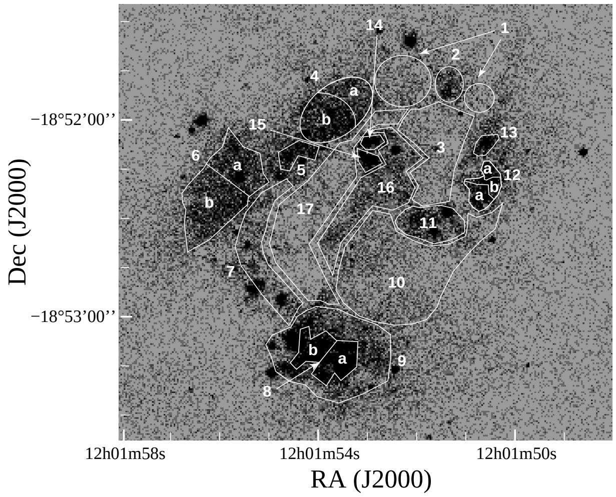

Figure 1. 0.3–6 keV Chandra ACIS-S image of The Antennae. The 21 regions used for the spectral analysis of the hot ISM are marked in white. A high-resolution color version of this figure can be found in Paper I.

Both the mapped-color image of the diffuse emission and the line-strength map (presented in Figure 4 and 6 of Paper I) guided us in selecting 21 spectrally similar regions for a proper spectral analysis. These regions are shown in Figure 1. The method used for the spectral extraction and analysis is fully described in Paper I.

Almost all regions could be fitted with a single thermal component. Only Region 4b required two thermal components with different kT; in this region, we could not constrain the low kT value (although we found a minimum in the χ^2 statistics at $kT = 0.20$ keV), and we could put only a lower limit ($kT > 0.54$ keV) to the higher temperature component. Almost all the single-temperature regions required a temperature of $kT \sim 0.6$ keV to fit the data, except for regions 5, 8b, and 14 ($kT \sim 0.3$ keV). Considering all the regions analyzed, the temperatures (both in the single- and two-temperature cases) range from $\sim$ 0.2 to $\sim$ 0.8 keV (including the errors). Our analysis yielded metal abundances that have acceptable constraints in the majority of regions, and led to the most important, and somewhat unexpected, result of our spectral analysis: the abundances of Silicon and Magnesium cover a wide range of values ranging from the very low values found in regions 2, 6a, 12a, and 12b ($Z \sim 0.2Z_{\odot}$) to the very high values observed in Region 5 ($Z \sim$10–20 $Z_{\odot}$). The intrinsic absorption throughout the hot ISM is generally low, with $N_H \sim 10^{20}$ cm^{-2} typical and often consistent with zero. The exceptions are the southern nucleus (regions 8a and 8b) and Region 7, which is significantly obscured also in the optical. In the optical and near infrared, Region 7 corresponds to the "Overlap Region," where the most active star formation is now occurring (Mirabel et al. 1998; Wilson et al. 2000; Zhang, Fall, & Whitmore 2001). These three regions show intrinsic absorption of $\sim 1-2\times10^{21}$ cm^{-2}.

3. HOT-GAS PARAMETERS

From the parameters determined from the spectral fits we estimated various properties of the emitting plasma, such as electron density n_e ($\approx\ n_H$), thermal energy content E_{th}, cooling time τ_c, and pressure p. Since we observe regions projected on the plane of the sky, we can only measure the "footprint" of each emitting region. To estimate the emitting volumes we adopted the following procedure. For all "single"-temperature regions, we assumed a depth of 200 pc for the emitting volume, corresponding to the typical depth of a spiral disk. In the case of Region 4b, where we have two temperatures, we assumed that the high- and low-temperature components are in pressure equilibrium, and derived the thicknesses for the volumes occupied by these two phases from the best-fit kTs, imposing the condition that they add up to a total value of $200K$ pc. The filling factor η is assumed to be unity in our calculations. A filling factor η close to unity for the hot phase of the ISM is plausible from recent results coming from 3D hydrodynamical simulations (η ranging between 0.17 and 0.44 for SN rate between Galactic and 16 times the Galactic value; see, e.g., de Avillez & Breitschwerdt 2004 and references therein). However, our parameters have only a slight dependence on it ($\propto\ \eta^{-1/2}$ or $\propto\ \eta^{1/2}$), hence our estimates are precise within a factor of two or less.

The calculated cooling times are in the 10^7–10^8 yr range and in agreement with the results of F03. The pressure is generally of the order of a few 10^{-11} dyne cm^{-2}, but reaches higher values (a few 10^{-10} dyne cm^{-2}) in the two nuclei and also in the regions corresponding to the hot-spot regions R1 and R2 of F03. These new values are in excess of those found in F03, possibly reflecting the fact that larger areas were averaged over in that work. F03 argued for a possible pressure equilibrium between the hot gas and the cold molecular clouds. Zhu, Seaquist, & Kuno (2003) derived from CO measurements a pressure of 4.2×10^{-11} for the northern nucleus (NGC 4038) and of 3.1×10^{-11} dyne cm^{-2} for the southern nucleus (NGC 4039). Our observations suggest that the hot-gas pressure is a few times higher than the CO estimate for the northern nucleus and almost an order of magnitude higher in the southern nucleus. Such a large pressure difference would imply that shock waves are being driven into the CO clouds. The hot ISM may therefore in part be responsible for compressing and fragmenting the CO clouds, triggering star formation. However, we must bear in mind the large uncertainties in the estimated pressures, due to the assumptions we had to make on the emitting volume and the small-scale properties of the clouds.

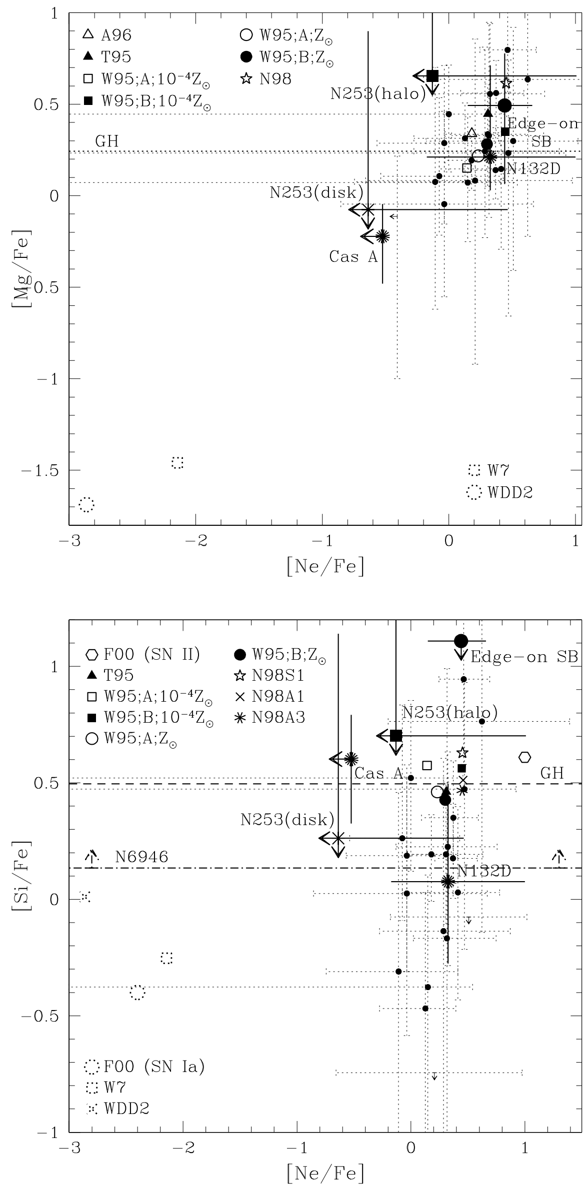

Figure 2. Abundance-ratio diagrams for regions of the Antennae hot ISM: [Ne/Fe] vs. [Mg/Fe] (left); [Ne/Fe] vs. [Si/Fe] (right). Abundance units refer to meteoritic abundances of Anders & Grevesse (1989). Each region is plotted with a small black dot (upper limits with black arrows). Dotted line symbols correspond to ratios expected in SNe Ia yields, while solid line symbols refer to the average stellar yield of SNe II. "F00" indicates values adopted in Finoguenov et al. (2000), while the other labels refer to the theoretical works listed in Nagataki & Sato (1998). Cas A and N132D SN ratios derived from the metallicities observed by BeppoSAX (Favata et al. 1997a, 1997b) are plotted too . Other symbols and lines refer to determinations of abundance ratios in other galaxies: the warm Galactic halo, NGC 253, NGC 6946 and the Strickland et al. (2004) sample of edge-on starbursts (see text for details).

4. ABUNDANCES

The elemental abundances of Ne-IX, Mg-XI, Si-XIII, and Fe-L that we measure in the hot ISM of The Antennae are generally consistent with the stellar abundances measured from optical data (∼0.5 solar; Fritze-v.Alvensleben 1998), except for a few regions (4b, 5, 7, 8a and 8b) where the measured abundances are clearly in excess of this value and, in the case of Region 5, even significantly super-solar. While all the other regions have metallicities consistent with solar (within the errors), Region 5 is showing particularly enhanced abundances for three out of the four elements we measured ($Z_{Ne} > 3.9$, $Z_{Mg} > 3.8$, $Z_{Fe} > 1.3$, at 90% confidence level). Such high X-ray derived metallicities of Fe and especially of the α elements are quite rare and have been rarely found in previous observations of other galaxies (e.g. Soria & Wu 2002; Schlegel et al. 2003). This could be due both to the peculiarity of Region 5 and to the fact that constraining abundances through X-ray fitting of low resolution spectra is always a challenging task.

The ratios between elemental abundances in each region can be related to the type of supernovae generating the metals. If the elemental enrichment results from Type II supernovae, one would expect [Ne/Fe] and [Mg/Fe] values approaching 0.3, and [Si/Fe] values approaching 0.5 on average; the corresponding values expected in Type Ia supernova enrichment are dramatically lower (Nagataki & Sato 1998). We used our results to explore the origin of the metals in The Antennae. The [Ne/Fe], [Mg/Fe], and [Si/Fe] ratios of each spectral region are plotted in diagrams displaying the [Ne/Fe] ratio vs. [Mg/Fe] ratio and [Ne/Fe] vs. [Si/Fe] (Figure 2). In these diagrams, we also show the theoretical stellar yields expected from SNe Ia and SNe II, taken from the compilations by Finoguenov et al. (2000) and Nagataki & Sato (1998). We also indicate the regions occupied by the type-II supernova remnants (SNR) Cas A and N132D, using the abundances measured by Favata et al. (1997a,b) from BeppoSAX data. To relate our results to other measurements of these ratios in the literature we plot also the values relative to the warm Galactic halo (Savage & Sembach 1996), to the emission both from the disk and from the northern halo of NGC 253 (Strickland et al. 2002), to the X-ray diffuse emission observed in NGC 6946 (Schlegel et al. 2003), and to the averaged value in the hot halo of a sample of ten nearby edge-on starbursts (Strickland et al. 2004).

Although the uncertainties are often large, almost all regions observed in The Antennae show [Ne/Fe] and [Mg/Fe] ratios fully consistent with a SN II-dominated enrichment scenario. However, the [Si/Fe] ratio is clearly lower than expected in a SN II enrichment scenario, and in some cases it could be consistent with SN Ia enrichment, although the uncertainties are quite large also for this ratio. The only two exceptions to these trends are regions 5 and 7, both located in the upper right corners of the diagrams. These two regions have a [Si/Fe] ratio fully consistent with an enrichment stemming entirely from type-II supernovae.

Although our measurements are affected by large uncertainties they represent clearly an improvement over the previous efforts aimed at measuring the α to Fe ratio in starburst galaxies. The only exception comes from the Strickland et al. (2004) sample of edge-on starburst galaxies. This data point, which has smaller error bars than our typical error bars, is consistent with the ratios observed in almost all the regions of The Antennae. However, note that their smaller error bars derive from the fact that they come from the observed hot halo emission in all ten galaxies of the sample. Moreover, in this sample they cannot put a stringent upper limit on the [Si/Fe] ratio, a thing that we were able to do in at least some of our regions.

4.1. X-ray abundances vs. Optical/Radio SF indicators

To further explore our results, we searched for correlations with age and star formation indicators for the different regions of The Antennae. NGC 4038/39 was observed by *HST*/WFPC2 (F336W, F439W, F555W, and F814W filters) in 1996 January (Whitmore et al. 1999). There were also VLA observations (in configurations BnA, CnB, and B at 6 and 4 cm) performed in 1997 January and 1998 September (Neff & Ulvestad 2000).

From the published data and our visual estimates it was possible to derive—for each region—four quantities that might correlate with ISM metal abundances: a mean cluster age, the relative strength of star formation, the star formation per unit area, and the number of SNRs per unit area. Details on how these quantities were calculated can be found in Baldi et al. (2005b).

Figure 3 displays the relations between the SF per unit area, SNRs per unit area and the mean abundance of α-elements in each region. There are no strong correlations between the different star-formation indicators we calculated and the mean abundances in the same regions. The “star-formation per unit area” and the number of “SNRs per unit area” are supposed to be among the best indicators of star formation. Yet, these two quantities appear uncorrelated with the metal abundances.

The hot-gas masses derived from the measure of the abundances may yield some clues toward an interpretation of this lack of correlations. Assuming the average SN II stellar yields listed in Nagataki & Sato (1998), we estimated the number of type-II SNe necessary to produce the observed metal masses in the hot ISM, and the time required to produce that number of SNe. If the resulting time is significantly shorter than 100 Myr, then the lack of correlations may either be related to the speed at which mixing occurs in the hot ISM or indicate that the metals are somehow removed from the hot phase of the ISM. Conversely, if the SN production time is $\geq$100 Myr, then mean cluster ages may not be relevant because over periods of 100 Myr or longer major fractions of the decaying galaxy orbits are traversed and it is unclear whether any relation could be established between regional abundances and the past local star-formation history.

A calculation for a range of theoretical models (see e.g. Nagataki & Sato 1998) for SN II average yields has been

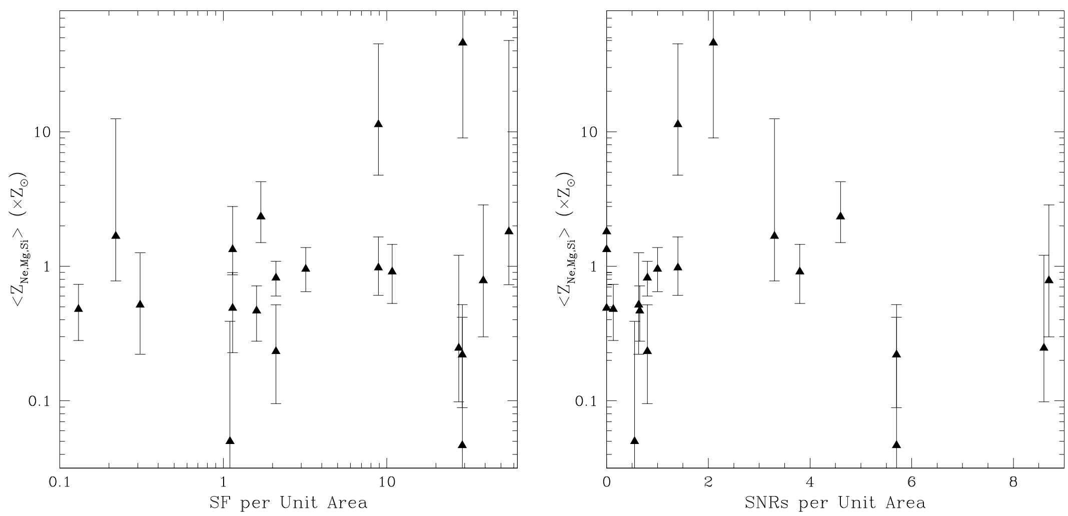

Figure 3. Diagrams of the mean abundances of α-elements in each spectral region of the Antennae hot ISM plotted versus star formation per unit area (left), and SNRs per unit area (right).

performed in Baldi et al. (2005b). In that paper, we estimated the time necessary to produce the required number of SNe II, assuming a constant SN rate throughout The Antennae. Neff & Ulvestad (2000) derived a SN rate directly associated with the compact radio sources detected in The Antennae of 0.03 yr^{-1}, assuming a typical SNR emits 6-cm radio emission for 30,000 yr and has the luminosity of Cas A. Applying instead the Condon & Yin (1990) method (based on the ratio of non-thermal radio luminosity to the radio-emitting SN rate in our Galaxy) to the total steep-spectrum radio emission of The Antennae, and not only to the detected compact sources, they predict a SN rate of 0.26 yr^{-1}. For both rate estimates the times required to produce the metals observed are quite short: in the $\sim$3.4–12 Myr range for a SN rate of 0.03 yr^{-1} and in the $\sim$0.4–1.4 Myr range for 0.26 yr^{-1}.
Indeed, 2 Myr is a relevant time threshold for mixing in a hot gas of the temperature we detect, corresponding to average velocities of $\sim$ 500 km s^{-1}. At 500 km s^{-1}, gas travels only $\sim$ 1 kpc in 2 Myr. If the time required to produce the metals is actually of this order of $\leq$2 Myr, it may be unlikely that efficient mixing takes place on a scale larger than a few hundred pc, and it is probably insufficient to destroy the correlation. Other factors may have destroyed the correlation as well like, e.g., (i) the presence of a significant fraction of the SN ejecta in a cool phase or (ii) in dust grains, or (iii) the escape of the ejecta in a galactic wind. Another possibility could be that the other metals are invisible in soft X-rays. Indeed, in a Chevalier & Clegg (1985) wind model the metals would be expected to be in much hotter ($T \sim 10^{7.5}$ K) gas. Therefore the hot gas observed could be primarily ambient ISM heated, but not particularly enriched, by Type II SNe.

5. SUMMARY AND CONCLUSIONS

In this paper we described the main results of an extensive study of the X-ray properties of the diffuse emission of The Antennae (NGC 4038/39), analyzing the entire 411 ks exposure obtained with *Chandra* ACIS-S.

To summarize:

1) Fitting the Fe-L, Ne-IX, Mg-XI and Si-XIII emission for the hot ISM, we find significant metal enrichment. Metal abundances are generally consistent with solar, but reach extremes of $\sim$ 20 solar in Region 5 and are significantly subsolar in a few regions.

2) We derived physical parameters of the hot gas, such as density, thermal energy, cooling times and pressure.

3) Comparison of elemental ratios with those expected from Type Ia and Type II SNe suggests that SNe II are mainly responsible for the metal enrichment of the hot ISM in The Antennae, although the measured [Si/Fe] ratios are mostly lower than those predicted for SN II yields. This may be due by poor data quality at the energy of the Si line (E$\sim$2 keV).

4) We report a remarkable lack of correlations between our abundance measurements and stellar age indicators, estimated from either the $Hubble$ observations of stellar clusters (Whitmore & Schweizer 1995; Whitmore et al. 1999) or VLA SNR estimates (Neff & Ulvestad 2000). The time required to produce the observed quantities of metals through type-II SN explosions is probably $\leq$2 Myr, implying that efficient mixing is unlikely to be the main agent destroying the expected correlation between abundances and radio-optical star-formation indicators. This may point toward the presence of a significant fraction of SN II ejecta in a cool phase, in dust grains, or

escaping in a wind of hot gas, undetectable at soft X-rays wavelengths.

ACKNOWLEDGMENTS

We thank the *Chandra* X-ray Center DS and SDS teams for their efforts in reducing the data and for developing the software used in the data reduction (SDP) and analysis (CIAO). We thank D.-W. Kim for useful discussions. This work was supported in part by NASA contract NAS8-39073 and NASA grants GO1-2115X and GO2-3135X. F.S. acknowledges partial support from the NSF through grant AST 02-05994.

REFERENCES

[1] Anders, E., & Grevesse, N. 1989, Geochimica et Cosmochimica Acta, 53, 197

[2] Baldi, A., Raymond, J.C., Fabbiano, G., Zezas, A., Rots, A.H., Schweizer, F., King, A.R., Ponman, T.J. 2005a, ApJSin press (astro-ph/0410192)

[3] Baldi, A., Raymond, J.C., Fabbiano, G., Zezas, A., Rots, A.H., Schweizer, F., King, A.R., Ponman, T.J. 2005b, ApJin press (astro-ph/0509034)

[4] Dahlem, M., Parmar, A., Oosterbroek, T., Orr, A., Weaver, K.A., Heckman, T.M. 2000, ApJ, 538, 555

[5] de Avillez, M.A., & Breitschwerdt, D. 2004, A&A, 425, 899

[6] Fabbiano, G., & Trinchieri, G. 1983, ApJ, 266, L5

[7] Fabbiano, G., Schweizer, F., & Mackie, G. 1997, ApJ, 478, 542

[8] Fabbiano, G., Zezas, A., Murray, S.S. 2001, ApJ, 554, 1035

[9] Fabbiano, G., Krauss, M., Zezas, A., Rots, A., & Neff, S. 2003, ApJ, 598, 272

[10] Fabbiano, G., Baldi, A., King, A.R., Ponman, T.J., Raymond, J., Read, A., Rots, A., Schweizer, F., & Zezas, A. 2004, ApJ, 605, L21

[11] Favata, F., Vink, J., Parmar, A.N., Kaastra, J.S., & Mineo, T. 1997, A&A, 324, L45

[12] Favata, F., Vink, J., dal Fiume, D., Parmar, A.N., Santangelo, A., Mineo, T., Preite-Martinez, A., Kaastra, J.S., & Bleeker, J.A.M. 1997, A&A, 324, L49

[13] Finoguenov, A., David, L.P., & Ponman, T.J. 2000, ApJ, 544, 188

[14] Fritze-v.Alvensleben, U. 1998, A&A, 336, 83

[15] Gibson, B.K., Loewenstein, M., & Mushotzky, R.F. 1997, MNRAS, 290, 623

[16] Heckman, T.M., 1999, Ap&SS, 266, 3

[17] Hibbard, J.E., van der Hulst, J.M., Barnes, J.E., & Rich, R.M. 2001, AJ, 122, 2969

[18] Martin, C.L., Kobulnicky, H.A., & Heckman, T.M. 2002, ApJ, 574, 663

[19] McKee, C.F., & Ostriker, J.P. 1977, ApJ, 218, 148

[20] Mirabel., I.F., Vigroux, L., Charmandaris, V., Sauvage, M., Gallais, P., Tran, D., Cesarsky, C., Maddus, S.C., & Duc, P.-A. 1998, A&A, 333, L1

[21] Nagataki, S., & Sato, K. 1998, ApJ, 504, 629

[22] Neff, S.G., & Ulvestad, J.S. 2000, AJ, 120, 670

[23] Pudritz, R.E. & Fiege, J.D., 2000, in ASP Conf. Series 168, New Perspectives on the Interstellar Medium, A.R. Taylor, T.L. Landecker & G. Joncas, (San Francisco: ASP), 235

[24] Read, A.M., Ponman, T.J., & Wolstencroft, R.D. 1995, MNRAS, 277, 397

[25] Sansom, A.E., Dotani, T., Okada, K., Yamashita, A., & Fabbiano, G. 1996, MNRAS, 281, 48

[26] Savage, B.D., & Sembach, K.R. 1996, ARA&A, 34, 279

[27] Schlegel, E.M., Holt, S.S., & Petre, R. 2003, ApJ, 598, 982

[28] Soria, R., & Wu, K. 2003, A&A, 410, 53

[29] Strickland, D.K., Heckman, T.M., Weaver, K.A., Hoopes, C.G., & Dahlem, M. 2002, ApJ, 568, 689

[30] Strickland, D.K., Heckman, T.M., Colbert, E.J.M., Hoopes, C.G., Weaver, K.A. 2004, ApJS, 151, 193

[31] Weaver, K.A., Heckman, T.M., & Dahlem, M. 2000, ApJ, 534, 684

[32] Weisskopf, M.C., O' Dell, S.L., & van Speybroeck, L.P. 1996, SPIE, 2805, 2

[33] Whitmore, B.C., & Schweizer, F. 1995, AJ, 109, 960

[34] Whitmore, B.C., Zhang, Q., Leitherer, C., Fall, S.M., Schweizer, F., & Miller, B.W. 1999, AJ, 118, 1551

[35] Wilson, C.D., Scoville, N., Madden, S.C., & Charmandaris, V. 2000, ApJ, 542, 120

[36] Zezas, A., Fabbiano, G., Rots, A.H., & Murray, S.S. 2002, ApJS, 142, 239

[37] Zhang, Q., Fall, S.M., & Whitmore, B.C. 2001, ApJ, 561, 727

[38] Zhu, M., Seaquist, E.R., & Kuno, N. 2003, ApJ, 588, 243

NEW INSIGHTS INTO ULTRALUMINOUS X-RAY SOURCES FROM DEEP *XMM-NEWTON* OBSERVATIONS

T.P. Roberts[1], A.-M. Stobbart[1], M.R. Goad[1], R.S.Warwick[1], J. Wilms[2], P. Uttley[3], and J.N. Reeves[3,4]

[1]X-ray & Observational Astronomy Group, Dept. of Physics & Astronomy, University of Leicester, University Road, Leicester, LE1 7RH, UK
[2]Astronomy & Astrophysics Group, Department of Physics, University of Warwick, Coventry, CV8 1GA, UK
[3]Exploration of the Universe Division, NASA Goddard Space Flight Center, Greenbelt Road, Greenbelt, MD 20771, USA
[3]Dept. of Physics & Astronomy, Johns Hopkins University, 3400 N Charles Street, Baltimore, MD 21218, USA

ABSTRACT

The controversy over whether ultraluminous X-ray sources (ULXs) contain a new intermediate-mass class of black holes (IMBHs) remains unresolved. We present new analyses of the deepest *XMM-Newton* observations of ULXs that address their underlying nature. We examine both empirical and physical modelling of the X-ray spectra of a sample of thirteen of the highest quality ULX datasets, and find that there are anomalies in modelling ULXs as accreting IMBHs with properties simply scaled-up from Galactic black holes. Most notably, spectral curvature above 2 keV in several sources implies the presence of an optically-thick, cool corona. We also present a new analysis of a 100 ks observation of Holmberg II X-1, in which a rigorous analysis of the temporal data limits the mass of its black hole to no more than 100 $M_\odot$. We argue that a combination of these results points towards many (though not necessarily all) ULXs containing black holes that are at most a few 10s of $M_\odot$ in size.

Key words: black hole physics - X-rays: binaries - X-rays: galaxies.

1. ULXS AND IMBHS

ULXs have garnered a great detail of attention since the launch of *Chandra* and *XMM-Newton*, as these missions have provided the first opportunity to study these remarkable objects in great detail (see e.g. Miller & Colbert 2004). The key question in these sources is whether their extreme X-ray luminosities originate in isotropic radiation from a compact object accreting below the Eddington rate - requiring the presence of an IMBH - or whether it can be explained by another means, with the prime suspects being anisotropic or super-Eddington radiation from a stellar-mass black hole.

The outstanding piece of recent evidence in support of the presence of IMBHs in ULXs derives from fitting their X-ray spectra with the same empirical model as used for Galactic black hole X-ray binaries (BHXRBs). It has been found that a number of luminous ULXs are well fitted by the combination of a soft multi-colour disc blackbody (MCDBB, representative of an accretion disc spectrum) plus a hard power-law continuum model (representative of a hot, optically thin corona). However, there is one crucial difference: the temperature of the accretion disc in these ULXs is a factor ~ 10 lower, at $\sim 0.1 - 0.2$ keV, than in Galactic systems. As the temperature of the innermost edge of an accretion disc scales with the mass of the compact object as $kT_{\rm in} \propto M_{\rm BH}^{-0.25}$, this implies very massive black holes in these ULXs, at ~ 1000 $M_\odot$ (e.g. Miller et al. 2003; Miller et al. 2004a).

However, recent analyses of high spectral quality ULX data have shown that some ULXs are best described by a variant of this empirical model where the power-law continuum dominates *at low energies* (e.g. Stobbart et al. 2004; Foschini et al. 2004), and the disc component is similar to that observed in stellar-mass black holes. Furthermore, in the case of NGC 5204 X-1 there is a clear ambiguity, with both model variants fitting the same data (Roberts et al. 2005). So a *bona fide* "alternate" empirical description for the spectra of some ULXs does exist, albeit one with serious physical challenges. In particular the origin of the dominant soft power-law is unclear - it appears too soft to originate in a jet, and cannot be disc-Comptonisation as it dominates well below the peak emissivity of the disc spectrum.

2. A SAMPLE OF BRIGHT ULXS

The existence of this second class of ULX spectral shape, and the ambiguity between this model and the "IMBH" spectrum in NGC 5204 X-1, led us to consider the following questions:

- How easy is it to differentiate the two spectral forms?
- How common is each type of spectrum?
- What are the physics underlying the alternate spectral model?

We have therefore selected and uniformly reduced a sample of 13 ULXs, comprising the highest quality EPIC spectral data available from the *XMM-Newton* archive, to address these questions. The data were primarily selected on the basis of datasets with $\sim$ 10 ks or more EPIC exposure, and a measured *ROSAT* High Resolution Imager count rate > 10 ct ks^{-1} (taken from Roberts & Warwick 2000 or Colbert & Ptak 2002). Though this sample is small, the ULXs are representative of the full range of ULX luminosity ($\sim 10^{39} - 2 \times 10^{40}$ erg s^{-1}), and with a minimum of a few thousand counts per source represent the best defined X-ray spectra of ULXs to date. More details on this work will appear in Stobbart et al. (2006).

2.1. Empirical spectral models

Our initial spectral fits were made utilising simple single component spectral models, subject only to absorption by material along the line-of-sight to the ULXs. The high definition and underlying complexity of the ULX spectra were highlighted by these fits, with none of the sources being well-fit (using a 95% probability of rejection criterion) by an absorbed MCDBB model, and only 5/13 being adequately fit by a power-law continuum (including the three lowest quality datasets).

The use of two-component models improved the fits considerably. In particular, the IMBH model (i.e. cool MCDBB + hard power-law) produced good fits to 8/13 datasets (using the same criterion as above), with an inner-disc temperature $kT_{\rm in} \sim 0.1 - 0.25$ keV and a power-law photon index $\Gamma \sim 1.6 - 2.5$. Again, the disc temperatures inferred in these sources lead to black hole mass estimates in the range ~ 1000 M$_{\odot}$. However, the anomaly in power-law slope discussed by Roberts et al. (2005) remains - though one might reasonably expect the IMBH accretion disc to be in a "high/soft" or "very high" state, given that it appears to be accreting at or above roughly 10% of the Eddington rate, these states typically (though not exclusively) show power-law continua with photon index $\Gamma > 2.4$ (McClintock & Remillard 2005). The power-law continua exhibited by these IMBH candidates therefore appear to possess photon indices that are somewhat on the low side.

The alternate empirical model (soft power-law, dominant at low energies, plus a warm MCDBB) also produced a total of 8/13 good fits. In fact, six of these sources were also well-fit by the IMBH model, hence spectral ambiguity is present in 6/13 of the ULXs even in our high data quality sample. Of the remaining sources, two apiece were uniquely well-fit by either the IMBH or alternate model, and the remaining three were well-fit by neither (though two favoured an IMBH fit, and one the alternate).

There is a potential discriminator between the two models that allows us to investigate which model the ambiguous sources prefer, namely curvature in the 2–10 keV range. This should be present in the alternate model (which is dominated by the MCDBB in this regime) but not the power-law-dominated IMBH model. We therefore examined the 2–10 keV data for each ULX by fitting both power-law and broken power-law models, and looking for a significant improvement between the two fits. This approach was vindicated by demonstrating that those sources best fit by the alternate model showed strong curvature ($> 4\sigma$ improvements in the broken power-law fit over the power-law fit, according to the F-test). Of the ambiguous sources, 3/6 also showed some evidence for curvature ($> 2\sigma$ significance) as, rather surprisingly, did two of the IMBH model sources. Hence we find at least marginal evidence for 2–10 keV curvature in $> 50\%$ of our spectra.

The above results suggests that the alternate model is at least a viable description of the spectrum of more than half of our sample. Hence we are once again faced with the problem of the dominant soft power-law. However, as there is no strong physical motivation for using a power-law to describe the soft excess apparent in these sources, we decided to test substituting another component, with the constraint that it should have morphological similarities to an absorbed power-law. We therefore attempted fits using a classical black body to describe the soft excess, and retained a MCDBB as the harder component (we describe this as a "dual thermal" model). We found this to be the most successful empirical description of the data, producing good fits to 10/13 ULXs, with typical parameters of $kT_{\rm BB} \sim 0.25$ keV and $kT_{\rm in} \sim 1 - 2$ keV. We speculate that this could describe the spectrum of the accretion disc around a stellar-mass black hole, with a related optically-thick outflow (or "black hole wind", c.f. King & Pounds 2003) producing the soft excess.

We demonstrate one interesting implication of these fits in Fig. 1. We essentially re-plot the results of Miller et al. (2004b) as elliptical regions in $kT_{\rm in} - L_{\rm X}$ space, representing the high-luminosity, low temperature IMBH candidate discs in the top left-hand corner, and the lower luminosity, warm discs of stellar-mass black holes in our own Galaxy in the bottom-right. In the left panel we demonstrate that when we model our sample of ULXs as IMBHs, we reproduce the results of Miller et al. (2004b), that is that the IMBH candidates sit in a separate part of $kT_{\rm in} - L_{\rm X}$ parameter space from stellar-mass black holes. However, the right panel demonstrates that when we use the (more successful) dual-thermal model, the ULXs appear to sit in a direct, high luminosity continuation of the stellar-mass black hole relationship (broadly $L_{\rm X} \propto T^4$ as the accretion rate increases, as expected for standard ac-

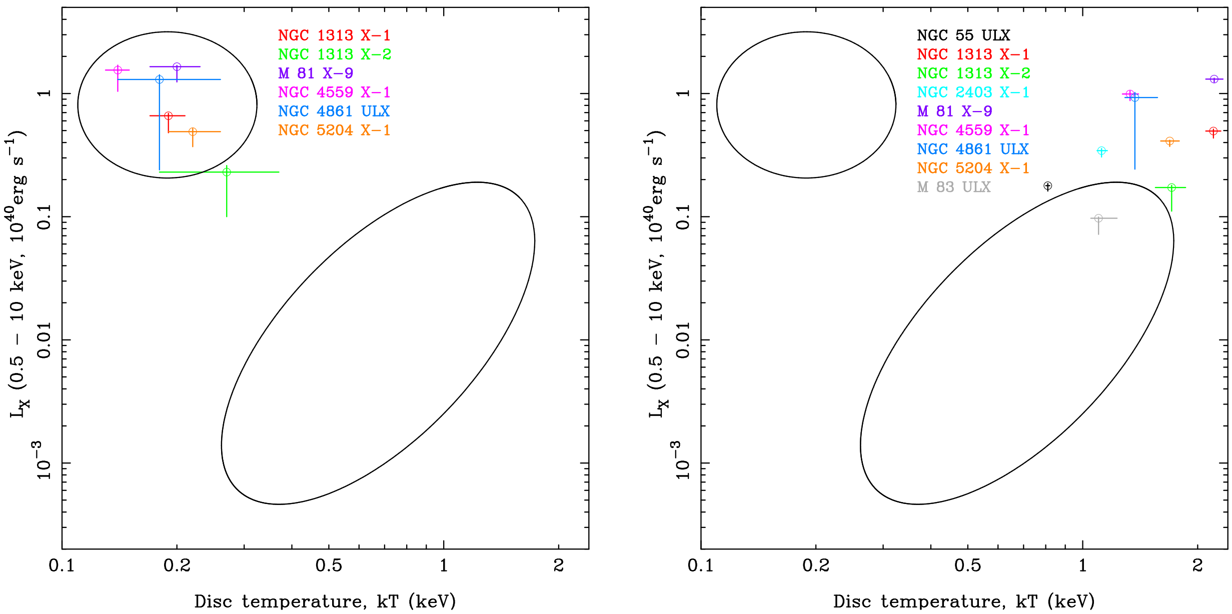

Figure 1. The relationship between accretion disc luminosity and temperature, calculated and displayed as per Miller et al. (2004b). The ellipses represent the regions in which the IMBH candidates (top left) and stellar-mass black holes (bottom right) lay in Figs. 1 & 2 of that paper. Left panel: We overlay data points from our IMBH fits (note that we only show 6 of 8 points; of the missing pair, one had a lower temperature [$\sim$ 80 eV] whilst the other had a temperature that was unconstrained). Right panel: The data points from our dual thermal model overlayed (in this case one disc was too hot to appear within the plotted range).

cretion discs). This evidence shows that, at the very least, the mass of the underlying black hole inferred from empirical spectral fitting of ULXs appears very dependent on the choice of model.

2.2. Physical spectral models

We next investigated the origin of the possible 2–10 keV curvature using more physically-motivated models. The "slim disc" model of an accretion disc (e.g. Watarai et al. 2001; XSPEC parameterisation courtesy K. Ebisawa) was only successful in fitting our spectra in 3/13 cases. Instead, we found a physically self-consistent accretion disc plus Comptonised corona model, using a `diskpn + eqpair` model in XSPEC (Gierliński et al. 2001, Coppi 2000), gave good fits to 11/13 sources (plus a further source that was only marginally rejected at the 95% criterion). All the fits display a cool disc component, with temperatures $\sim 0.1 - 0.3$ keV, as would be expected from IMBHs. However, the majority of these fits also show a second remarkable characteristic; the spectral curvature present in many sources originates in a coronal component that is optically thick, with typical optical depths of $\tau \sim 10 - 40$. This is very puzzling, because if ULXs are to be understood as direct higher-mass analogies of high-state BHXRBs, then their coronae should presumably be similarly optically thin ($\tau < 1$). This only occurs in two of our sources, leaving this pair as the best accreting IMBH candidate ULXs within our sample. For the remaining ULXs, that possess apparent optically-thick coronae, it is evident that they are not simple scaled-up Galactic BHXRBs in a classic high/soft state, and we may perhaps need new insight to explain their spectra.

3. HOLMBERG II X-1

This source is regarded as the archetypal luminous ($L_X > 10^{40}$ erg s^{-1}) nearby ULX, and has been widely studied both in X-rays (e.g. Dewangan et al. 2004) and over complementary wavebands (e.g. Kaaret, Ward & Zezas 2004; Miller, Mushotzky & Neff 2005). We were awarded a 100-ks observation of this source in *XMM-Newton* AO-3, the results of which we summarise here (see also Goad et al. 2005).

3.1. Spectra

Though more than 60% of this observation was lost to space weather, we were still able to extract the first reasonable signal-to-noise RGS spectrum of an ULX. This showed a smooth continuum shape, modelled simply as an absorbed power-law continuum ($N_H \sim 2 \times 10^{21}$ cm^{-2}, $\Gamma \sim 2.6$) with the exception of an excess of counts slightly above 0.5 keV (see Fig. 1 of Goad et al. 2005). This could be fit by an O VII triplet, but a much better solution was found by allowing the abundance of the absorbing material to drop to $\sim$ 0.6 of the solar value.

Interestingly, this result strongly affects the EPIC data modelling. In particular, using a 0.6-solar abundance

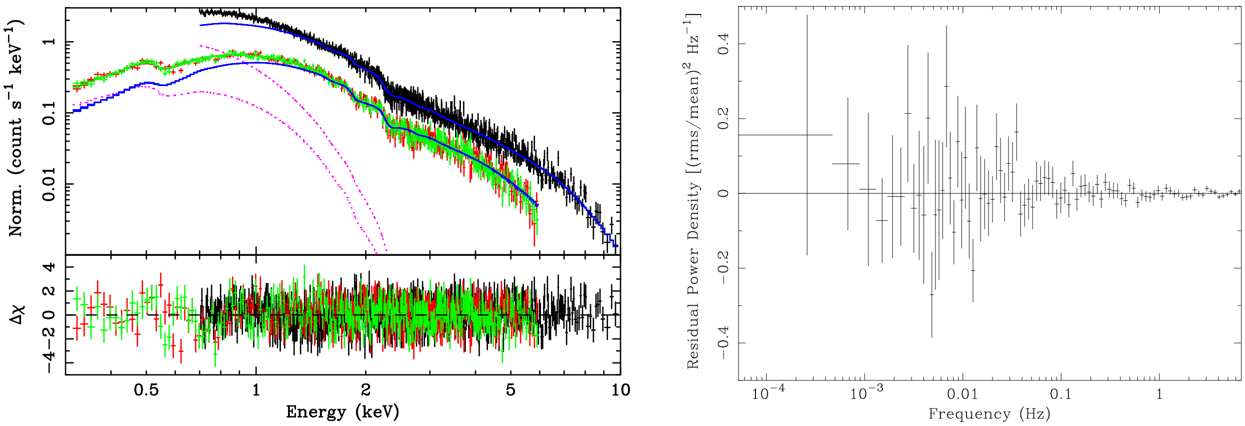

Figure 2. Left panel: EPIC X-ray spectra of Ho II X-1. The pn data points are displayed in black, and the MOS in grey. We show the modelled contributions of the accretion disc (dotted lines) and corona (solid lines) separately in the top part of the panel, and show the model fit residuals in the lower part. Right panel: the residual power density after fitting the PSD of Ho II with a constant. This demonstrates the lack of variability power in the source.

TBABS model in XSPEC (and interstellar abundances set to the values of Wilms, Allen & McCray 2000) greatly reduces the size of the apparent soft excess, and so the mass of the BH estimated from the IMBH model is reduced to $\sim 33\%$ of its value assuming a solar abundance absorber. However, the best fit to the data was again found to be the physically self-consistent accretion disc + corona model, with $kT_{\rm in} \sim 0.2$ keV and $\tau \sim 4-9$ (i.e. a cool disc and optically thick corona). The EPIC spectral data, with this best-fit model, are shown in Fig. 2. Note there is no detection of an Fe Kα line in this dataset; formally, we place a 90% upper limit of 25 eV on the equivalent width of a narrow 6.4 keV Fe Kα feature.

3.2. Timing

The EPIC timing data showed Ho II X-1 to be remarkably invariant during the observation. A power spectral density (PSD) analysis was performed, finding that no power was evident (above the Poisson noise level) in the $\sim 10^{-4} - 6$ Hz range (see Fig. 2). This likely rules out Ho II X-1 being in a high/soft state, as a comparison to Galactic black holes and AGN shows they generally have a red noise spectrum with measureable RMS variability in this state[1]. It does not rule out a state with a band-limited PSD, such as occurs in the low/hard or some very high states. However, the strong limits placed by the non-detection of power in the observed frequency interval implies any power must be present at higher frequencies. Assuming that BH timing properties scale linearly with mass (e.g. Uttley et al. 2002), we can place an upper limit on the mass of Ho II X-1 of 100 $M_\odot$ if it is in the low or certain very high states. Encouragingly, GRS 1915+105 shows very similar variability characteristics in its "χ-class" of behaviour, which is thought to occur whilst it is in the very high state.

[1]We note that dilution by photons from the accretion disc should not be a problem for Ho II X-1 if it contains an IMBH, as the 0.3–6 keV band we derive the PSD from is dominated by the putative coronal component. However, it has been brought to our attention that there may be a dimunition of intrinsic variability in the coronae of high/soft state sources at the highest luminosities (J. Homan, *priv. comm.*), which merits further quantification.

4. RADICAL SOLUTIONS

Whilst it is evident from this work that optically-thick coronae may be common in ULXs, what is their origin? One possible explanation is offered by the model of Zhang et al. (2000), that explains accretion discs as a two-layer system, with a cool ($0.2 - 0.5$ keV) interior seeding a warm, optically thick ($1 - 1.5$ keV, $\tau \sim 10$) Comptonising upper disc layer. This model therefore offers an explanation for both spectral components seen in our modelling. Crucially, it has also successfully been used to describe the X-ray spectrum of GRS 1915+105. We therefore speculate that our spectral modelling, considered along with the mass limit from Ho II X-1, argues that Ho II X-1 and many other ULXs may be analogues of GRS 1915+105. Whilst ULXs may still possess larger BH masses than GRS1915+105 (i.e. 20 - 100 $M_\odot$, so still technically IMBHs), we suggest they are operating in similar accretion states, with a key link being that the accretion is persistently at around the Eddington limit.

Obviously, we cannot rule out cool discs being the signature of a larger, ~ 1000 $M_\odot$ IMBH. Indeed, a weakness of the above model is how we manage to see photons from the inner disc layer through an optically thick exterior. However, we note there are also weaknesses with a literal interpretation of cool disc parameters, most notably in the case of PG quasars. Similar soft spectral components - also modelled as cool discs - are seen in PG quasars, where their temperature has been shown to be completely independent of the mass of the BH (Gierliński & Done 2004). This implies a radically different origin for the soft excesses in PG quasars - and, by extension, ULXs - such as in an outflow (as suggested in our dual-thermal model), or perhaps even as atomic features on the accretion disc spectrum.

5. CONCLUDING COMMENTS

If ULXs do contain $\sim$ 1000 $M_\odot$ IMBHs, as suggested by empirical modelling of their spectra, then one might reasonably assume from their luminosities that they are accreting at $\sim 10\%$ of the Eddington rate, and so should behave like scaled-up versions of BHXRBs in the high-state. The detection of spectral curvature in the 2–10 keV range in the majority of our sample of ULXs, that can be physically modelled as a cool, optically-thick corona, argues that something different is happening in many ULXs. One explanation could be that these ULXs are operating in a fashion similar to GRS 1915+105, as suggested by the timing results for Ho II X-1, in which case the ULXs might harbour black holes not much more massive than in Galactic BHXRBs. This would bring X-ray spectral results more into line with other arguments on ULXs that suggest that the majority of sources do not contain IMBHs. For example, King (2004) argues that the sheer numbers of ULXs in the most extreme star-forming environments makes it very unlikely that they can all contain IMBHs, and the modelling of Rappaport, Podsiadlowski & Pfahl (2005) demonstrates many ordinary high-mass BHXRBs (that one would expect to find in these environments) have a mass transfer rate that is substantially super-Eddington, providing an adequate reservoir of fuel for ULXs. Not least, it would agree with observations of accreting sources in our own Galaxy that show many - most notably GRS 1915+105 - do experience episodes of radiating at a super-Eddington level (cf.. McClintock & Remillard 2005).

However, we certainly cannot exclude ULXs from containing $\sim$ 1000 $M_\odot$ IMBHs at the current point in time, and indeed two of the sources in our sample do appear consistent with this interpretation. Ultimately it may prove that the only measurement that can resolve the debate on the underlying nature of ULXs will be a dynamical mass limit for the black hole from its orbital motion, as is the case for Galactic BHXRBs. Until then, more and deeper X-ray observations are required to advance our knowledge of these extraordinary X-ray sources.

ACKNOWLEDGMENTS

TPR, AMS and MRG gratefully acknowledge funding from PPARC. This work is based on observations obtained with *XMM-Newton*, an ESA science mission with instruments and contributions directly funded by ESA member states and NASA.

REFERENCES

Colbert E.J.M., Ptak A.F., 2002, ApJS, 143, 25

Coppi, P.S., 2000, *HEAD*, 5.2311

Dewangan, G., Miyaji, T., Griffiths, R.E., Lehmann, I., 2004, ApJ, 608, L57

Foschini, L., Rodriguez, J., Fuchs, Y., Ho, L.C., Dadina, M., Di Cocco, G., Courvoisier, T.J.-L., Malaguti, G., 2004, A&A, 416, 529

Gierliński, M., Done, C., 2004, MNRAS, 349, L7.

Gierliński, M., Maciolek-Niedzwiecki, A., Ebisawa, K., 2001, MNRAS, 325, 1253

Goad M.R., Roberts T.P., Reeves J., Uttley P., 2005, MNRAS, in press (astro-ph/0510185)

Kaaret P., Ward M.J., Zezas A., 2004, MNRAS, 351, L83

King A., 2004, MNRAS, 347, L18

King A., Pounds K.A., 2003, MNRAS, 345, 657

McClintock J.E., Remillard R.A., 2005, to appear in Compact Stellar X-ray Sources, eds. W.H.G. Lewin and M. van der Klis. (astro-ph/0306213)

Miller, J.M., Fabbiano, G., Miller, M.C., Fabian, A.C., 2003, ApJ, 585, L37

Miller, J.M., Fabian, A.C., Miller, M.C., 2004a, ApJ, 607, 931

Miller, J.M., Fabian, A.C., Miller, M.C., 2004b, ApJ, 614, L117

Miller M.C., Colbert E.J.M., 2004, Int. J. Mod. Phys. D, 13, 1

Miller N.A., Mushotzky R.F., Neff S.G., ApJ, 623, L109

Rappaport S.A., Podsiadlowski Ph., Pfahl E., 2005, MNRAS, 356, 401

Roberts T.P., Warwick R.S., 2000, MNRAS, 315, 98

Roberts, T.P., Warwick, R.S., Ward, M.J., Goad, M.R., Jenkins, L.P., 2005, MNRAS, 357, 1363

Stobbart, A., Roberts, T.P., Warwick, R.S., 2004, MNRAS, 351, 1063

Stobbart, A., Roberts, T.P., Wilms, J., 2006, *in preparation*

Uttley, P., McHardy, I.M., Papadakis, I.E., 2002, MNRAS, 332, 231

Watarai, K., Mizuno, T., Mineshige, S., 2001, ApJ, 549, L77

Wilms J., Allen A., McCray R., 2000, ApJ, 542, 914

Zhang, S.N., Cui, W., Chen, W., Yao, Y., Zhang, X., Sun, X., Wu, X.-B., Xu, H., 2000, Science, 287, 1239

SPECTRAL STUDY OF ULTRA-LUMINOUS COMPACT X-RAY SOURCES WITH *XMM-NEWTON* AND *CHANDRA*

R. Miyawaki[1], M. Sugiho[1], A. Kubota[2], K. Makishima[1,2], M. Namiki[3], T. Tanaka[4], and N. Tsunoda[2,5]

[1]Department of Physics, University of Tokyo, Tokyo 113-0033, Japan
[2]Institute of Physical and Chemical Research (RIKEN), Wako 351-0198, Japan
[3]Department of Earth and Space Science, Osaka University, Osaka 560-0043, Japan
[4]Japan Aerospace Exploration Agency, Institute of Space and Astronautical Science, Sagamihara 229-8510, Japan
[5]Department of Physics, Tokyo University of Science, Tokyo 162-8601, Japan

ABSTRACT

Using the *ASCA*, *XMM-Newton*, and *Chandra* data, luminosity-dependent spectral changes of the ultra-luminous X-ray source (ULX) M 81 X-9 were studied. When the luminosity was below a threshold of $\sim 1.5\times10^{40}$ erg s^{-1}, the source consistently exhibited power-law spectra. In contrast, the spectra at higher luminosities were more convex, favoring a multi-color-disk modeling. A p-free disk model with $p \sim 0.6$ gave a still better fit to the high-luminosity spectra of M81 X-9, suggesting the presence of a slim disk. Another ULX, NGC 1313 Source B, also showed a similar luminosity-dependent spectral change. These results agree with the *ASCA* report on the two ULXs in IC 342 (Kubota et al., 2001).

Key words: galaxies: individual (M 81 / NGC 1313) ; X-rays: galaxies.

1. INTRODUCTION

Ultra-luminous compact X-ray sources (ULXs) are point-like off-center X-ray sources in nearby galaxies, with their luminosity reaching 10^{39-40} erg s^{-1}. Since their luminosity largely exceeds the Eddington limit of a neutron star, ULXs are important and interesting objects as possible candidates for intermediate-mass black holes (Colbert & Mushotzky, 1999, Makishima et al., 2000).

Detailed spectral study of ULXs have become possible since the *ASCA* era. Spectra of about 10 ULXs obtained with *ASCA* were mostly described successfully by multi-color disk (MCD) blackbody model from a standard accretion disk, and others by power-law (PL) model (Makishima et al., 2000, Mizuno et al., 2001). Moreover, two ULXs in IC 342 showed spectral transitions between the

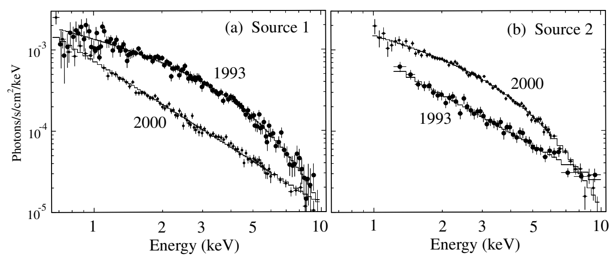

Figure 1. The ASCA spectra of IC 342 Source 1 (panel a) and Source 2 (panel b) obtained in two observations. The detector response and absorption are removed. From Kubota et al. (2001)

MCD-type and PL-type states (Kubota et al., 2001), as clearly seen in figure 1.

Recently, *XMM-Newton* and *Chandra* are providing us with a much large sample of ULXs. In contract to the *ASCA* results, spectra of most ULXs obtained with these satellites prefer the PL model to the MCD model (e.g., Roberts et al., 2004, Swartz et al., 2004), and there is evidence for very cool disks in several ULXs (Miller et al., 2003, 2004). There seems to be a systematic difference between the *ASCA* results and those from *XMM-Newton* and *Chandra*. In order to examine this issue, we analyzed archival data of two luminous nearby ULXs which have been observed repeatedly, namely, M81 X-9 and NGC 1313 Source B.

2. SPECTRAL ANALYSIS OF M 81 X-9

2.1. Observation and Data Reduction

As a typical ULX observed repeatedly over a decade since *ASCA*, we have selected M 81 X-9 ULX, located in a dwarf galaxy Holmberg IX in the M 81 group. Because

Table 1. A summary of observations and spectral studies of M 81 X-9.

	Observation date	L_x^{**}	χ^2/d.o.f(PL)	χ^2/d.o.f(MCD)	Preferred model parameter***
*ASCA**	1993-1998(average)	1.4	66/72	486.3/72	PL 1.58±0.03
	1999-04	1.9	486.5/318	359.3/318	MCD 1.24±0.03 keV
XMM-Newton	2001-04-22	2.1	508.7/324	392.0/324	MCD 1.36±0.03 keV
	2002-04-10	1.1	663.3/644	1178.5/644	PL 1.77±0.03
	2002-04-16	1.3	739.5/747	1262.4/747	PL 1.82±0.03
Chandra	2002-12-28	1.1	236.3/225	447.8/225	PL 1.63±0.04
	2003-06-09	1.3	254.4/240	396/240	PL 1.82±0.04
	2003-09-03	0.9	268.0/200	430.0/200	PL 1.62±0.06

* From Ezoe et al. (2001), La Parola et al. (2001), and Wang (2002).
** The X-ray luminosity (0.5-10 keV) in units of 10^{40} erg s^{-1}, assuming a distance of 3.6 Mpc.
*** The MCD $T_{\rm in}$ or the PL photon index, whichever is preferred.

of the explosion of SN 1993J, this object was observed 19 times with *ASCA* over 1993-1998, and the spectra from these observations were successfully described by the PL model with photon index of 1.58 (Ezoe et al., 2001). However, La Parola et al. (2001) and Wang (2002) reported from the observation on April 1999 that it became more luminous, and its spectrum turned into the MCD type with the innermost disk temperature of $T_{\rm in} = 1.24$ keV.

Observations of this object have been repeated also with *XMM-Newton* and *Chandra*, and 3 observation data with the *EPIC* onboard *XMM-Newton* and 5 data with the *ACIS* onboard *Chandra* are archival by August 2005. Although the two *XMM-Newton* datasets acquired in 2002 were already analyzed by Miller et al. (2004) and the three *Chandra* data from December 2002 to September 2003 by Unks et al. (2003), here we re-analyzed these data by ourselves. We did not utilize two Chandra datasets obtained in 2004, because they suffered from significant ($\geq$ 10 %) pile up. Table 1 summarizes the datasets employed in the present work.

We extracted spectra from each observation using the data reduction software *SAS* version 6.5.0 for *XMM-Newton* and *CIAO* version 3.2.2 for *Chandra*. Background data were extracted from regions neighboring to the source. For the 2001 April 21 observations with *XMM-Newton*, we used only the MOS1 data because the fields of view of PN and MOS2 did not fully cover the source region, which is located about 13 arcminutes off the telescope aim-points.

2.2. Spectral Properties

We fitted each spectrum of M 81 X-9 by PL (*powerlaw*) or MCD (*diskbb*) models using the software *XSPEC* version 11.0.2. Table 1 summarizes the luminosity, the fit goodness of the two models, and the parameter of the more favored model. Figure 3 shows $\Delta\chi^2$ as a function of luminosity. Here, $\Delta\chi^2$ was calculated as a difference

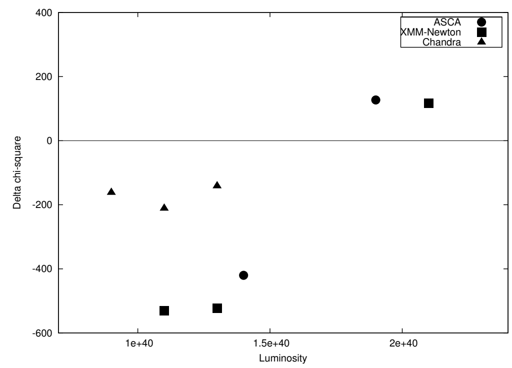

Figure 3. The difference in the fit goodness between the MCD and PL models, namely $\Delta\chi^2 \equiv \chi^2_{PL} - \chi^2_{MCD}$, plotted as a function of the 0.5-10 keV luminosity. Circles, squares, and triangles stand for ASCA, XMM-Newton, and Chandra, respectively.

between the χ^2 by the PL model and that by the MCD model; positive values mean an MCD-preferred spectrum and negative values a PL-preferred one. As was the case with *ASCA*, the most luminous *XMM-Newton* data showed an MCD-like spectrum, and the fainter two PL-type spectra. In the three *Chandra* observations, the object was rather dim, and the spectrum was PL-like. Thus, the three satellites give consistent results in that the spectrum becomes MCD-like when the source is luminous, while it becomes PL-like when the luminosity is low, with the threshold luminosity at about 1.5×10^{40} erg s^{-1}.

In figure 2, we show two typical spectra acquired on the brighter (2.1×10^{40} erg s^{-1}) and the fainter (1.1×10^{40} erg s^{-1}) occasions. Thus, the brighter spectrum clearly exhibits a convex shape, in contrast to the fainter one which is much more straight in shape. Our results on the fainter spectrum roughly agree with the results by Miller et al. (2004).

In order to more directly visualize the difference between the two spectra, we show in figure 4 (left) their spectral

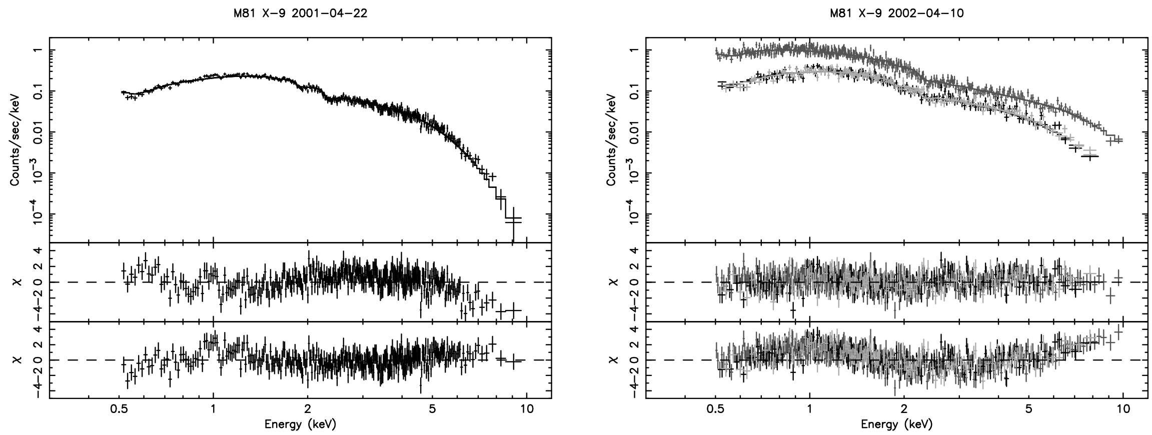

Figure 2. The left panel shows the XMM-Newton MOS1 spectrum of M 81 X-9 on the brighter occasion (2001-04-22), with the solid line describing the best-fit MCD model. The right panel shows the MOS1 (black), MOS2 (light gray), and PN (dark gray) spectra on the fainter occasion (2002-04-10), with the solid lines describing the best-fit PL model. The middle and bottom panels show the fit residuals from the PL and MCD model fits, respectively.

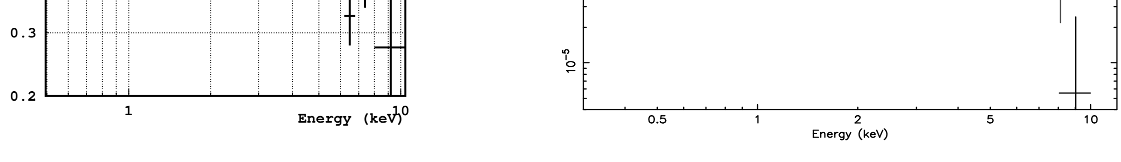

Figure 4. Comparison of the two spectra in figure 2, in the form of spectral ratios (left) and response-removed presentations (right).

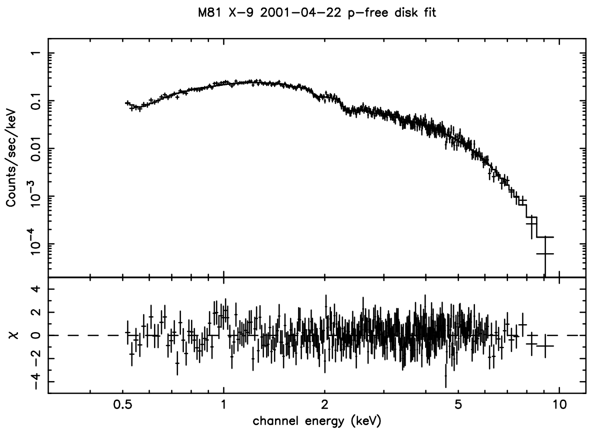

Figure 5. The same spectrum as the left panel of figure 2, but fitted with a p-free disk model.

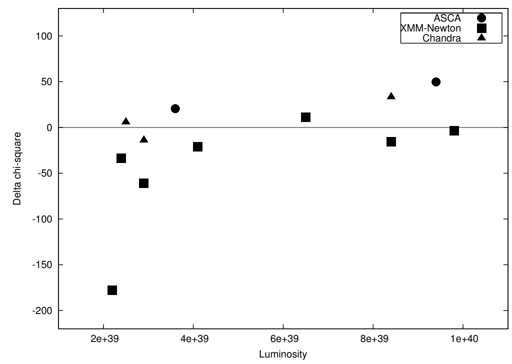

Figure 6. The same as figure 3, but for NGC 1313 Source B.

ratios. Thus, the two spectra have very different shapes, in agreement with the model fitting results. Finally, in order to understand the actual shape of the two spectra, we show them in figure 4 (right) with the detector response removed. As expected from the ratio, the spectrum becomes clearly curved as the luminosity increases. This behavior is essentially the same as the *ASCA* results on the ULXs in IC 342 (Kubota et al., 2001), which are reproduced here as figure 1.

2.3. A p-free Disk Model Fit

Although the spectrum of M 81 X-9 on the brighter occasion preferred the MCD model as shown in the previous sub-section, the fit is not yet fully acceptable.Actually in figure 2, the spectrum is slightly deviated in shape from the MCD model. Therefore, we may modify the MCD model to achieve a better fit. The simplest modification may be so-called p-free disk model (e.g., Mineshige et al., 2000, and Watarai et al., 2001). The model assumes that the disk temperature scales as r^{-p}, where r is the radius and p is a free parameter, whereas $p = 0.75$ implies the MCD model. The p-free disk model gives a good approximation to a slim disk (Watarai et al., 2001), which is expected to form under very high accretion rates. As the standard disk gradually changes into a slim disk, the value of p is predicted to start decreasing from 0.75, and finally approaches 0.5. When p gets smaller, the soft energy part of the spectrum becomes more enhanced.

In figure 5, We actually fitted the brighter *EPIC* spectrum by the p-free disk model. Comparing the fit residual with that in figure 2 left ($\chi^2_\nu = 1.21$), the fit has been significantly improved and has become acceptable ($\chi^2_\nu = 0.98$). The best-fit model parameters are $T_{\rm in} = 1.77 \pm 0.12$ keV and $p = 0.60 \pm 0.02$. Since the value of p is significant smaller than 0.75 of the MCD model, the MCD-type spectrum may be in fact emitted by a slim disk around the central object (most likely an intermediate-mass black hole), instead of a standard disk. Further details will be reported elsewhere (Tsunoda et al., in preparation).

3. SPECTRAL ANALYSIS FOR NGC 1313 SOURCE B

As another target for our spectral analysis, we have selected NGC 1313 Source B, which is also a typical ULX observed repeatedly for a decade. Two observations were performed with *ASCA*, and both spectra were described successfully by the MCD model, when the 0.5-10 keV source luminosity was 9.4×10^{39} and 3.6×10^{39} erg s^{-1} at an assumed distance of 4.5 Mpc (Makishima et al. 2000, Mizuno et al. 2001). By August 2005, 9 *XMM-Newton EPIC* datasets and 5 *Chandra ACIS* data sets of this object became publicly available. We did not utilize two *XMM-Newton* datasets (2005 December 9 and 27) because they suffered from high background over the observations, and two *Chandra* datasets (2002 November 9 and 2004 February 22) suffering from significant pile up. Although some of these observations were reported by Miller et al. (2003), Wang et al. (2004), Zampieri et al. (2004), and Turolla et al. (2005), we re-analyzed these datasets by ourselves in order to study the luminosity-dependent spectral changes in a unified way.

As summarized in table 2, the luminosity of this object through the *XMM-Newton* and *Chandra* observations varied between 2.2×10^{39} and 9.8×10^{39} erg s^{-1}. In figure 6, we show $\Delta\chi^2$ calculated in the same way as in figure 3. Although the results are not as clear as those for M81 X-9, we can see a tendency that the spectrum changes into MCD-like as luminosity increases. Among them, we have selected the 2003 December 21 data (8.4×10^{39} erg s^{-1}) and the 2000 October 17 data (2.2×10^{39} erg s^{-1}), both with *EPIC* MOS1, as representing relatively brighter and fainter states, respectively. Other datasets had poorer statistics. Like in the case of M81 X-9, figure 7 (left) compares the two spectra in the form of spectral ratios, whereas figure 7 (right) in the response-removed representations. We can see that the spectrum becomes again curved as the luminosity increases. These results are similar to those of M 81 X-9.

Table 2. The same as table 1, but for NGC 1313 Source B.

	Observation date	L_{x}^{**}	χ^2/d.o.f(PL)	χ^2/d.o.f(MCD)	Preferred model parameter***
*ASCA**	1993-07-12	9.4	174.2/130	124.5/130	MCD 1.47±0.08 keV
	1995-11-29	3.6	110.3/74	89.8/74	MCD 1.07±0.07 keV
XMM-Newton	2000-10-17	2.2	195.4/222	373.0/222	PL 2.32±0.07
	2003-11-25	6.5	53.0/50	42/50	PL 1.90±0.16 or MCD $1.34^{+0.14}_{-0.12}$ keV
	2003-12-21	8.4	336.0/314	351.7/314	PL 1.78±0.05 or MCD 1.62±0.06 keV
	2003-12-23	9.8	182.6/179	186.2/179	PL 1.72±0.06 or MCD 1.72±0.09 keV
	2003-12-25	4.1	70.5/82	91.8/82	PL 2.10±0.13
	2004-01-08	2.9	134.2/156	195.0/156	PL 2.39±0.09
	2004-01-16	2.4	57.0/67	90.5/67	PL 2.35±0.14
Chandra	2002-10-13	8.4	204.8/175	171.5/175	MCD 1.66±0.07 keV
	2003-10-02	2.9	75.6/56	89.6/56	PL 1.93±0.14 or MCD $1.41^{+0.06}_{-0.16}$ keV
	2004-03-10	2.5	41.9/26	36.1/26	PL $2.04^{+0.24}_{-0.22}$ or MCD $1.17^{+0.16}_{-0.14}$ keV

* From Makishima et al. (2000) and Mizuno et al. (2001).
** In units of 10^{39} erg s^{-1}, assuming a distance of 4.5 Mpc.
*** Both parameters were shown in case that a preferred model cannot be constrained.

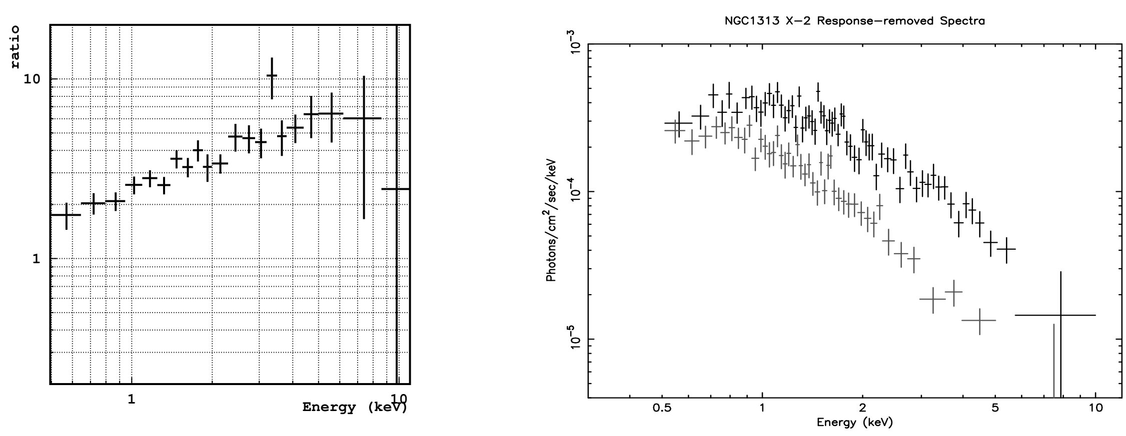

Figure 7. The same as figure 4, but for NGC 1313 Source B.

4. CONCLUSION

In order to investigate spectral properties and in particular search for spectral transitions, we analyzed *XMM-Newton* and *Chandra* archival data of two typical ULXs, M 81 X-9 and NGC 1313 Source B. Spectra of the two ULXs showed consistent luminosity-dependent changes through the three satellites including *ASCA*. That is, the spectrum exhibited a transition from PL-type ones to MCD-type ones, as the source luminosity increased across a certain threshold. Such a spectral transition is reminiscent of those observed with *ASCA* from two ULXs in IC 342. This means that the same spectral transition has been confirmed from four ULXs in total. As to M 81 X-9, a p-free disk model significantly improved the fit to the high-luminosity spectrum, and the obtained value of p was smaller, 0.60 ± 0.02, than that of the MCD model. This object possibly forms a slim disk when luminosity becomes higher than $\sim1.5\times10^{40}$ erg s^{-1}. We therefore conclude that the *XMM-Newton* and *Chandra* data are consistent with the original *ASCA* results, at least as to those four luminous ULXs.

REFERENCES

Colbert, E.J.M. & Mushotzky, R.F. 1999, ApJ, 519, 89

Ezoe, Y., Iyomoto, N., Makishima, K. 2001, PASJ, 53, 69

Kubota, A., Mizuno, T., Makishima, K., et al. 2001, ApJ, 547L, 119

La Parola, V., Peres, G., Fabbiano, G., et al. 2001, ApJ, 556, 47

Makishima, K., Kubota, A., Mizuno, T., et al. 2000, ApJ, 535, 632

Miller, J.M., Fabbiano, G., Miller, M.C., et al. 2003, ApJ, 585L, 37

Miller, J.M., Fabian, A.C., Miller, M.C. 2004, ApJ, 606, 131

Mineshige, S., Kawaguchi, T., Takeuchi, M., et al. 2000, PASJ, 52, 499

Mizuno, T., Kubota, A., Makishima, K. 2001, ApJ, 554, 1282

Roberts, T.P., Warwick, R.S., Ward, M.J., et al. 2004, MNRAS, 349, 1193

Swartz, D.A., Ghosh, K.K., Tennant, A.F., et al. 2004, ApJS, 154, 519

Turolla, R., Mucciarelli, P., Zampieri, L., et al. astro-ph/0506341

Unks, B.E., Slane, P.O., Erikson, K.A., et al. 2003, American Astronomical Society Meeting 203, #81.08

Wang, Q.D. 2002, MNRAS, 332, 764

Wang, Q.D., Yao, Y., Fukui, W., et al. 2004, ApJ, 609, 113

Watarai, K., Mizuno, T., Mineshige, S. 2001, ApJ, 549, L77

Zampieri, L., Mucciarelli, P., Falomo, R., et al. 2004, ApJ, 603, 523

OPTICAL SEARCH FOR SUPERNOVA REMNANTS IN TWO-SPIRAL GALAXIES

A.Akyuz [1], S. Balman [2], D. Bhattacharya[3], E. Sonbas[1], and E. Cekmecelioglu[1]

[1] University of Cukurova, Dept. Of Physics, 01330 Adana, TURKEY
[2]Dept. of Physics, Middle East Technical University, 06531 Ankara, TURKEY
[3]Institute of Geophysics and Planetary Physics, University of California, Riverside, CA 92521, USA

ABSTRACT

We present the results of an optical search for Supernova Remnants (SNRs) in the spiral galaxies NGC6946 and NGC628. The SNR identification technique consisted of constructing continuum-subtracted H_α and [SII] $\lambda\lambda$ 6716,6731 images and then using [SII] / H_α ratios obtained from the image. 32 emission nebulae have been detected as SNR candidates in NGC6946. 22 of them were previously identified by Matonick et al (1997). We found five SNR candidates in the spiral galaxy NGC628. We will compare and contrast the new SNR candidates and our optical data with the existing Chandra and XMM observation of the two galaxies of interest and VLA radio observation of NGC6946. Interference-filter CCD images of two spiral galaxies were taken in 2004 September with the f/7.7 1.5 m Russian-Turkish Telescope at Turkish National Observatory.

Key words: SNR;Optical Observation.

1. INTRODUCTION

Supernova remnants are important probes of the interstellar medium. Although the sample of Galactic remnants is large it is plagued by interstellar extinction and uncertain distances. These problems are much less in extragalactic samples.A number of spiral galaxies have had SNRs cataloged for them but the overall remains small (DOdorico, Dopita & Benvetui 1980, Magnier et al.1995). SNR surveys have been carried out at optical , radio and X-ray wavelengths (Pannuti at al. 2002,Blair & Long 2004).

2. SNR IDENTIFICATION TECHNIQUE

In this work, we use [SII] / H_α ratio to carry out or search for SNRs in NGC6946 and NGC628 (Mathewson & Clarke (1973a)). Basic reduction of our images was accomplished using MIDAS.The twelve exposures for H_α and [SII] and three continuum exposures of each field were combined to obtain a deeper field image and increase S/N for faintest objects. Preliminary SNR candidates were found by blinking between continuum-subtracted [SII] and H_α images. If objects were almost as bright, in [SII] as in H_α they were considered as possible SNR candidates. 32 SNR candidates for NGC6946, (22 of them were identified previously by Matonick et al.1997, hereafter MF97), and 5 SNR candidates for NGC628 were identified. (Fig1 and Fig2). These are the objects that had count rate ratio in the final analysis in excess of the [SII]/$H_\alpha > 0.45$. The list of new SNR candidates in NGC6946 and NGC628 are given in Table 1 and Table 2 respectively.

Table 1. NGC 6946 New Supernova Remnant Candidates

SNR NO	RA (J2000)	DEC (J2000)	[[SII]]/H
TUG 1	20:34:47.4	60:08:20.8	0.57
TUG 2	20:34:45.1	60:11:52.1	0.58
TUG 3	20:35:12.9	60:09:09.5	0.86
TUG 4	20:34:54.5	60:09:08.6	0.62
TUG 5	20:35:02.3	60:10:58.1	0.56
TUG 6	20:34:51.6	60:10:30.4	0.67
TUG 7	20:35:13.0	60:08:58.7	0.95
TUG 8	20:34:24.2	60:07:22.3	0.83
TUG 9	20:34:52.9	60:05:30.4	0.60
TUG 10	20:34:46.9	60:07:29.7	0.67

3. COMPARISON OF MULTIWAVELENGHT OBSERVATIONS

NGC6946 was observed by the ACIS instrument on board Chandra X - Ray Observatory (Holt et al., 2003). The authors detect 72 point sources with luminosities

Table 2. NGC 628 Supernova Remnant Candidates

SNR NO	RA (J2000)	DEC (J2000)	[[SII]]/H
1	1:36:39.8	15:49:07.3	0.88
2	1:36:39.3	15:45:49.6	0.92
3	1:36:47.0	15:45:13.2	0.92
4	1:36:45.5	15:43:06.2	0.73
5	1:36:49.1	15:43:34.2	0.95

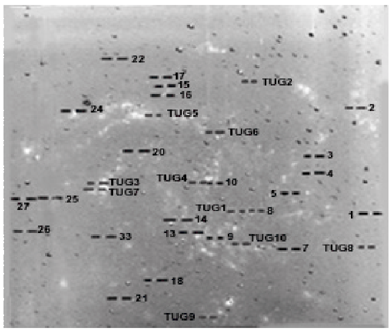

Figure 1. [SII]-continuum image of NGC6946 with SNRs

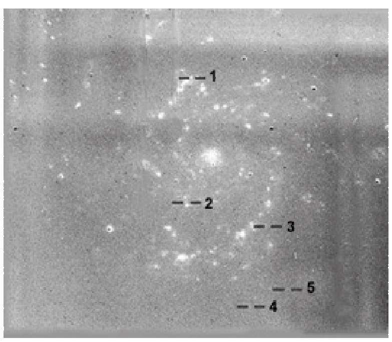

Figure 2. [SII]-continuum image of NGC628 with SNRs

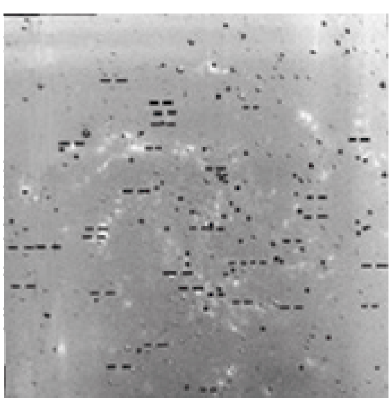

Figure 3. H_α image of NGC6946 with Chandra X-ray point sources. Dashed lines indicate SNR candidates and filled circles indicate X-ray sources

greater than 7 x 10^{36} (d5.9 Mpc)^2 ergs^{-1}. We have taken these 72 X - ray sources and projected onto continuum subtracted H_α image of NGC6946. It is shown in Figure3. We have not found any positional coincidence with the X-ray point sources within 2” errors radius of our SNR candidates except for the one previously identified by MF97. NGC6946 was also observed with the Very Large Array (Lacey et al., 1997). The authors detect 118 radio sources. 37 of the candidate sources have been identified as possible SNR or background object. Except one previously identified by MF97 any positional coincidence have not been recovered within 5” error radius between optically identified SNRs and radio sources defined as possible SNRs. NGC628 was observed by XMM - Newton in January 2003. Soria et al. (2004) detect 77 point sources with luminosities 2 x 10^{37} ergs^{-1}. There is no match with five optically identified possible SNR candidates in NGC628. Six historical supernovae have been detected in NGC6946. Only five of these were in the field of our NGC6946 image. We were able to identify optical counterpart for only one (SN1917A) of the five historical supernovae that have occurred in NGC6946. SN 1917A has positional coincidence with one of our SNR (TUG10) candidates. NGC628 was observed by XMM - Newton (Soria et al., 2004). There is no match with five optically identified possible SNR candidates in NGC628.

4. CONCLUSION

We have performed an optical search for SNRs in two spiral galaxies. The technique consist of imaging the galaxies using narrow H_α and [SII] filters and find emission nebulae with [SII]/ $H_\alpha > 0.45$ to identify SNRs. We have detected 10 new SNR candidates in NGC 6946 and 5 other new ones in NGC628. We also have scheduled observations at TUG to obtain spectra of some of the reference stars in the fields in order to calibrate the flux ratio of the H_α and [SII] emission lines; the work is in progress.

REFERENCES

Blair, W. P. & Long,K. S.2004, 155,101 - 121

D’Odorico, et al., 1980, A&AS 40, 67D

Holt,S.S., et al., 2003, ApJ, 588, 762

Lacey, C, Duric, N., & Gross, W.M, 1997, ApJS, 109,417

Magnier, E., et al., 1995, A&AS, 114, 215 - 245

Mathewson, D. S. & Clarke,J.N., 1973,ApJ, 180, 725

Matonick D.M., et al., 1997, ApJS, 113, 333

Pannuti,T.G., et al., 2000,ApJ, 565,966

Soria,R. et al., 2004, A&A 413,107

A DETAILED REFLECTION GRATING SPECTROMETER ANALYSIS OF THE OUTFLOW OF NGC 253

M. Bauer[1], W. Pietsch[1], D. Breitschwerdt[2], M. Ehle[3], M. J. Freyberg[1], A. Read[4], and G. Trinchieri[5]

[1]Max-Planck-Institut für extraterrestrische Physik, Giessenbachstraße, 85748 Garching, Germany
[2]Institut für Astronomie der Universität Wien, Türkenschanzstr. 17, A-1180 Wien, Austria
[3]European Space Astronomy Centre, ESA, P.O. Box 50727, 28080 Madrid, Spain
[4]Department of Physics & Astronomy, University of Leicester, Leicester LE1 7RH, UK
[5]INAF Osservatorio Astronomico di Brera, via Brera 28, 20121 Milano, Italy

ABSTRACT

NGC 253 is an edge-on starburst galaxy in the Sculptor group. Observations in X-rays by *ROSAT*, XMM-Newton and *Chandra* show a mixture of extended and point source emission in disk and halo (Pietsch et al., 2000, 2001; Strickland et al., 2000; Vogler & Pietsch, 1999). Especially interesting is the connection between the starburst driven outflow from the nuclear region into the halo of the galaxy (plume). We analyzed XMM-Newton data, taken with the Reflection Grating Spectrometer (RGS) in 2000 and 2003 with a total low background exposure time of 127.8 ks. We extracted spectra of the outflow for different regions. Depending on the distance to the center along the south-east semi minor axis of NGC 253, the spectra show many individual emission lines with varying intensity. We used line ratios to characterize the temperature and the ionization mechanism in these regions. Furthermore we extracted narrow-band RGS images to map the spatial origin of the different emission lines.

Key words: X-rays: galaxies; Galaxies: individual: NGC 253; Galaxies: spiral; Galaxies: starburst; interstellar medium: jets and outflows.

1. INTRODUCTION AND OBSERVATIONS

The edge-on ($i = 86°$) galaxy NGC 253 is one of the best nearby (2.58 Mpc) examples of a nuclear starburst galaxy. It is well studied in many wavelength regimes. Especially important for sensitive soft X-ray observations is the very low galactic foreground absorption ($N_{\rm H} = 1.3 \times 10^{20}$ cm^{-2}) towards NGC 253 making it a perfect object to study the interaction of the starburst nucleus with the halo.

The nuclear region of NGC 253 was observed with XMM-Newton RGS in 2000 and 2003 with a total low background exposure time of 127.8 ks. The brightest regions in X-rays are the nuclear starburst region and emanating from that, a hollow cone shaped structure (plume) along the south-east minor axis which can be seen as extended bright soft X-ray emission in EPIC PN images. It has been interpreted as an outflow of hot interstellar medium from the starburst nucleus into the halo of the galaxy. Barely visible is an outflow to the north-west, due to high absorption of the intervening NGC 253 disk. The observation geometry led to a RGS dispersion direction that was approximately aligned to the NGC 253 major axis.

2. RESULTS

We extracted high resolution RGS spectra from several regions along the plume of NGC 253. As the galaxy covers the whole RGS detector CCDs, we used the new Science Analysis Software (SAS) task `rgsbkgmodel` to obtain a background spectrum which is not contaminated by emission of the galaxy. The resulting spectra are shown in Fig. 1. The extraction regions have a width of $0.5'$ in the cross dispersion direction and lie parallel to the major axis of the galaxy. We were able to identify many individual emission lines. In region SE 3 however, located farthest from the center, the S/N level is too low to draw reliable conclusions. Region NW is strongly affected by absorption from the disk of NGC 253. The line strength of individual lines changes with distance from the center of the galaxy, i.e. along the outflow. Lines at the shortest wavelengths vanish first from the spectra. Except for the iron lines in the center region the oxygen lines are the strongest lines in all spectra.

We used line ratios from different elements, most of them in their highest ionization state to derive temperatures for the different extraction regions. In contrast to the usual spectral fits we get temperatures free of abundance bias with small errors. The obtained temperatures range from 0.17 to 0.77 keV along the outflow (see Table 1). We did

Table 1. Temperatures of the plasma for different regions of the outflow of NGC 253 derived from line ratios of different elements. For region SE 3 no temperatures could be derived as the lines are too weak.

Region	Temperature in keV			
	Si	Mg	Ne	O
NW		0.40±0.04	0.26±0.06	0.17±0.02
Center	0.77±0.10	0.48±0.04	0.31±0.05	0.23±0.03
SE 1		0.40±0.05	0.23±0.02	0.24±0.03
SE 2			0.22±0.05	0.21±0.02

not include the temperatures derived from Fe XVII in Table 1 as they show errors in the order of 100 %. The broad range of temperatures may be caused by plasma which is not in equilibrium and/or reflects distributions of temperatures in the extraction regions. Narrowband RGS images can help to resolve this issue. Fig. 2 shows a selection of images in the Fe XVII and O VIII lines. A comparison of emission of Fe XVII at $\sim$ 15 Å (2p-3d) and at $\sim$ 17 Å (2p-3s), for example, shows that the emission originates to a certain degree from different regions. In the temperature calculation we assume that the lines emerge from the same region of space. If this is not the case the derived results are wrong. This may be the case for Fe XVII and therefore we obtained the large errors.

The diagnostic lines of Fe XVII are commonly used to derive the ionizing mechanism in plasmas. In the center region of NGC 253 as well as in the regions NW and SE 2 the line strenghts indicate a predominantly collisional ionized plasma. Region SE 1 however shows an inverted line ratio. Here the lines at 17 Å are stronger than the lines at 15 Å. Collisions between electrons and ions seem to be of less importance. This is not expected for an outflow where the X-ray emission is created at the border of the outflow, the region where the ejected gas collides with the surrounding interstellar material. It could be well possible that the strong 2p-3s emission is created in a photoionized region outside of the outflow. A possible region can be seen in Fig. 2 in the Fe XVII image at 17 Å, 0.7′ south of the galactic center. The very bright source coincides with source X33 from Pietsch et al. (2001).

REFERENCES

Pietsch, W., Roberts, T. P., Sako, M., et al. 2001, A&A, 365, L174

Pietsch, W., Vogler, A., Klein, U., & Zinnecker, H. 2000, A&A, 360, 24

Strickland, D. K., Heckman, T. M., Weaver, K. A., & Dahlem, M. 2000, AJ, 120, 2965

Vogler, A. & Pietsch, W. 1999, A&A, 342, 101

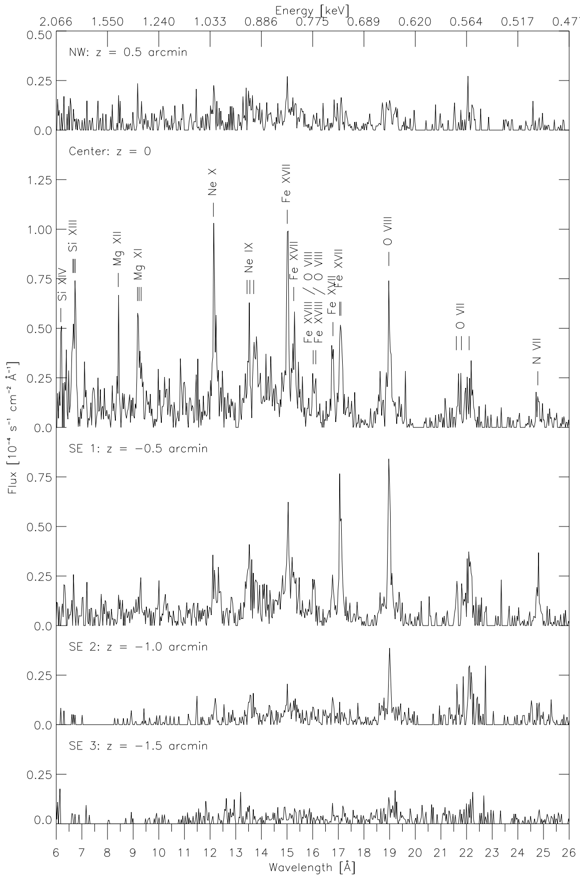

Figure 1. RGS spectra of NGC 253 extracted from different regions along the outflow. The label gives the position of the extraction region along the minor axis relative to the center of the galaxy in arcmin.

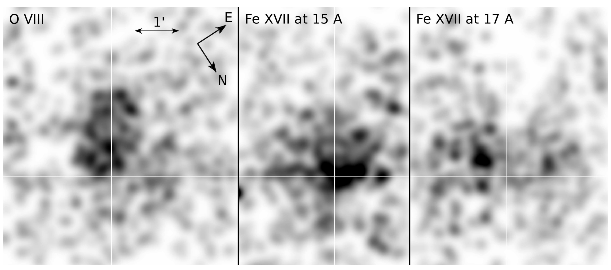

Figure 2. RGS images of NGC 253 in different lines. The RGS data allows to filter for very narrow wavelength bands. Shown here are images in the O VIII and Fe XVII lines. The strong O VIII emission nicely traces the outflow region. The horizontal white line marks the position of the disk of NGC 253. The vertical white line is the direction of the minor axis, i.e. along the outflow.

X-RAY PROPERTIES OF THE POINT SOURCES DETECTED INSIDE THE GALAXY NGC 300

S. Carpano[1], **J. Wilms**[2], **M. Schirmer**[3], **and E. Kendziorra**[1]

[1]Institut für Astronomie und Astrophysik, Universität Tübingen, Germany
[2]Department of Physics, University of Warwick, Coventry, UK
[3]Isaac Newton Group, Santa Cruz de La Palma, Spain

ABSTRACT

We present properties of the X-ray point sources detected in the nearby spiral galaxy NGC 300. The galaxy was observed with *XMM-Newton* in 2000 December/2001 January for a total of 66 ksec. A total of 163 sources were detected in the energy range of 0.3–6 keV, 86 sources of which are within the D_{25} optical disk. We report on the global properties of these sources, such as their hardness ratio and X-ray fluxes. We combine this information with the optical counterparts found in B, V, and R images from the 2.2 m MPG/ESO telescope and we cross-correlate the X-ray sources found inside the disk with SIMBAD, the USNO-A2.0 catalog, and radio catalogues. A full description of our results can be found in Carpano et al. (2005).

Key words: Galaxies: individual: NGC 300 – X-rays: galaxies.

1. INTRODUCTION

NGC 300 is a normal dwarf galaxy of type SA(s)d belonging to the Sculptor galaxy group. Due to its small distance (~1.88 Mpc; Gieren et al., 2005), its low Galactic column density ($N_\mathrm{H} = 3.6 \times 10^{20}\,\mathrm{cm}^{-2}$; Dickey & Lockman, 1990) and its face-on orientation, this galaxy is an ideal target for the study of the entire X-ray population of a typical normal quiescent spiral galaxy. The major axes of the D_{25} optical disk are 13.3 kpc and 9.4 kpc ($22' \times 15'$; de Vaucouleurs et al., 1991).

2. SOURCE CATALOG

NGC 300 has been observed by *XMM-Newton* during orbit 192 and orbit 195 for 37 ksec and 47 ksec respectively. Event and attitude files of each instrument were merged for both orbits using the `merge` task. Point source detection was then performed on the three cameras using the maximum likelihood approach of the `edetect_chain` task.

After removing sources associated with the galaxy cluster CL 0053−37, a total of 163 sources were found above a maximum likelihood threshold of 10 in the 0.3–6.0 keV band, 86 sources of which are within the D_{25} optical disk.

3. COLORS

We define the X-ray colors with:

$$\mathrm{HR}_\mathrm{hard} = \frac{H-M}{H+M+S}, \quad \text{and} \quad \mathrm{HR}_\mathrm{soft} = \frac{M-S}{H+M+S}$$

where S, M, and H are the total count rates in the soft (0.3–1.0 keV), medium (1.0–2.0 keV), and hard (2.0–6.0 keV) energy bands. Comparing the color-color diagram for sources inside the D_{25} optical disk and having more than 20 net counts with empirical color-color diagrams (see Carpano et al., 2005), we were able to characterize the shape of the X-ray spectrum for each source individually and to estimate source fluxes. These are between $\sim 3.5 \times 10^{-13}\,\mathrm{erg\,cm^{-2}\,s^{-1}}$ and $\sim 7 \times 10^{-16}\,\mathrm{erg\,cm^{-2}\,s^{-1}}$.

4. OPTICAL COUNTERPARTS AND CATALOGS

In addition to the X-ray data, observations with the 2.2 m MPG/ESO telescope on La Silla were performed. We searched for all possible optical counterparts in the merged BVR optical image and then calculated their fluxes in each of these three optical bands. Results are tabulated by Carpano et al. (2005). We also cross-correlated the X-ray sources with SIMBAD, the USNO-A2.0 catalog, and radio catalogues, finding

- 14 sources already observed in the X-rays,
- 9 (suspected) supernova remnants (SNR),
- 11 radio sources (3 associated with SNR, 8 possible AGN),

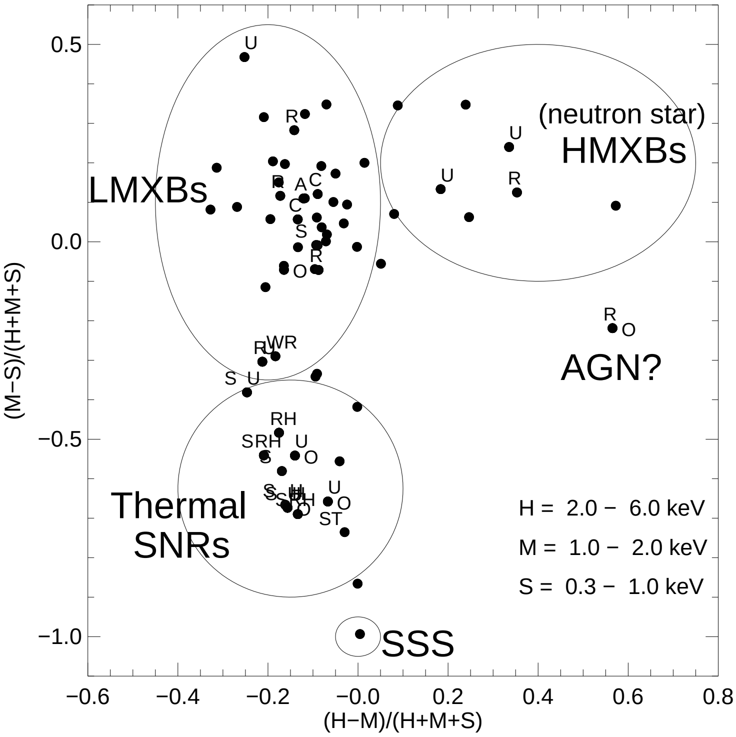

Figure 1. Color-color diagram for sources inside the optical disk. Supernova remnants are labeled with an 'S', radio sources with a 'R', H ii *regions with an 'H', Cepheid stars with a 'C', association of stars with an 'A', stars in NGC 300 with an 'ST', Wolf-Rayet stars with a 'WR' and sources from the USNO catalog with an 'U'. Sources with* $\log(F_X/F_{vis}) < -1$ *(Maccacaro et al., 2005) are labeled with 'O'.*

- 2 associations of stars, 8 H ii (ionized) regions, 2 Cepheid variable stars, 3 foreground stars/stars in NGC 300, 10 USNO-A2.0 counterparts.

5. SOURCE CLASSIFICATION

Using the source identification from catalogs, we classify the sources according to their X-ray colors (Fig. 1). SSSs are at the very bottom of the color-color diagram and soft sources are expected to be thermal SNR. SNR dominated by non-thermal emission (Crab-like objects) are expected to have harder spectra. Hard sources are likely X-ray binaries (XRB), which we classify into X-ray soft low-mass and harder high-mass XRB following Prestwich et al. (2005). Black-hole HMXB and LMXB are assumed to have similar spectral shape. Foreground stars are expected to have a $\log(F_{\mathrm{X}}/F_{\mathrm{vis}}) < -1$ (Maccacaro et al., 2005) and to be soft (therefore being prone to be confused with 'Thermal SNRs').

Note that there are overlaps from the different categories in the color-color diagram due to similar spectra and/or absorption. Strongly absorbed SSSs, e.g., can fall into the SNR group, whilst strongly absorbed or non-thermal SNRs can be confused with LMXBs.

Six sources in the thermal SNR group have SIMBAD counterparts (some of them have also radio and/or H ii region counterparts), and one known SNR (lying in the LMXB group) has be found to be a non-thermal X-ray spectrum. One source, having a radio and a bright optical counterpart, is likely identified as a background AGN. The brightest source is associated with a Wolf-Rayet star.

REFERENCES

Carpano, S., Wilms, J., Schirmer, M., & Kendziorra, E. 2005, A&A, in press

Dickey, J. M. & Lockman, F. J. 1990, ARA&A, 28, 215

de Vaucouleurs, G., de Vaucouleurs, A., Corwin, jr., H., et al. 1991, Third Catalogue of Bright Galaxies (New York: Springer)

Gieren, W., Pietrzyński, G., Soszyński, I., Bresolin, F., Kudritzki, R.-P., Minniti, D. & Storm, J. 2005, ApJ, 628, 695

Maccacaro, T., Gioia, I. M., Wolter, A., Zamorani, G. & Stocke, J. T. 1988, ApJ, 326, 680

Prestwich, A. H., Irwin, J. A., Kilgard, R. E., Krauss, M. I., Zezas, A., Primini, F., Kaaret, P. & Boroson, B. 2003, ApJ, 595, 719

REVEALING THE SUPERNOVA REMNANTS OF M33 WITH *CHANDRA* AND *XMM-NEWTON*

Parviz Ghavamian[1], Knox S. Long[2], William P. Blair[1], Manami Sasaki[3], Terrance J. Gaetz[3], and Paul P. Plucinsky[3]

[1]Department of Physics and Astronomy, Johns Hopkins University, Baltimore, MD, U.S.A., 21218-2686
[2]Space Telescope Science Institute, Baltimore, MD, U.S.A., 21218
[3]Harvard-Smithsonian Center for Astrophysics, Cambridge, MA, U.S.A., 02138

ABSTRACT

We present results of a search for supernova remnants (SNRs) in archival Chandra images of M33. We have identified X-ray SNRs by comparing the list of Chandra X-ray sources in M33 with tabulations of SNR candidates identified from (1) elevated [S II]/Halpha ratios in the optical, and (2) radio spectral indices. Of the 98 optically known SNRs in M33, 22 have been detected at $> 3\sigma$ level in the soft band (0.35-1.1 keV). At least four of these SNR candidates are spatially extended. We have also found new optical counterparts to two soft X-ray SNRs in M33, tentatively increasing the total number of known optically emitting SNRs in M33 to 100. The total number of identified SNRs with X-ray counterparts, including those exclusively detected by the XMM-Newton survey of M33, is now 37. We find that while there are a similar number of confirmed X-ray SNRs in M33 and the LMC with X-ray luminosities in excess of 10^{35} ergs s^{-1}, nearly 40% of the LMC SNRs are brighter than 10^{35} ergs s^{-1}, while only 13% of the M33 SNRs exceed this luminosity. The differences in luminosity distributions cannot be fully explained by uncertainty in spectral model parameters, and is not fully accounted for by abundance differences between the galaxies.

Key words: galaxies: individual (M33) – galaxies: ISM – shock waves – supernova remnants.

1. INTRODUCTION

Due to the low inclination ($<$ 55 degrees) and proximity (795 kpc) of M33, a detailed study of the the X-ray source population of this galaxy is particularly rewarding. Here we present results of a search for supernova remnants (SNRs) in archival *Chandra* and *XMM-Newton* images of this galaxy, utilizing spatial extent and hardness ratios as discriminants. We compare the list of *Chandra* and *XMM-Newton* X-ray sources with narrowband KPNO Mosaic images from the NOAO archive (Massey et al. 2002) to search for new optical SNRs at the positions of soft X-ray sources. Drawing together both SNRs with optical counterparts and SNR candidates lacking optical counterparts, we have generated an X-ray luminosity distribution for the M33 SNRs. Here we present a characterization of the X-ray spectral properties of this distribution and compare it to those of the SMC and LMC. A full description of this work can be found in Ghavamian et al. (2005).

2. OBSERVATIONS

The *Chandra* datasets analyzed here were acquired during Cycle 1 (ObsID 786 in ACIS-S imaging mode, ObsID 1730 in ACIS-I imaging mode) and Cycle 2 (ObsID 2023 in ACIS-I imaging mode). The Cycle 1 observations targeted the bright nuclear source of M33, while the Cycle 2 pointing was aimed at NGC 604, the giant starburst H II region along the northern spiral arm. Using CIAO version 3.0.2, we applied the CXC CTI correction to the level 1 event files and screened the data to remove background flare events and restrict the energy range of the resulting images to 0.35−8 keV. The final exposure times for the ObsID 786, 1730 and 2023 datasets were 46.3 ks, 49.4 ks and 88.8 ks, respectively.

2.1. X-ray Source Detection

We used the CIAO routine Wavdetect to search for X-ray sources in the *Chandra* data. We optimized our search for spatially extended X-ray emission from SNRs by conducting our Wavdetect runs on spatial scales of $0.''5$, $1''$, $2''$, $4''$, $8''$, $16''$, $32''$ and $64''$. We filtered each events file to create images in each of the following bands: 0.35−1.1 keV (S, or soft), 1.1−2.6 keV (M, or medium), 2.6−8.0 keV (H, or hard) and 0.35−8.0 keV (broad). The number of unique sources detected in the broad band images of ObsIDs 786, 1730 and 2023 was 166 (207) at the 3σ (2σ) level. We compared the list of

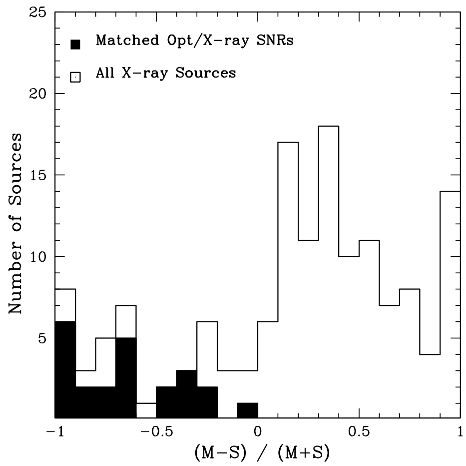

Figure 1. Hardness ratios for the 166 sources detected in the Chandra observations of M33, where S and M are defined as emission in the 0.35−1.1 keV and 1.1−2.6 keV range, respectively. The hardness ratios of soft Chandra sources matching the 22 Gordon et al. (1998) SNRs are shown for comparison (a 23rd source lacking an optical counterpart but exhibiting soft X-ray emission characteristic of a SNR is also included).

X-ray sources with the catalogue of M33 SNRs identified optically by Gordon et al. (1998) by their elevated [S II]/Hα line ratios (≥ 0.4). We performed the cross-correlation in two steps. First, we obtained a culled list of sources in all three bands that matched the coordinates of Gordon et al. (1998) SNRs to within a generous coincidence radius of 20$''$. Next, we looked for secondary signs of a match, such as evidence of extended morphology. In the majority of cases the X-ray emission from SNRs is dominated by thermal emission (lines + bremsstrahlung continuum) from shocks in ISM and ejecta material. The thermal emission is typically soft, peaking below 1 keV. Therefore, we concentrated our search for SNRs on the soft band images (0.35−1.1 keV) of M33.

3. SUPERNOVA REMNANTS DETECTED WITH *CHANDRA* AND *XMM-NEWTON*

Of the detected X-ray sources in the archival data, we find that 22 match optical SNRs from the optical catalogue at $\geq 3\sigma$ level in the S band (**Fig.** 1). In their *XMM-Newton* survey of M33, Pietsch et al. (2004) found X-ray counterparts to 13 additional optical SNRs not detected in the *Chandra* observations. These remnants are either intrinsically too faint to be detected in the given exposure times, are located too far off the *Chandra* optical axis (rendered undetectable by smearing of the PSF and/or high detector background), or are located outside the *Chandra* field of view. However, the *XMM-Newton* survey also identified 13 additional soft X-ray sources lacking optical counterparts as SNR candidates, based on their hardness ratios. We were able to identify optical counterparts to two of these sources in the KPNO Mosaic images.

Another relationship we can measure from the *Chandra* data is the cumulative luminosity distribution, $N(>L)$, of the M33 SNRs in the X-rays. We utilized the PIMMS online tool of the Chandra X-ray Center for the calculations and assumed a Raymond-Smith model, $kT = 1$ keV and 0.2 solar abundances. We fixed the M33 column to be N_H(M33) = 7×10^{20} cm^{-2}, the best fit value for the brightest SNR detected in the *Chandra* observations. We used N_H(LMC) = N_H(SMC) = 2×10^{20} cm^{-2}. The Galactic column used for all three galaxies was N_H(Gal) = 5×10^{20} cm^{-2}. The assumed distances to M33, the LMC and SMC were 795, 50 and 60 kpc, respectively. We find that while there are a similar number of confirmed X-ray SNRs in M33 and the LMC with X-ray luminosities in excess of 10^{35} ergs s^{-1}, nearly 40% of the LMC SNRs are brighter than 10^{36} ergs s^{-1}, while only 13% of the M33 sample exceed this luminosity. Including X-ray SNR candidates from the *XMM-Newton* survey increases the fraction of M33 SNRs brighter than 10^{36} ergs s^{-1} to 22%, still only half the LMC fraction. The differences in luminosity distributions cannot be fully explained by uncertainty in spectral model parameters, and is not fully accounted for by abundance differences between the galaxies. An explanation for this result is a focus of our ongoing investigation.

4. A DEEP *CHANDRA* SURVEY OF M33

The work outlined here is a prelude to a much more detailed investigation of M33 planned for Cycle 7 of *Chandra* . Our group (M. Sasaki, P.I.) has been awarded 1.4 Ms observing time to perform a survey of the entire galaxy with $\leq 1''$ resolution (*Chandra* ACIS-I Survey of M33: ChASeM33) down to a luminosity of 5×10^{34} ergs s^{-1} for point sources and 10^{35} ergs s^{-1} for diffuse sources. The rich data set from this survey, together with what promises to be an iconic image, will be part of the legacy of *Chandra* .

REFERENCES

Ghavamian, P., et al. 2005, AJ, 130, 553

Gordon, S. M., Kirshner, R. P. Long, K. S. & Smith, R. C. 1998, ApJ Suppl. 117, 89

Long, K. S., Blair, W. P., Kirshner, R. P. & Winkler, P. F. 1990, ApJ Suppl. 72, 61

Massey, P., et al. 2002, AAS 199, 130.05

Pietsch, W., et al. 2004, A&A 426, 11

Sasaki, M., Haberl, F. & Pietsch, W. 2002, A&A, 143, 391

van der Heyden, K. J., Bleeker, J. A. M. & Kaastra, J. S. 2004, A&A, 421, 1031

THE ULTRA LUMINOUS X-RAY SOURCES IN THE HIGH VELOCITY SYSTEM OF NGC 1275

O. González-Martín[1,2]*, A.C. Fabian[2] and J.S. Sanders[2]

[1]Instituto de Astrofísica de Andalucía (CSIC), Apdo 3004, 18080 Granada, Spain

[2]Institute of Astronomy, Madingley Road, Cambridge CB3 0HA

ABSTRACT

We report the results of a study of X-ray point sources coincident with the High Velocity System (HVS) projected in from of NGC 1275. A very deep X-ray image of the core of the Perseus cluster made with the *Chandra Observatory* has been used. We find a population of Ultra-Luminous X-ray sources. As with the the ULX populations in the Antennae and Cartwheel galaxies, those in the HVS are associated with a region of very active star formation. Several sources have possible optical counterparts found on *HST* images, although the brightest one does not. Absorbed power-law models fit the X-ray spectra, with most having a photon index between 2 and 3.

Key words: Perseus - NGC 1275- ULX.

1. INTRODUCTION

The study of Ultra-Luminous X-ray sources (ULX) has been greatly expanded by the high spatial resolution and spectral grasp of the *Chandra* and *XMM-Newton* observatories, respectively. ULX sources (Fabbiano & White 2003; Miller & Colbert 2004) have 2–10 keV X-ray luminosities exceeding $10^{39}\,\mathrm{erg\,s^{-1}}$ and they are not active galactic nuclei. Their luminosity exceeds that for a $10\,\mathrm{M_\odot}$ black hole accreting at the Eddington limit which radiates isotropically and so have created much interest in the possibility that they contain even higher mass black holes, such as InterMediate Black Holes (IMBH) of $\sim 10^3\,\mathrm{M_\odot}$ (Makishima et al. 2000). Alternatively they may appear so luminous because of beaming (Reynolds et al 1999) or due to super Eddington accretion (Begelman 2002).

Here we report on the discovery of a population of 8 point X-ray sources to the N of the nucleus of NGC 1275, which is the central galaxy in the Perseus cluster. A datailed analysis of the optical counterpart and X-ray spectral energy distribution have been performed.

*E-mail: omaira@iaa.es

2. IMAGING AND SPECTRAL ANALYSIS

The total exposure time, after removing periods containing flares, is 890 ks. All of the datasets were reprocessed to use the latest appropriate gain file. The CIAO LC_CLEAN tool was used to remove periods 20 per cent away from the median count rate for all the lightcurves. The CIAO CELLDETECT source detection routine was then used on the reprocessed level 2 event data to produce a preliminary list of point sources. As the X-ray diffuse emission of the NGC 1275 is very strong, the source list may well include false detections in high background level regions. Therefore problematic sources embeded in such regions have been excluded in our analysis. We have detected 8 bright sources close to the nucleus of NGC 1275, located in the northen inner radio lobe of 3C 84 (in the same region as the HVS). There are no sources associated with the southern lobe, thus we assume these sources are associated with the HVS.

We have used archival *HST* observations of NGC 1275 in order to search for optical counterparts. The galaxy was imaged with the WFPC2 camera on *HST* using the F814W ($\sim$ I) and F702W ($\sim$ R) broad-band filters. Several coincidences between X-ray sources and optical knots of emission (F814W) can be seen in Fig. 1. The *HST* image shows many highly absorbed features. When we compare in detail, sources N7 and N8 are located in star forming regions, while N2 and N6 have a point-like counterpart. Therefore, we have found a possible correlation between compact X-ray sources and regions of vigorous star formation. In order to investigate the emission mechanism of these ULX, the X-ray to optical flux ratios have been computed between the F702W and F814W *HST* bands and 1.0–7.0 keV band.

We extracted X-ray spectra for all the detected sources close to the HVS. The background region was either a source-free circular annulus or several circles surrounding each source. We extracted spectra from each of the datasets. These spectra were summed to form a total spectrum for each source. The spectra were fitted using XSPEC v.11.3.2., grouping the data to include at least 20 counts per spectral bin. In spectral fitting we excluded

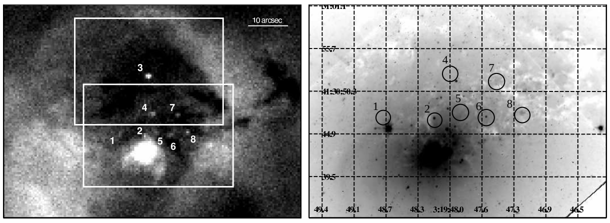

Figure 1. Left: Broadband (0.5–7.0 keV) X-ray smoothed image. Right: HST*/WFPC2 F814W broadband image centred in source 5. Note that source N3, out of HST image, have not optical counterpart.*

N	$N_H(10^{21}cm^{-2})$	Γ	χ^2/d.o.f.	$\log L_X$
1	$2.5^{(a)}$	$3.20^{+0.23}_{-0.37}$	112.90/101	39.51
2	$2.72^{+1.43}_{-0.87}$	$1.78^{+0.30}_{-0.24}$	101.50/109	39.86
3	$2.49^{+0.40}_{-0.40}$	$2.08^{+0.09}_{-0.09}$	153.86/142	40.22
4	$2.05^{+0.91}_{-0.96}$	$2.29^{+0.44}_{-0.28}$	156.24/152	39.91
5	$2.64^{+1.23}_{-0.93}$	$2.92^{+1.44}_{-0.36}$	124.09/139	39.90
6	$3.74^{+1.57}_{-1.39}$	$3.51^{+0.48}_{-0.66}$	102.58/92	39.84
7	$4.03^{+1.78}_{-1.45}$	$3.20^{+1.39}_{-0.48}$	133.69/135	39.95
8	$2.66^{+1.00}_{-0.91}$	$2.13^{+0.52}_{-0.25}$	150.81/138	39.93

Table 1. Spectral fits and 0.5–7.0 keV luminosities. (a) The column density of source N1 has been fixed.

any events with energies above 7.0 keV or below 0.5 keV. Table 1 summarizes our spectral results in terms of the absorbing column density, photon index and luminosities. Note that in all the cases the single component power law give satisfactory fits. The lower limit of the luminosity of point sources in the image, if at the distance of NGC 1275, is $L_X(0.5 - 7.0\,\mathrm{keV}) = 3.2 \times 10^{39}\mathrm{erg\ s^{-1}}$, which is already above the Eddington limit for a neutron star binary ($L_X \sim 3 \times 10^{38}\mathrm{erg\ s^{-1}}$) and is also above the limit of canonical ULX, i.e. $\geq 10^{39}\mathrm{erg\ s^{-1}}$.

Time variability analysis has been performed. The data characteristics allows us determine short variation in 16 days and long-term variability of 2 years. We extracted light-curves, using DMEXTRACT CIAO task for the two brightest sources (N3 and N4) binned with bin sizes between 500 and 5000 s. In both cases the points were consistent with the respective mean values and variability has not been found.

3. DISCUSSION

Chandra has revealed significant populations of ULX in the interacting systems of the Antennae (NGC 4038/9; Zezas et al. 2002) and the Cartwheel ring galaxy (Gao et al. 2003), where dramatic events have stimulated massive star formation. We have reported here on another example in the HVS of NGC 1275 which is interacting with the ICM of the Perseus cluster. The sources are spatially associated with the distribution of absorbing clouds seen in soft X-ray and optical (Fig.1) images. Furthermore, optical identification has been found in several of the X-ray sources. The optical brightness of these counterparts are too high to be individual stars and so they may be associated with young star clusters. Our interpretation of this correspondence is that the regions are especially active, indicating a real link between ULX and star-forming regions. In M31 and the Milky Way (Grimm et al. 2002), XRB have luminosities consistent with the Eddington limit of a $\sim 2M_\odot$ accreting object. They produce luminosities about one order of magnitude below the limiting luminosity in our sample. It is possible that our ULX consist of at least 15 'normal' XRB clustered together, perhaps in a young star cluster. However in other objects we know that variability requires the presence of intrinsically luminous X-ray sources Alternative possibilities are that black hole sources, with masses in the range of galactic black hole binaries, are mildly beamed (Reynolds et al. 1999). Spectral and timing features however rule out this possibility in some ULX.

Our optical studies have clearly shown that the ULX have very high X-Ray to optical flux ratios. X-ray selected AGN from the *Rosat all sky survey* tend to have $\log(F_X/F_{opt}) \sim 1$. Thus the ULX do not have the optical properties expected if their were simple extensions of AGN (IMBH). However, low mass X-ray binaries in the Milky Way have $F_X/F_{opt} \sim 100 - 10000$ (Mushotzky 2004). The results found in our system indicate that we have a mixed group of objects. At least 4 out of 8 sources (N3, N4, N5 and N8) have high X-ray to optical flux ratios. At least 3 out of 8 (N1, N2 and N6) have lower X-ray to optical ratios, possibly because they lie in star clusters.

Time variability is frequently observed in ULX (e.g. Liu et al. 2002), arguing that most of them are single compact objects. Unfortunately, our data are consistent with no significant variability.

Finally, our results add to the growing evidence that some episodes of rapid star formation lead to the production of ULX. Young, massive, star clusters may be involved in some, but not all of the sources.

REFERENCES

[1] Begelman M.C., 2002, ApJ, 568, L97

[2] Fabbiano G., White N.E., 2003, astro-ph/0307077

[3] Gao Y. et al.,2003, ApJ, 596, L171

[4] Grimm H., et al., MNRAS, 339, 793

[5] Liu J. et al., 2002, ApJ, 581, L93

[6] Makishima K. et al., 2000, ApJ, 535, 632

[7] Miller J.M., Colbert E., 2004, IJ Mod. Phys., 13, 1

[8] Mushotzky R., 2004, Prog. of Th. Phys. Sup., 155, 27

[9] Reynolds C. et al., 1999, ApJ, 521, 99

[10] Zezas A. et al.,2002, ApJ Supplement, 142, 239

THE ULTRALUMINOUS X-RAY SOURCE IC 342 X-1 AND ITS ENVIRONMENT

F. Grisé, M. Pakull, and C. Motch

Observatoire Astronomique, 11 rue de l'Université, 67000 STRASBOURG, France

ABSTRACT

We present optical observations of a ULX in the nearby spiral galaxy IC 342. This variable source has an average X-ray luminosity of some 10^{40} erg/s. At the position of the source there is an ionized nebula (the "Tooth") having huge dimensions (280 x 130 pc), much larger than normal supernova remnants. Our optical spectra reveal highly supersonic expansion velocities and emission line ratios typical of SNRs. It has been claimed that two [OIII] λ5007 bright regions in the nebula might be indicative of excitation by non-isotropic emission from the ULX. However, our continuum subtracted [OIII] λ5007 image reveals that O^{++} ions are rather smoothly distributed in the nebula, fully consistent with shock excitation. Within the nebula we find two candidate stars (V=24.0 & 24.6) in the Chandra X-ray error circle. Both are substantially reddened being consistent with the patchy interstellar absorption. We will discuss the nature of this source in the framework of what is currently known about optical counterparts of ULXs.

Key words: galaxies: individual (IC 342), ISM: supernova remnants, X-rays: galaxies, X-rays: binaries.

1. INTRODUCTION

The two main hypotheses put forward to explain the high X-ray luminosities of ULXs are intermediate mass black holes (IMBHs) having 10^2 to 10^5 solar masses (Colbert & Mushotzky, 1999) or non-isotropic emission from a stellar mass black hole beamed into our line-of-sight (King et al., 2001).

We present optical observations of one of these sources, carried out in 2003 and 2004 with the 8.2m SUBARU telescope. This ULX is located in the spiral galaxy IC 342, at a distance of some 4.0 Mpc, although the distance is not precisely known due to high foreground obscuration. Previously detected in an Einstein observation (Fabbiano & Trinchieri, 1987), IC342 X-1 was seen several times with ROSAT and ASCA, and later with Chandra and XMM-Newton, but in different states.

The first optical observation was done by Pakull & Mirioni (2002), revealing the presence of a nebula coincident with the ROSAT position of the ULX, which was named the "Tooth" nebula, descriptive of its morphology.

Another optical study made independently by Roberts et al. (2003), has obtained results consistent with the previous one, e.g, a [SII]/H_α emission-line flux ratio of 1.1 consistent with a supernova remnant.

2. RESULTS

At the position of the X-ray source there is an ionized nebula having huge dimensions (280 x 130 pc), much larger than normal supernova remnants (Fig. 1).

Inside the Chandra error circle of the X-ray source, there are two possible optical counterparts (astrometrical error $\sim 0.2''$) :

- candidate 1 at $03^h45^m55.60^s$, $+68°04'55.3''$ with a magnitude V=24.0 (V-I=1.5). Absolute magnitude M_V=-6.5 $\pm$ 0.5
- candidate 2 at $03^h45^m55.70^s$, $+68°04'54.5''$ with a magnitude V=24.6 (V-I=1.3). Absolute magnitude M_V=-5.9 $\pm$ 0.5

These two possible counterparts have V-I consistent with the extinction E(B-V)=0.8$\pm$0.1 towards the nebula in IC 342, so they are both likely members of the galaxy.

Unlike the study made by Roberts et al. (2003), the [OIII] emission seems to closely follow that of H_α (Fig. 1). Accordingly, we do not confirm the presence of high excitation [OIII] blobs which could have been suggestive of anisotropic X-ray emission (and ionisation) by the X-ray source.

Figure 2 presents the low resolution spectrum of the nebula around IC 342 X-1 (slit orientation is north-south) which confirms the previous studies with a high [SII]/H_α emission line flux ratio of 1.1, constant along the nebula. We can also note a high [OI]λ6300/H_α flux ratio of 0.26, all these ratios being typical of SNRs. Our [OIII]/H_β ratio, with a value of 1.0, does not show strong variations in

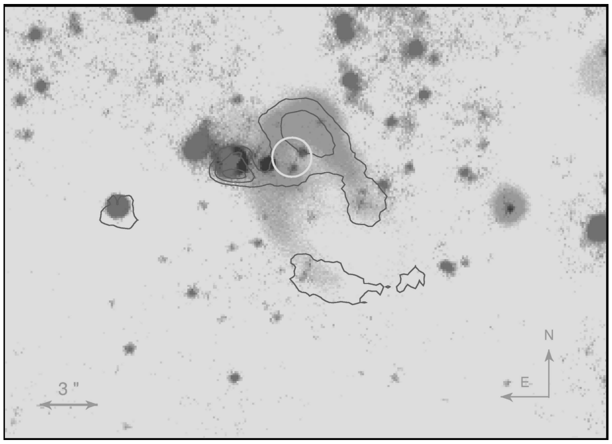

Figure 1. Structure of the "Tooth" around IC 342 X-1. The image shows the continuum subtracted H_α and V band representing the continuum. The continuum subtracted [OIII] emission is shown with contours. The uncertainty in the position of the X-ray source is indicated by an error circle with a 90% confidence radius of 1.2″.

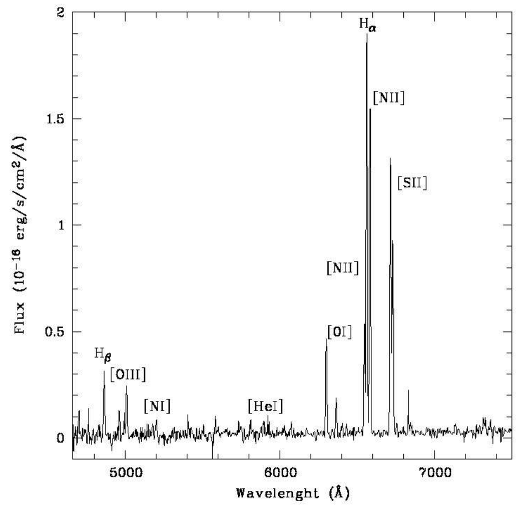

Figure 2. Low resolution spectrum of the nebula around IC 342 X-1. Emission features other than annotated are residuals of telluric lines or cosmic rays.

the main body of the nebula in agreement with our continuum subtracted [OIII] image. Table 1 presents the emission line flux ratios (vs. H_β) of the nebula, corrected for reddening.

Candidate 1 is present in our long slit spectrum. Unfortunately, the continuum of the star is not visible in the blue end of the spectrum because of the high reddening (Galactic extinction : E(B-V)=0.56). It seems that there is in addition a local extinction with E(B-V)=0.26 deduced from the H_α/H_β ratio. We have carefully searched for the HeIIλ4686 emission line present in some other ULXs and revealing X-ray ionization, but the spectrum is not sufficiently sensitive in this wavelength domain. We derive an upper limit for an emission line flux ratio [HeII]λ4686/H_β of about 0.1.

Element	λ(Å)	$I(\lambda)/I(H_\beta)$
H_β	4861	1.0 ± 0.1
[OIII]	4959	0.3 ± 0.08
	5007	0.7 ± 0.09
[NI]	5198+5200	0.3 ± 0.08
[HeI]	5876	0.1 ± 0.05
[OI]	6300	0.8 ± 0.1
	6363	0.3 ± 0.08
[NII]	6548	0.7 ± 0.15
	6583	2.4 ± 0.25
H_α	6563	2.9 ± 0.3
[SII]	6717	1.8 ± 0.25
	6731	1.3 ± 0.2
[ArIII]	7136	0.05 ± 0.03
[OII]	7320+7330	0.10 ± 0.07

Table 1. Emission line flux ratios of the nebula surrounding IC 342 X-1, corrected for reddening. c(H_β)=1.13 corresponding to E(B-V)=0.82

3. CONCLUSION AND PERSPECTIVES

IC 342 X-1 is one of the most studied ULX, and it starts to reveal some of its secrets. We conclude that the nebula is mainly shock-ionized, with no or little X-ray ionization. Like other ULX bubbles, the Tooth is probably either a supernova remnant that reflects tfhe formation of the compact star in the ULX or it is inflated by relativistic wind/jets as in the system W50/S433.
We have found in the Chandra error circle two possible optical counterparts. Their absolute visual magnitude is consistent with the X-ray heated accretion disk counterparts of ULXs Holmberg IX X-1 and NGC 1313 X-2. Much fainter candidates, including the possible presence of a poor cluster as observed in these archetypal ULXs, cannot presently be excluded for IC 342 X-1. Future optical observations will be crucial to reveal nature and evolutionary state of the exciting class of ultraluminous X-ray emitters.

REFERENCES

Colbert, E. & Mushotzky, R. 1999, ApJ, 519, 89

Fabbiano, G. & Trinchieri, G. 1987, ApJ, 315, 46

King, A., Davies, M., Ward, M., Fabbiano, G., & Elvis, M. 2001, ApJ, 552, L109

Pakull, M. & Mirioni, L. 2002, astro-ph/0202488

Roberts, T., Goad, M., Ward, M., & Warwick, R. 2003, MNRAS, 342, 709R

DARK MATTER HALOS OF EARLY-TYPE GALAXIES

P. J. Humphrey[1], **D. A. Buote**[1], **F. Gastaldello**[1], **L. Zappacosta**[1], **J. S. Bullock**[1], **F. Brighenti**[2,3] **& W. G. Mathews**[2]

[1]Dept. of Physics & Astronomy, University of California, Irvine, Irvine, CA 92697
[2]University of California Observatories, Lick Observatory, University of California at Santa Cruz, Santa Cruz, CA 95064
[3]Dipartimento di Astronomia, Università di Bologna, Via Ranzani 1, Bologna 40127, Italy

ABSTRACT

Cosmological simulations of galaxy formation predict a universal form for the mass profile of dark matter (DM) halos from cluster to galaxy scales. Remarkably few interesting constraints exist, however, on DM halos in early-type galaxies. Using *Chandra* we present the temperature, density and mass profiles of a small sample of early-type galaxies, revealing significant DM in each case. When a component is included to account for stellar mass and the DM halo is allowed to respond adiabatically to the baryonic condensation into stars, the mass profiles are well-fitted by the universal profile, with Virial masses and concentrations in agreement with simulations. However, only ∼half, or less, of the mass within $\mathrm{R_e}$ seems attributable to the stars, implying stellar $\mathrm{M_*/L_B}$ ∼1–5.

Key words: galaxies: elliptical and lenticular, cD— galaxies: ISM— dark matter.

1. INTRODUCTION

The nature of DM within the Universe is one of the fundamental problems facing modern physics. N-body cosmological simulations predict a "universal" profile for DM halos over a wide range of mass-scales (Navarro et al., 1997, hereafter NFW). In an hierarchical formation scenario the early epoch of formation of low-mass halos should "freeze in" more tightly concentrated halos at the galaxy scale than are observed in clusters (Bullock et al., 2001). What is less clear, however, is the way in which the DM halo responds to the condensation of baryons into stars. If the galaxy is assembled by a series of mergers, however, the baryonic and dark matter may be mixed in such a way that the total gravitating mass follows the NFW profile (Loeb & Peebles, 2003). Alternatively, present-day ellipticals may retain the "memory" of the original contraction (Gnedin et al., 2004). We present X-ray determined mass profiles for 7 early-type galaxies, spanning the mass range $\sim 10^{12}$–$\sim 10^{13}\mathrm{M_\odot}$, chosen from the *Chandra* archive to be sufficiently bright and relaxed enough to yield interesting mass constraints. Two companion posters, Gastaldello et al and Zappacosta et al (both this volume) address DM halos at galaxy and group scales.

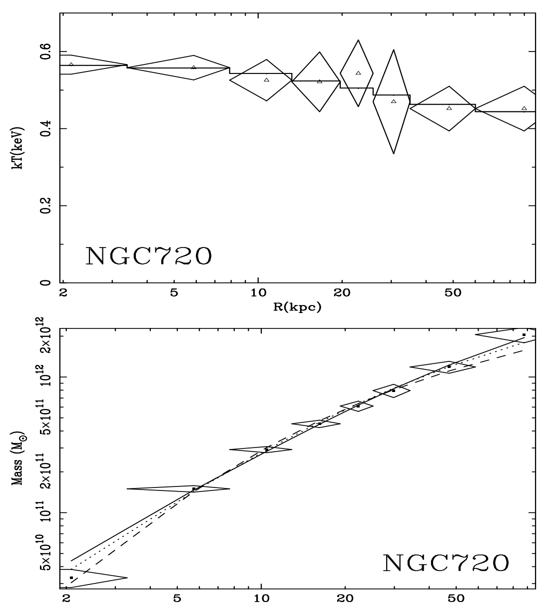

Figure 1 Temperature *(upper panel)* and mass *(lower panel)* profiles of NGC 720. The mass data are shown with models comprising simple NFW (dashed line), NFW plus stellar (dotted line) and compressed NFW plus stellar (solid line) potentials.

2. DATA ANALYSIS

The *Chandra* data were processed with *CIAO* 3.2.2, following standard procedures. Due to the low surface brightness of the data, special care was taken in treating the background, for which we adopted a modelling procedure (see Humphrey et al, 2005). We fitted the spectra from concentric annuli with an APEC model (plus unresolved point-source component in $\mathrm{D_{25}}$) to determine temperature and density. The best-fitting abundances were

Table 1: Best-fit values of $\mathrm{M_{vir}}$, in units of $10^{12}\mathrm{M_\odot}$, and c for the different mass models fitted. Where no error is quoted the parameter value was fixed. Error bars are at 1-σ. Figures in square parentheses are systematic error estimates (see text). Other figures in parentheses represent the change in the best-fit value if $\mathrm{M_*/L_B}$ is varied by $\pm$20%.

Galaxy		NFW			Compressed NFW+ stars		
	χ^2/dof	$\mathrm{M_{vir}}$	c	χ^2/dof	$\mathrm{M_{vir}}$	c	$\mathrm{M_*/L_B}$
NGC 720	2/9	$3.4^{+1.5}_{-0.9}$	47$\pm$15	1/9	$6.1^{+5.2}_{-2.4}$	19^{+8}_{-6}	3.3
		$[^{+1.7}_{-0.7}]$	[$\pm$8]		$[^{+15}_{-1.2}](^{+1.4}_{-0.9})$	$[^{+2}_{-7}](\pm4)$	
NGC 1407	23/11	$9.0^{+6.3}_{-3.5}$	36^{+13}_{-9}	18/11	300(>30)	4.6$\pm$4.2	4.7
		$[^{+4.3}_{-3.7}]$	$[^{+14}_{-8}]$		[-250](-230)	$[^{+7.2}_{-1.9}](\pm4.1)$	
NGC 4125	23/11	$1.0^{+0.2}_{-0.1}$	88$\pm$14	19/11	$1.8^{+0.8}_{-0.4}$	25^{+8}_{-6}	2.4
		$[^{+0.3}_{-0.4}]$	$[^{+44}_{-7}]$		$[^{+0.2}_{-1.1}](^{+0.7}_{-0.3})$	[+38]($\pm$10)	
NGC 4261	23/12	$1.5^{+0.3}_{-0.2}$	160$\pm$20	21/12	$2.6^{+1.8}_{-1.0}$	38^{+23}_{-14}	4.6
		$[^{+0.4}_{-0.2}]$	$[^{+10}_{-30}]$		$[\pm1.2](^{+2.0}_{-0.7})$	$[^{+23}_{-18}](\pm26)$	
NGC 4472	53/21	10^{+4}_{-3}	30^{+7}_{-5}	30/20	55^{+160}_{-28}	11$\pm$4	0.87$\pm$0.14
		$[^{+0.4}_{-0.6}]$	$[^{+20}_{-2}]$		$[^{+2}_{-30}]$	$[^{+1.7}_{-0.8}]$	
NGC 4649	30/7	$2.5^{+0.4}_{-0.3}$	140$\pm$10	21/7	17^{+36}_{-9}	24$\pm$8	4.7
		$[^{+0.1}_{-1.0}]$	$[^{+30}_{-4}]$		$[^{+2}_{-11}](^{+130}_{-10})$	$[^{+13}_{-1}](\pm18)$	
NGC 6482	0.6/5	$2.3^{+0.4}_{-0.3}$	99$\pm$16	0.4/5	$3.5^{+1.3}_{-0.9}$	36^{+9}_{-7}	1.2
		$[^{+0.2}_{-0.1}]$	[$\pm$4]		$[\pm0.3](^{+0.6}_{-0.4})$	[$\pm$2]($\pm$9)	

similar to other early-type galaxies (Humphrey & Buote, 2005).

3. MASS PROFILES

The gravitating mass profiles were inferred from the temperature and density profiles in two ways. First, we used parameterised models for each, although we did not find a universal profile fitted either, and derived mass profiles under the assumption of hydrostatic equilibrium (we discuss the possible impact of low-significance asymmetries in some systems— e.g. Randall et al. 2004— in Humphrey et al, 2005, in prep). The mass profiles were clearly more extended than the optical light, indicating significant DM. Within $\mathrm{R_e}$, we found $\mathrm{M/L_B}$ for the gravitating matter varied from 2.3–9.3 $\mathrm{M_\odot/L_\odot}$. In Fig. 1, we show the best-fit temperature and mass profiles for NGC 720. Alternatively, we also used the temperature profile, and an assumed mass profile (see below) to derive a density model, which we fitted to the data. This procedure gave more robust mass constraints. These techniques are outlined in Humphrey et al (2005).

Simple NFW fits to the data gave very large ($\gg 20$) values for c, the halo concentration, in contrast to the typical values predicted by simulations ($\sim$15 e.g. Bullock et al., 2001). To investigate whether baryonic matter affects the mass profile, we included an Hernquist (1990) mass component to trace the stars and allowed the DM halo to be compressed due to baryonic condensation (Gnedin et al., 2004). Assuming all mass within $\mathrm{R_e}$ is stellar did not give meaningful fits. Fixing stellar mass ($\mathrm{M_*}$) within $\mathrm{R_e}$ to be half of the total reduced c, bringing $\mathrm{M_{vir}}$ and c into better agreement with simulations. This model fitted all the galaxies well. We note that if adiabatic compression of the DM halo was turned off, for a fixed $\mathrm{M_*/L_B}$, c was significantly higher.

Our results were very sensitive to $\mathrm{M_*/L_B}$, which could only be constrained in NGC 4472 (in which it was $\sim$1). In general, though, we found $\mathrm{M_{vir}}$ and c were consistent with simulations (Bullock et al., 2001), albeit very uncertain. In Table 1 we show a summary of our results and, in addition, the sensitivity to $\mathrm{M_*/L_B}$ and the spectral analysis choices (e.g. N_H or background modelling).

ACKNOWLEDGMENTS

We thank Oleg Gnedin for making available his adiabatic contraction code. Support for this work was provided by NASA under grant NNG04GE76G issued through the Office of Space Sciences Long-Term Space Astrophysics Program.

REFERENCES

Bullock, J. S., Kolatt, T. S., Sigad, Y., Somerville, R. S., Kravtsov, A. V., Klypin, A. A., Primack, J. R., & Dekel, A. 2001, MNRAS, 321, 559

Gnedin, O. Y., Kravtsov, A. V., Klypin, A. A., & Nagai, D. 2004, ApJ, 616, 16

Hernquist, L. 1990, ApJ, 356, 359

Humphrey, P. J. & Buote, D. A. 2005, ApJ, submitted, astro-ph/0504008

Loeb, A. & Peebles, P. J. E. 2003, ApJ, 589, 29

Navarro, J. F., Frenk, C. S., & White, S. D. M. 1997, ApJ, 490, 493

Randall, S. W., Sarazin, C. L., & Irwin, J. A. 2004, ApJ, 600, 729

THE BIRTHPLACE OF LMXBS: FIELD VS. GLOBULAR CLUSTER POPULATIONS IN EARLY-TYPE GALAXIES

J. Irwin

Department of Astronomy, University of Michigan, Ann Arbor, MI 48109-1042, USA

ABSTRACT

Recent *Chandra* studies of low-mass X-ray binaries (LMXBs) within early-type galaxies have found that LMXBs are commonly located within globular clusters of the galaxies. However, whether all LMXBs are formed within globular clusters has remained an open question. If all LMXBs formed within globular clusters, the summed X-ray luminosity of the LMXBs in a galaxy should be directly proportional to the number of globular clusters in the galaxy regardless of where the LMXBs currently reside. We have compared these two quantities over the same angular area for a sample of 12 elliptical and S0 galaxies observed with *Chandra*, and found that the correlation between the two quantities is weaker than expected if all LMXBs formed within globular clusters. This indicates that a significant number of the LMXBs were formed in the field, and naturally accounts for the spread in field–to–cluster fractions of LMXBs from galaxy to galaxy. We also find that the "pollution" of globular cluster LMXBs into the field has been minimal within elliptical galaxies but there is evidence that roughly half of the LMXBs originally in the globular clusters of S0 galaxies in our sample have escaped into the field.

Key words: LaTeX; ESA; X-rays.

1. INTRODUCTION

While it was expected that *Chandra* would resolve many low-mass X-ray binaries (LMXBs) in nearby galaxies, it was quite unexpected that such a large percentage of LMXBs would reside within globular clusters of the host galaxies. Also unexpected was the variation in the fraction of LMXBs within globular clusters from galaxy to galaxy, ranging from almost 70% in NGC 1399 to a more modest 18% in NGC 1553 (Angelini et al. 2001; Sarazin et al. 2003).

Given the much higher (> 100 times) efficiency of creating LMXBs within globular clusters than in the field, it is natural to ask if *all* (or nearly all) LMXBs are formed within globular clusters. In this scenario, the LMXBs found presently in the field actually formed within globular clusters, but escaped to the field at a later time, either through interactions within the globular cluster or through the tidal disruption or destruction of the globular cluster over time. This was first suggested by Grindlay (1984) for the case of Galactic X-ray bursting binaries, and extended to LMXBs within early-type galaxies by White, Sarazin, & Kulkarni (2002).

To address this issue we have compared the total X-ray luminosity emanating from LMXBs in a galaxy to the number of globular clusters in the galaxy for a sample of galaxies. If all LMXBs formed within globular clusters, there should be a linear relation between these two quantities regardless of where the LMXBs currently reside. On the other hand, if there is a significant population of LMXBs created in the field, the relation between the number of LMXBs and globular clusters should be weaker, as the field component becomes more dominant in galaxies with fewer globular clusters. This would also predict that the fraction of LMXBs found within globular clusters is larger for galaxies with more globular clusters per unit light, which could account for the measured spread in the fraction of LMXBs within globular clusters from galaxy to galaxy.

2. THE DATA REDUCTION

We have determined L_X, the total X-ray luminosity emanating from LMXBs in a given galaxy. L_X was determined by summing the individual X-ray luminosities of the detected sources and adding to this an estimate of the unresolved LMXB emission (determined by the amount of diffuse emission in hard energy channels, where gaseous X-ray emission should be minimal). This was done for a sample of 12 galaxies for which good estimates of the total number of globular clusters per unit light (the globular cluster specific frequency, S_N) could be obtained from the literature. For each galaxy, L_X was normalized by the optical luminosity of the galaxy in order to compare galaxies of different sizes. We were careful to determine L_X/L_{opt} only over the same angular area of the *Chandra* detector for which S_N was determined from optical data (primarily *HST* WFPC2 data), since S_N can vary substantially with galactic radius. We also eliminated all X-ray sources with X-ray luminosities exceeding 5×10^{38} ergs s^{-1} from the study to avoid the few brightest X-ray sources from dominating L_X.

3. RESULTS

Figure 1 shows the relation between L_X/L_{opt} vs. S_N for our sample of 12 galaxies. Although there is a clear relation between the two quantities, the best-fit relation does *not* go through the origin. If it had gone through the origin, this would imply that a galaxy without any globular clusters would not contain any LMXBs – this is expected if *all* LMXBs formed within globular clusters. However, the non-zero $y-$intercept (significant at the 8.0σ level) implies that there is indeed a component to the LMXB population that forms in the field (and are not simply LMXBs that escaped from globular clusters).

If we fit a linear relation to the data of the form $(L_X/L_{opt})_{total} = (L_X/L_{opt})_{GC} + (L_X/L_{opt})_{Field}$ = A * S_N + B, we can use the best-fit constants A and B to predict the fraction of LMXBs that formed within globular clusters. That is, the fraction of LMXBs formed in globular clusters is (A * S_N)/(A * S_N + B) for each galaxy. This is not to be confused with the *present-day* fractions of LMXBs within globular clusters, which can be substantially lower than the initial fraction if some LMXBs were lost from globular clusters over time. For the elliptical galaxies in our sample, the predicted (initial) fraction is consistent with or only slightly less than the measured (present-day) fraction. Conversely, for the three S0s in the sample, the initial fractions were much greater than the present-day fraction. This indicates that LMXBs within globular clusters of S0 galaxies have been removed from globular clusters at a much higher rate than within elliptical galaxies. It is possible that this is due to the tidal disruption (but not destruction) of globular clusters within S0 galaxies. Such an effect is expected to be more pronounced within S0 galaxies than in elliptical galaxies, owing to the presence of disks in S0s that are lacking in ellipticals. Gravitational shocks caused by the passage of a globular cluster through a disk are much stronger than passage through a bulge distribution (Fall & Zhang 2001), leading to a greater number of LMXBs ejected from globular clusters in S0s than in ellipticals. Clearly, more observations are needed to confirm this hypothesis.

4. CONCLUSIONS

Our main conclusions are that (1) LMXBs can be formed in the field of early-type galaxies, despite the fact that it is much easier to form them within globular clusters – a galaxy without any globular clusters would still contain LMXBs, and (2) it appears that some LMXBs within S0 galaxies have escaped from globular clusters into the field to join the LMXBs that were truly formed in the field. This effect is not seen (or to a much lesser extent) in elliptical galaxies, possibly due to the fact that elliptical galaxies lack a disk that might be necessary to tidally disrupt globular clusters to the point where they could lose their LMXBs into the field.

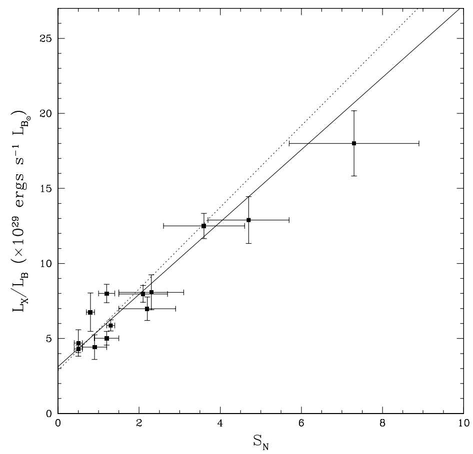

Figure 1. Relation between L_X/L_{opt} vs. S_N for a sample of 12 galaxies. The fact that the best-fit relation does not pass through the origin indicates that there is a population of LMXBs in each galaxy that did not form within globular clusters, but formed in the field instead. The y-intercept represents the fraction of L_X/L_{opt} attributed to field-born LMXBs in each galaxy.

REFERENCES

Angelini, L., Loewenstein, M., & Mushotzky, R. F. 2001, ApJ, 557, L35

Fall, S. M., & Zhang, Q. 2001, ApJ, 561, 751

Grindlay, J. E. 1984, Adv. Space Res., 3, 19

Sarazin, C. L., Kundu, A., Irwin, J. A., Sivakoff, G. R., Blanton, E. L., & Randall, S. W. 2003, ApJ, 595, 743

White, R. E., Sarazin, C. L., & Kulkarni, S. R. 2002, ApJ, 571, L23

A DEEP XMM–NEWTON SERENDIPITOUS SURVEY OF A MIDDLE–LATITUDE AREA

N. La Palombara[1], G. Novara[1], N. Carangelo[1], A. De Luca[1], P. Caraveo[1], R.P. Mignani[2], and G.F. Bignami[3]

[1]INAF/IASF-Milano, via Bassini 15, I–20133 Milano (I)
[2]European Southern Observatory, Karl Schwarzschild Strasse 2, D–85740 Garching (D)
[3]Centre d'Etude Spatiale des Rayonnements (CESR), CNRS–UPS, 9 Avenue du colonel Roche, F–31028 Toulouse (F)

ABSTRACT

The radio–quiet neutron star 1E1207.4-5209 has been the target of a 260 ks *XMM–Newton* observation. It is the longest observation ever performed at intermediate galactic latitude ($b \simeq 10°$), which is a rather unexplored region of the X–ray sky. Here we report on the performed source detection, which yielded an harvest of about 200 serendipitous sources above a limiting flux of 2×10^{-15} erg cm^{-2} sec^{-1}, in the 0.3-8 keV energy range. Their log$N$–log$S$ distribution is different from those measured either in the Galactic Plane or at high galactic latitudes. An identification is proposed for the brightest sources in our sample and the discovery of a previously unknown Seyfert–2 galaxy is discussed. A complete description of this work is reported in Novara et al. (2005).

Key words: Galaxies: Seyfert – X–rays: general.

1. X–RAY ANALYSIS

During the *XMM–Newton* observation of 1E1207.4-5209 all the three *EPIC* focal plane cameras (Turner et al. 2001; Strüder et al. 2001) were active: the two *MOS* cameras were operated in *Full Frame* mode, in order to cover the whole *field–of–view* of 30 arcmin; the *pn* camera was operated in *Small Window* mode, where only the on–target CCD is read–out. Therefore we used only the *MOS* data to perform the source detection.

In order to maximize the *signal–to–noise* ratio (*S/N*) of our serendipitous sources and to reach lower flux limits, we 'merged' the data of the two cameras. We performed the source detection in both the two coarse energy ranges 0.5–2 and 2–10 keV and eight fine ranges between 0.3 and 8 keV (since above 8 keV the instrument effective area decreases rapidly). The source detection was based on the *maximum detection likelihood* criterium. Selecting all the sources with likelihood $L > 8.5$ in at least one of our energy ranges and matching those detected in several energy intervals we found a total of 196 sources (with a position accuracy of $\sim$ 5"). We detected 135 sources between 0.5 and 2 keV and 89 sources between 2 and 10 keV, at a flux limit of 1.3×10^{-15} and 3.4×10^{-15} erg cm^{-2} s^{-1}, respectively; 68 of them were detected in both energy bands. In order to evaluate their flux, we assumed a template AGN spectrum, i.e. a power–law with photon–index Γ=1.75 and an hydrogen column density N_H of 1.28×10^{21} cm^{-2}, corresponding to the total galactic column density.

In Fig. 1 we show the cumulative log$N$–log$S$ distributions for the sources detected in the two energy ranges. For comparison, we have superimposed to our data the lower and upper limits of the log$N$–log$S$ distributions measured by Baldi et al. (2002) for a survey at high galactic latitude ($|b| > 27°$). Moreover, in the same figure we have also reported the log$N$–log$S$ distributions, as well

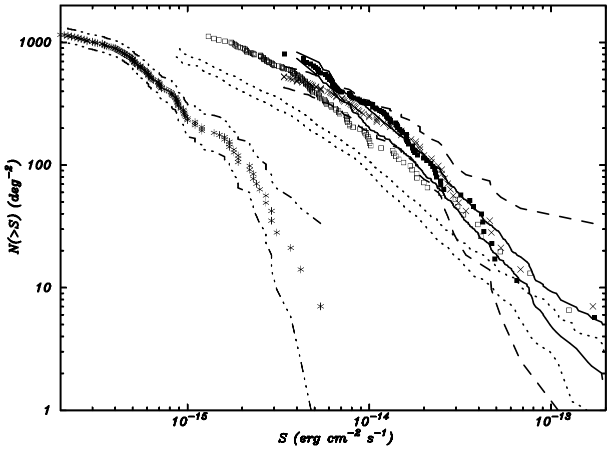

*Figure 1. Log$N$–log$S$ distribution of the detected sources in the energy ranges 0.5–2 keV (*open squares*) and 2–10 keV (*filled squares*). The dotted and the solid lines, respectively, trace the upper and lower limits obtained by Baldi et al. (2002) in the same energy ranges but at higher galactic latitudes. The asterisks and the crosses are the distributions measured by* CHANDRA *in the galactic plane (in the 0.5–2 and 2–10 keV ranges, respectively), while the dot–dashed and the dashed lines represent the corresponding limits (Ebisawa et al. 2005))*

as the 90 % confidence limits, measured by *CHANDRA* in the galactic plane (Ebisawa et al. 2005). In the soft energy band, the log$N$–log$S$ distribution of our sources is well above the high–latitude upper limit, expecially at low X–ray fluxes. Since Ebisawa et al. (2005) find that most of their soft sources detected in the galactic plane (show with the asterisks) are nearby X–ray active stars, it is possible that our excess is due to additional, more distant galactic sources, which are missed looking at $b \sim 0°$ but can be detected just outside the galactic plane. On the other hand, in the hard energy band the distribution of our sources is in good agreement with both the high latitude and the galactic plane ones. Here we expect that the effect of the galactic absorption is negligible, therefore the extragalactic sources dominate the log$N$–log$S$ distribution at all galactic latitudes, with just a small contribution of the *softer* galactic sources.

2. SOURCE IDENTIFICATION

The detected X–ray sources were cross–correlated with the *GSC* ($B_{lim} \simeq 22.5$) and the *USNO* ($V_{lim} \simeq 21$) optical catalogues, assuming a 5" radius error–circle. In such a way, we found at least one optical candidate counterpart for 95 of the 196 sources. The remaining sources lack any optical counterpart since, in view of the length of our X–ray exposure, the expected limiting magnitude of the possible counterparts is $V \simeq 25$. In order to reach this limit and to find all the missing counterparts, a complete optical coverage of the *EPIC* field at the 2.2 m ESO telescope has already been performed and the data analysis is now in progress.

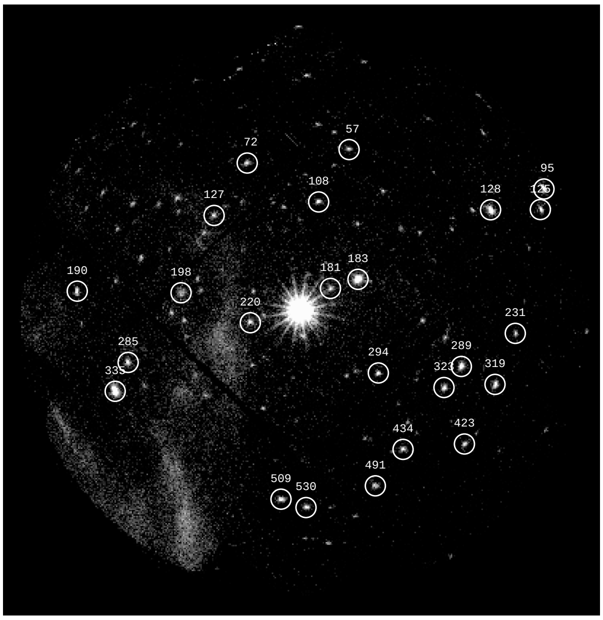

Figure 2. Image of the sky distribution of the 24 brightest sources, in the energy range 0.3–8 keV.

We also performed a spectral analysis of the 24 brightest sources, which have more than 500 counts (Fig. 2). Based on both the best–fit single–component emission model and the X–ray/optical flux ratio, it was possible to propose an AGN identification for 13 sources and a star identification for 7 sources; for the remaining 4 sources it was not possible to suggest any identification. Therefore we find that roughly one third of the brightest sources could belong to the Galaxy. Such a percentage is in agreement with the results obtained by previous surveys, which showed that the stellar content decreases from $\sim$85% to $\sim$30% moving from the galactic plane to high galactic latitudes (Motch et al. 1997; Zickgraf et al. 2003).

Finally, we focused on the analysis of one of the four identified sources (i.e. source #127 in Fig. 2), which shows a very hard and highly absorbed spectrum, with a prominent feature at $\sim$6 keV, ascribable to Fe emission line (Fig. 3). We found that its optical counterpart is the spiral galaxy ESO 217-G29, with magnitudes Bj=16.74 and F=14.93 and optical redshift z=0.032 (Visvanathan & van den Bergh 1992). Assuming a simple power–law spectrum, the estimated X–ray/optical flux ratio is $>$0.02. All these parameters suggested an AGN identification for this source. According to the AGN unification model, we tried to fit its spectrum with a complex emission model composed by primary power–law, a warm and a cold reflection component and a Gaussian component to model the Fe line. We checked that the source spectrum is well described by this model only with a redshift z=0.057, i.e. very different from the optical one. On the other hand, in order to obtain a good spectral fit with z=0.032 it is necessary to replace the Gaussian line with a relativistic one (i.e. a *laor* or a *diskline* component). The unabsorbed flux of the primary nuclear component implies that f_X/f_{opt}=0.41, a value well within the AGN range (Krautter et al. 1999). The X–ray luminosity of the source in the 2–10 keV energy band, corrected by the absorption and with the redshift at 0.032, is $2.59^{+1.84}_{-1.07} \times 10^{42}$ erg s^{-1}, corresponding to a low luminosity Seyfert galaxy. Since the hydrogen column density associated to the torus of dust around the AGN nucleus is $\simeq 8 \times 10^{22}$ cm^{-2}, we propose that this source could be a new, low–luminosity Seyfert–2 galaxy discovered serendipitously in our field.

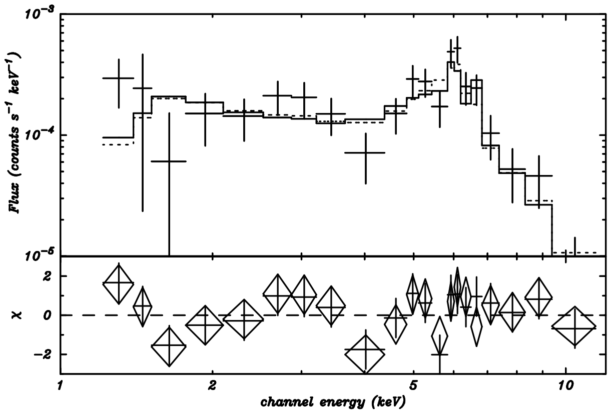

Figure 3. Top*: comparison of the spectrum of source #127 with the best–fit model and z=0.032, in the case of both a* laor *(solid line) and a* diskline *(dashed line) model for the Fe line.* Bottom*: data - model residuals (in σ) for the diskline (crosses) and the laor (diamonds) model.*

ACKNOWLEDGMENTS

We are grateful to K. Ebisawa for providing us the log$N$-log$S$ data of the *Chandra* observation of the galactic plane. The Guide Star Catalog used in this work was produced at the Space Telescope Science Institute under U.S. Government grant. This research has made use of the USNOFS Image and Catalogue Archive operated by the United States Naval Observatory at the Flagstaff Station (http://www.nofs.navy.mil/data/fchpix/).

REFERENCES

Baldi, A., Molendi, S., Comastri, A., et al. 2002, ApJ, 564, 190

Ebisawa, K., Tsujimoto, M., Paizis, A., et al. 2005, ApJ accepted astro-ph/0507185

Krautter, J., Zickgraf, F.-J., Appenzeller, I., et al. 1999, A&A, 350, 743

Motch, C., Guillout, P., Haberl, F., et al. 1997, A&A, 318, 111

Novara, G., La Palombara, N., Carangelo, N., et al. 2005, A&A accepted astro-ph/0510674

Strüder, L., Briel, U., Dennerl, K., et al. 2001, A&A, 365, L18

Turner, M. J. L., Abbey, A., Arnaud, M., et al. 2001, A&A, 365, L27

Visvanathan, N. & van den Bergh, S. 1992, AJ, 103, 1057

Zickgraf, F.-J., Engels, D., Hagen, H.-J., Reimers, D., & Voges, W. 2003, A&A, 406, 535

LUMINOSITY FUNCTION OF X-RAY SOURCES IN THE GALACTIC BULGE

H. Mori[1], **Y. Maeda**[1], **Y. Ueda**[2], **and H. Inoue**[1]
[1]ISAS/JAXA, 3-1-1 Yoshinodai, Sagamihara, Kanagawa, Japan
[2]Kyoto University, Sakyo-ku, Kyoto, Japan

ABSTRACT

We studied the luminosity function of X-ray sources in the Galactic bulge using a flux-limited sample selected from the *ROSAT Bright Source Catalogue* (hereafter *RBSC*). By using the spectral colors, 78 sources were picked up from the Galactic bulge. From the 78 selected sources, we constructed the luminosity function of the Galactic bulge sources with a luminosity of $> 10^{34}$ erg s^{-1}. Most of the X-ray sources are likely Low-Mass X-ray Binaries (hereafter LMXBs). Compared with the luminosity functions of LMXBs in the bulges in other galaxies, we found that there is a good correlation between the number of LMXBs and the B-band luminosity in the host bulges. The luminosity function of the LMXBs over the wide luminosity range of $10^{34} - 10^{40}$ erg s^{-1} can be commonly represented by the power-law with three indices (0.4, 0.8, and 1.8) and two break luminosities of $\sim 10^{36}$ and 5×10^{38} erg s^{-1}.

Key words: Bulge, Luminosity function, LMXBs.

1. INTRODUCTION

The galactic bulge is a spherical structure surrounding the galactic center over ~ 3 kpc. The bulge is considered as a vestige of galaxy evolution (e.g., Gilmore 1999). Therefore the galactic bulge is believed as a key to understand the galaxy evolution. Since the bulge is old, its stars with relatively large masses had already ended their lives and evolved into compact stars, such as a neutron star (hereafter NS) or a black hole (hereafter BH). Hence the X-ray wavelengths provide us new insights into the bulge that are sensitive to the stellar population with higher masses. For this aim, we selected the Galactic bulge. There have been many past studies on the Galactic LMXBs (e.g., Grimm et al. 2002), however no attention had been paid to the Galactic bulge, mainly due to the poor detection limit of a non-imaging instruments. In order to pick up the LMXBs in the Galactic bulge, we used the *RBSC* sample (Voges et al. 1999), which enables us to determine the positions of the X-ray sources with high accuracy and to perform an unbiased population study of the Galactic bulge.

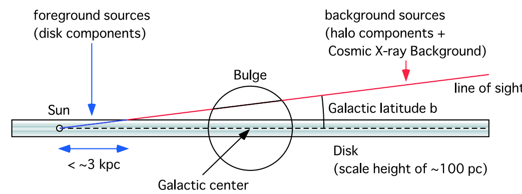

Figure 1. Schematic view of the cross section of our Galaxy

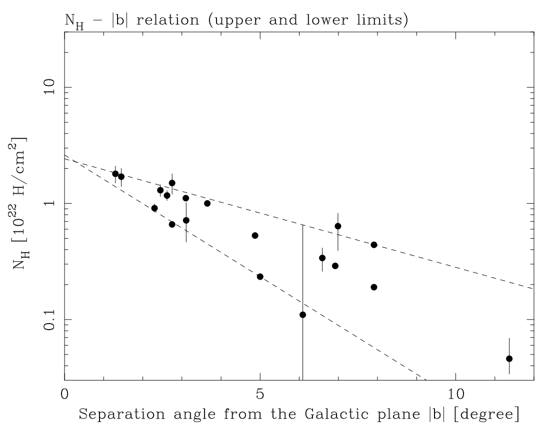

Figure 2. Column densities towards the Galactic bulge LMXBs dependent on their Galactic latitude $|b|$

2. X-RAY SOURCES IN THE GALACTIC BULGE

Fig. 1 shows a schematic view of our Galaxy, which consists of the Galactic disk and bulge. The Galactic bulge is a gas-less spheroid with a scale angle of ~ 12 degrees from the Galactic center. As shown in Fig. 1, the Galactic bulge sources are contaminated along a line of sight by foreground sources in the Galactic disk and background ones in the Galactic halo or extragalaxies. Since the Galactic absorption is attributed to interstellar medium (hereafter ISM) which mainly distributes along the Galactic disk, the foreground sources are suffered from relatively low absorption. We can thus remove the foreground sources by testing if their low-energy absorption columns are large enough for the disk ISM in the line of sight or not. The *RBSC* provides us with two hardness ratios designated as HR1 and HR2. The spectral colors (HR1, HR2) serve as a good measure of absorption column if we assume an appropriate spectral model.

Fig. 2 shows the column densities to the known Galactic bulge sources. The column densities can be modelled by a simple exponential function of the Galactic latitude $|b|$ (for details, Mori et al. 2005). Using this $|b|$-dependent model of the Galactic absorption, we estimated the colors of the *RBSC* sources when they are located in the Galactic bulge. We considered the power-law spectrum with indices of 0.5–3.0 (see Schulz 1999). In total, the colors of 78 *RBSC* objects are consistent within 90% confidence level that they are not located in front of the Galactic bulge. Since only 17% of these sources are likely extragalactic origin (see Miyaji et al. 2000), the 78 sources mainly inhabit in the Galactic bulge.

3. LUMINOSITY FUNCTION

Since the distances to the Galactic bulge sources are expected as nearly constant (8.5 ± 1.7 kpc), we can make the luminosity function of the 78 Galactic bulge sources as shown in Fig. 3. The error box corresponds to the uncertainties of the distances, and the absorption columns and photon indices in spectra when we convert the source count rates to the unabsorbed X-ray fluxes. We also corrected the incompleteness of the source detection below the luminosities of 10^{35} erg s^{-1}. The extragalactic component was also subtracted using the high latitude data.

Over the luminosity range of $10^{35} - 10^{38}$ erg s^{-1}, we fit the luminosity function by a single power-law model. The best fit parameter of the power-law index is ~ 0.4. Since the Galactic bulge is old and the X-ray luminosities of each source are larger than 10^{34} erg s^{-1}, most of the Galactic bulge sources are considered to be LMXBs.

4. DISCUSSION

We compared the cumulative luminosity function of the LMXBs in the Galactic bulge with those in the M31 bulge (Kong et al. 2002) and elliptical galaxies (Kim & Fabbiano 2004). Fig. 4 shows these luminosity functions where the number of LMXBs is normalized by the B-band luminosity of its host bulge. As seen in Fig. 4, the normalized luminosity functions are consistent with each others in the overlapped luminosity ranges. This result indicates that the number of LMXBs in the galactic bulges is well proportional to their size, and that the luminosity

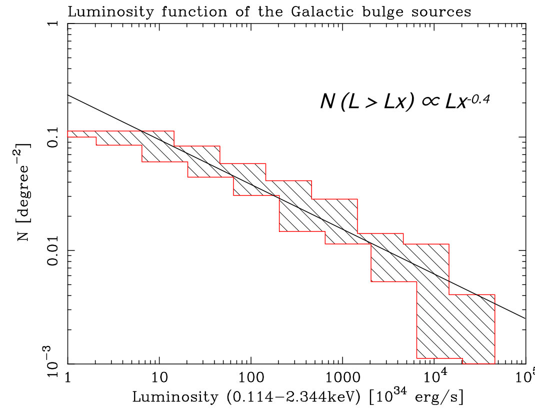

Figure 3. Cumulative luminosity function of the X-ray sources in the Bulge

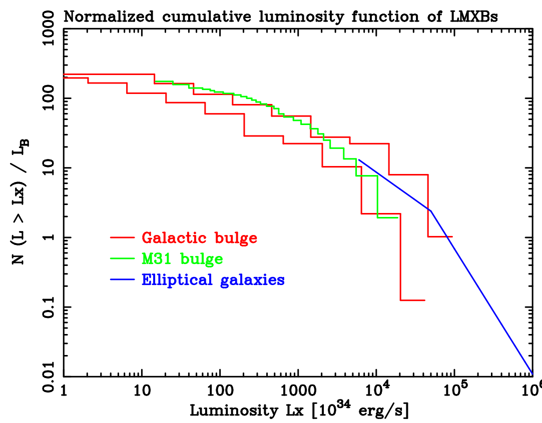

Figure 4. Luminosity function of the LMXBs normalized by the B-band luminosities of the host bulges

function of the LMXBs over the wide luminosity range of $10^{34} - 10^{40}$ erg s^{-1} is represented by the power-law model, whose slope becomes steeper (0.4, 0.8, and 1.8) as the luminosity increases.

REFERENCES

Gilmore, G. 1999, The Formation of Galactic Bulges , 1

Grimm, H.-J., Gilfanov, M., & Sunyaev, R. 2002, A&A, 391, 923

Kim, D. & Fabbiano, G. 2004, ApJ, 611, 846

Kong, A. K. H., Garcia, M. R., Primini, F. A., Murray, S. S., Di Stefano, R., & McClintock, J. E. 2002, ApJ, 577, 738

Mori, H. 2005, Ph. D thesis (Tokyo Univ.)

Miyaji, T., Hasinger, G., & Schmidt, M. 2000, A&A, 353, 25

Voges, W., et al. 1999, A&A, 349, 389